AWARD NUMBER: W81XWH-19-1-0443

TITLE: The Role of Astrocytes and Microglia in Exercise-induced Neuroplasticity in Parkinson's Disease

PRINCIPAL INVESTIGATOR: Michael W. Jakowec, PhD,

CONTRACTING ORGANIZATION: University of Southern California, Los Angeles, CA

REPORT DATE: October 2020

TYPE OF REPORT: Annual

PREPARED FOR: U.S. Army Medical Research and Development Command
Fort Detrick, Maryland, 21702-5012

REPORT DOCUMENTATION PAGE

Form Approved
OMB No. 0704-0188

1. REPORT DATE	2. REPORT TYPE	3. DATES COVERED
October 2020	Annual	01Sep2019-31Aug2020

4. TITLE AND SUBTITLE

The Role of Astrocytes and Microglia in Exercise-induced Neuroplasticity in Parkinson's Disease

5a. CONTRACT NUMBER

5b. GRANT NUMBER
W81XWH-19-1-0443

5c. PROGRAM ELEMENT NUMBER

6. AUTHOR(S)
Michael W. Jakowec, PhD (PI)

E-Mail: mjakowec@surgery.usc.edu

5d. PROJECT NUMBER
PD180100

5e. TASK NUMBER

5f. WORK UNIT NUMBER

7. PERFORMING ORGANIZATION NAME(S) AND ADDRESS(ES)

Michael Jakowec, PhD
1333 San Pablo St. MCA-241
Department of Neurology
University of Southern California, LA, CA, 90033

Rosemarie Gonzales, University of Southern California, Dept. Contracts and Grants, 1540 Marengo St. Suite 701, LA, CO, 90033

8. PERFORMING ORGANIZATION REPORT NUMBER

9. SPONSORING / MONITORING AGENCY NAME(S) AND ADDRESS(ES)

U.S. Army Medical Research and Development Command
Fort Detrick, Maryland, 21702-5012

10. SPONSOR/MONITOR'S ACRONYM(S)

11. SPONSOR/MONITOR'S REPORT NUMBER(S)

12. DISTRIBUTION / AVAILABILITY STATEMENT

Approved for Public Release; Distribution Unlimited

13. SUPPLEMENTARY NOTES

14. ABSTRACT

Recent studies in our labs have implicated a role for glial cells (astrocytes and microglia) in exercise-induced synaptogenesis and synaptic repair. The primary goal of this application is to investigate the role of astrocytes, microglia and peripheral monocytes in regulating exercise induced synaptogenesis and behavioral recovery in Parkinson's disease. Studies in this application will explore region specific metabolic changes mediated by exercise, using imaging tools and molecular biology approaches to determine the mechanistic roles of glial cells, metabolism and immune processes associated with exercise induced neuroplasticity and potential disease modification. **Specific Aim 1** will test the hypothesis that exercise induced astrocytic activation and elevated lactate metabolism regulates synaptogenesis and behavioral recovery in an animal model of PD. **Specific Aim 2** will test the hypothesis that activation of anti-inflammatory resident microglia and infiltrating peripheral mononuclear cells regulate synaptogenesis in the striatum and Prefrontal cortex of exercised 6-OHDA mice. We will further test the hypothesis that anti- vs. pro-inflammatory serum immune soluble factors (cytokines and BDNF) are associated with exercise benefits in PD.

15. SUBJECT TERMS

16. SECURITY CLASSIFICATION OF:			17. LIMITATION OF ABSTRACT	18. NUMBER OF PAGES	19a. NAME OF RESPONSIBLE PERSON
a. REPORT	b. ABSTRACT	c. THIS PAGE			19b. TELEPHONE NUMBER *(include area code)*
Unclassified	Unclassified	Unclassified	Unclassified	56	USAMRMC

Standard Form 298 (Rev. 8-98)
Prescribed by ANSI Std. Z39.18

TABLE OF CONTENTS

1. Introduction

Parkinson' disease (PD) is characterized by motor and non-motor (cognitive) impairments that lead to a progressive decline in quality of life (QoL) and increased morbidity. While there is no cure, research from our labs and others have demonstrated a role for exercise in improving motor/nonmotor features, QoL and repair of corticostriatal synaptic circuits). Recent studies in our labs have implicated a role for glial cells (astrocytes and microglia) in exercise-induced synaptogenesis and synaptic repair. It has long been known that activated glial cells accompany tissue damage in PD and contribute to an inflammatory cascade responsible for persistent injury that results in onset and progression of clinical disease. Astrocytes are essential for metabolic processes in the brain and are important in synaptic transmission. They couple multiple neurons and synapses into functional assemblies. Astrocytes also respond to increased synaptic neurotransmission via ability to sense extracellular concentrations of K^+ and glutamate. Neurons and astrocytes are metabolically coupled such that, even in the presence of cellular oxygen, astrocytes generate high levels of lactate through aerobic glycolysis and shuttle high-energy metabolites to neurons engaged in elevated synaptic activity. Astrocytes are also tightly associated with blood vessels and contribute to the blood brain barrier. In addition, synaptic loss and dysfunction, cell death, and neurite loss occurs in the presence of activated microglia, secretion of pro-inflammatory cytokines and chemokines, and recruitment of monocytes from the periphery. However, published studies and recent preliminary data from our lab have demonstrated that mechanisms capable of controlling pro-inflammatory activities in the CNS are induced by intensive exercise and involve production of anti-inflammatory cytokines (including the trophic factor BDNF), regional activation of microglia, and recruitment of monocytes with a "regulatory" phenotype to sites of synaptogenesis.

The primary goal of this application is to investigate the role of astrocytes, microglia and peripheral monocytes in regulating exercise induced synaptogenesis and behavioral recovery in PD. Studies in this application will explore region specific metabolic changes mediated by exercise, using imaging tools and molecular biology approaches to determine the mechanistic roles of glial cells, metabolism and immune processes associated with exercise induced neuroplasticity and potential disease modification.

Specific Aim 1 will test the hypothesis that exercise induced astrocytic activation and elevated lactate metabolism regulates synaptogenesis and behavioral recovery in an animal model of PD. This hypothesis is based on our preliminary data and recent reports demonstrating the importance of astrocytes and lactate metabolism in synaptic transmission, synaptogenesis and learning. We will also test whether exercise-induced changes in astrocytic activation and lactate metabolism is associated with increases in regional cerebral glucose uptake (rCGU) due to exercise. Studies will utilize a novel transgenic mouse model, established in our lab, which expresses astrocyte-specific red fluorescent protein tdTomato (ACT mouse) to isolate astrocytes. We have also developed a shRNA viral vector to selectively knock-down MCT-4, which we hypothesize to be critical for establishing the metabolic relationship between astrocytes and activated neuronal circuits through the ANLS.

Specific Aim 2 will test the hypothesis that activation of anti-inflammatory resident microglia and infiltrating peripheral mononuclear cells regulate synaptogenesis in the striatum and PFC of exercised 6-OHDA mice. We will further test the hypothesis that anti- vs. pro-inflammatory serum immune soluble factors (cytokines and BDNF) are associated with exercise benefits in PD. Our preliminary experiments in animals and pilot clinical study support this hypothesis. The CNS mononuclear cell population was more responsive to activation, which when cultured in the presence of stimuli secreted significantly higher amounts of IL-10, TGFβ, and BDNF suggesting enhancement of synaptic plasticity in these regions. processes are related to exercise benefits of cognitive function in physically (exercise) active PD subjects.

Impact: Studies from this application will (i) elucidate the role of glia in mediating exercise-induced neuroplasticity in PD and its models, (ii) support that changes in neuronal metabolism in conjunction with activation of astrocytes and microglia support improved synaptogenesis, leading to improved motor and cognitive behavior, and (iii) demonstrate how small energetic molecules like glucose and lactate in conjunction with components of the peripheral immune system (monocytes) link region-specific neuronal activation in the brain with non-neuronal cells (glia) at sites of circuitry activation. Understanding the mechanisms of exercise-induced neuroplasticity are critical to the development of strategies to treat patients suffering from degenerative brain disorders such as PD. Indeed, our studies in both animal models of PD and in patients with PD have led to widespread adoption of exercise and physical therapy as standard of care. The immediate impact of the studies in this application will shed additional mechanistic light on the benefits of exercise to reveal region specificity, allowing refinement of neurological physical therapy approaches. The long-term clinical impact will provide a framework for future clinical studies to determine if exercise (i) can modify disease progression, (ii) can impact immune components to promote synaptogenesis and restoration of motor and cognitive circuits, and (iii) whether benefits can be enhanced by including additional components of a healthy

lifestyle, including diet, mindfulness, and stress management. Finally, it is possible that the data will reveal potential for the addition of supplemental pharmacological interventions designed to target astrocytes, microglia and components of the peripheral immune system), and interventions that modify metabolism.

2. KEYWORDS

Parkinson's disease, exercise, metabolism, astrocytes, immune system, microglia, 6-OHDA, cognition, neuroplasticity, synaptogenesis.

3. ACCOMPLISHMENTS IN YEAR 1

3.1. Major Goals

The Following Section 3.1. outlines the major scientific goals achieved during Year 1. The Figure below highlights graphically the progress of the overall study. The Following Table lists the Statement of Word (SOW) with achievements in Year 1 highlighted in yellow. Following the Table are bullet points of major achievement and goals reached in Year 1.

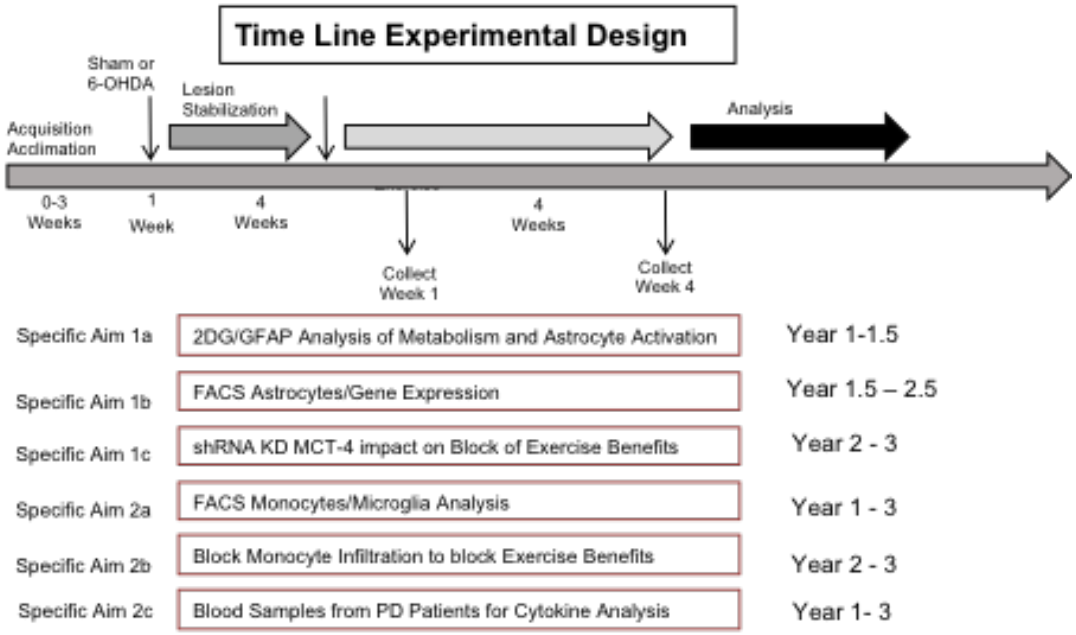

Lab 1 **University of Southern California**
1333 San Pablo St. MCA-241/3/5
Los Angeles, CA 90033
PI: M. Jakowec (MJ)

Lab 2 **University of Southern California**
1333 San Pablo St. MCA-B6/8
Los Angeles, CA 90033
Co-I: D. Holschneider/ Zhou Wang (DH/ZW)

Lab 3 **University of Southern California**
1333 San Pablo St., MCA-246
Los Angeles, CA 90033
Co-PI: B. Lund (BL)
Co-IP: W. Gilmore
Co-PI: G. Petzinger

Tasks in Specific Aim 1a	Timeline Month	Lab Group
Hiring and Training of Study Staff	All personnel are currently employed in labs	1, 2, 3
IACUC Approval for entire project (addendum to ongoing approved projects)	1	1, 2, 3

Milestone Achieved	2	1, 2, 3
6-OHDA lesioning of mice, stabilization of lesion, exercise regimen	2-6	1,2
2DG studies in Sham±exercise and 6-OHDA ± exercise mice	4-8	2
Milestone Achieved	8	1,2
GFAP analysis of astrocyte activation by IHC	4-8	1
Analysis of outcome data including correlation studies	8-9	1,2
Milestone Achieved	10	1,2
Analysis of data, completion of Aim 1b, report, publication, data storing	14	1,2
Tasks in Specific Aim 1b		
IACUC Approval for entire project (addendum to ongoing approved projects)	1	1,2
Milestone Achieved	2	1,2
6-OHDA lesioning of mice, stabilization of lesion, exercise regimen, breeding ACT mice	6-12	1,2
Construction and validation of ACT mouse	Completed	2
Milestone Achieved	Completed	2
FACS analysis of ACT mouse astrocytes	9-12	2
Analysis of ACT astrocytes by qRT-PCR and RNAseq	10-14	2
Milestone Achieved	14	2
Tasks in Specific Aim 1c		
Hiring and Training of Study Staff	All personnel are currently employed in labs	2
IACUC Approval for entire project (addendum to ongoing approved projects)	1	2
Milestone Achieved	2	2
6-OHDA lesioning of mice, stabilization of lesion, exercise regimen	14-18	2
Milestone Achieved	18	2
Construction of shRNA vector	Completed	2
Milestone Achieved	Completed	2
Validation of shRNA to KD MCT2 in astrocyte cultures	6	2
Milestone Achieved	8	2
Stereotaxic targeting of vector to mouse brain	14-18	2
Molecular and behavioral outcome measures	18-24	2
Analysis of data	20-24	2
Milestone Achieved	24-28	2
Tasks in Specific Aim 2a		
Hiring and Training of Study Staff	All personnel are currently employed in labs	3
IACUC Approval for entire project (addendum to ongoing approved projects)	1	3
Milestone Achieved	2	3
6-OHDA lesioning of mice, stabilization of lesion, exercise regimen	4-8	1, 3
FACS analysis microglia phenotype/function brain serum	8-18	1, 3
Milestone Achieved	18	1, 3
Tasks in Specific Aim 2b		
Hiring and Training of Study Staff	All personnel are currently employed in labs	1, 3
IACUC Approval for entire project (addendum to ongoing approved projects)	1	1, 3
Milestone Achieved	2	1, 3
6-OHDA lesioning of mice, stabilization of lesion, exercise regimen	18-22	1
Blocking monocyte infiltration, behavioral molecular study of effects	24-28	1, 3

Milestone Achieved	30	1, 3
Tasks in Specific Aim 2c		
IRB approval of addendum to current protocol	1-2	3
Begin subject recruitment	Currently underway as part of ongoing IRB approved project	3
Collection of samples	6-24	3
Analysis of serum cytokines in PD patients at baseline, 9, 18 months	6-24	3
Milestone Achieved	24-30	3
Analysis of data, completion of Aim 2c, report, publication, data storing	36	3
Tasks Overall		
Subtask 1: Coordinate with Data Core for monitoring data collection rates and data quality	Every 6 months	1, 2, 3
Perform all analyses according to specifications, share output and findings with all investigators	Every 6 months	1, 2, 3
Work with data core and dissemination of findings (abstracts, presentation, publications, DOD)		1, 2, 3
Completion of Studies	36	1, 2, 3

Major Goals Achieve in Year 1

Specific Aim 1a will test the hypothesis that exercise leads to increase regional Cerebral Glucose Uptake and astrocytic phenotypic activation. We will utilize [^{14}C]-2-deoxyglucose autoradiography mapping to measure glucose uptake in the brain and GFAP IHC as a phenotypic marker of astrocytic activation. This study is supported by our preliminary data showing exercise-related increase in astrocyte morphology consistent with activation. Adjacent brain slices will be used to examine for co-localization/correlation between increase in rCGU and astrocytic GFAP.

- Approval of IACUC for use of vertebrate animals

- Conducting studies of [^{14}C]-2-deoxyglucose autoradiography mapping to measure glucose uptake in the brains of 6-OHDA mice subjected to exercise or that remain sedentary. All parameters for studies in Aim 1A are validated and currently underway. Brains have been harvested from non-lesioned mice with and without exercise and subjected to [^{14}C]-2-deoxyglucose autoradiography mapping.

- Significant number of 6-OHDA lesioned mice have been established to carryout studies in Aim 1. The site of the lesions in the basal ganglia have been verified with immunohistochemical staining for tyrosine hydroxylase. The impact of the 6-OHDA lesion in the dorsomedial stratum and its impact on motor and cognitive behaviors has been verified using rotarod, novel object recognition, open field, and pole test.

Specific Aim 1b will test the hypothesis that exercise leads to an increase of lactate metabolism of activated astrocytes in brain regions identified in SA1a and including PFC, dSTR, ERC, and vCB. Using our ACT transgenic mouse, FACS enrichment of astrocytes from these regions will be examined for expression of mRNA transcripts and proteins of interest including MCT-4 and LDHa and GLUT1 using qRT-PCR and WIB. We will also examine for astrocyte phenotype (S100A10, thrombospondin-1/2).

- Construction of the ART mouse expressing the red fluorescent protein tdTomato has been completed and validated using immunohistochemistry and microscopy. Currently these mice are continuing to be bred to achieve enough numbers to be used in studies as outlined in Year 2 of the research proposal.

Specific Aim 1c will test the hypothesis that astrocyte mediated lactate transport is important in exercise-induced synaptogenesis. For these studies we have designed shRNA viral vector to selectively knock-down MCT-4 expression in astrocytes within the dSTR. Behavioral analysis will be conducted to examine recovery of motor and cognition. Molecular analysis will be used to quantitate synaptogenesis using IHC and Golgi. We will also test whether knock-down of MCT-4 leads to decreased expression of GLUT-1, and LDHa using qRT-PCR and WIB in the PFC and dSTR.

- Construction of the shRNA vector to knockdown MCT4 expression has been constructed and validated in both in vitro (astrocyte cell cultures) and in vivo (injections into the mouse striatum).

- Studies have been carried out addressing Aim 1B where ACT mice have been administered L-lactate and the activation of genes of interest involve in metabolism and neurotrophic factor expression have been evaluated. These studies have been complemented with in vitro studies in astrocyte cultures. A manuscript describing these outcome measures is currently in review.

Specific Aim 2a will test the hypothesis that exercise leads to the activation of anti-inflammatory microglia in the STR and PFC. This Aim will utilize FACS analysis phenotypically identify and examine functional capacity as well as identifying infiltrating cells derived from peripheral blood.

- Mice to be used in this study have been constructed and validated.

- We have validated the FACS approach to be used in these studies. This Aim will be carried out in Year 2.

Specific Aim 2b will test the hypothesis that peripheral monocyte infiltration to the STR and PFC may regulate exercise-induced synaptogenesis and behavioral recovery. To test this hypothesis, we will block peripheral monocyte infiltration using Natalizumab, an inhibitor of integrin $\alpha 4\beta 1$. We will use Golgi staining for dendritic spine density and IHC for markers of synaptogenesis (PSD95, synaptophysin) at the termination of the exercise intervention. Analysis will be conducted in the STR and PFC. We will conduct behavioral analysis of motor and cognitive function at completion of exercise.

- We have established and validated the 6-OHDA lesioning of mice for this aim. Studies are underway for Year 2 to determine infiltration of peripheral monocytes to he striatum and to determine if blocking the integrin receptor will block exercise-enhanced uptake to the striatum.

Specific Aim 2c will test the hypothesis that an increased level of serum anti-inflammatory (IL-10, TGFβ, and BDNF) vs. pro-inflammatory cytokines (TNFα, IL-1β, IL-6, and IL-2) is associated with higher levels of exercise intensity (average total METS/hr./week) and fitness levels (motor and/or cardiovascular) over an 18-month period in PD subjects. We will also examine whether increase level of serum anti-inflammatory vs. pro-inflammatory cytokines are associated with higher cognitive (executive function, EF) function at baseline, 9 and 18 months of follow up.

- Addendum to IRB (PI: Dr. G. M. Petzinger, MD) to conduct blood collection and analysis of samples outlined in Specific Aim 2.

- Blood Samples are being analyzed for the presence of immune markers at the early time point (baseline) and we have completed the analysis of 46 samples (baseline) 20 samples (9 months) and 14 samples (18 months). Data are currently undergoing analyses and statistical validation.

3.2. Opportunities for Training and Professional Development Provided by Project

This project has provided the following opportunities for training and development.

- Research electives for 5 undergraduate students
- Components of this project and data collection will be part of the doctoral thesis work of 3 USC doctoral students in the USC Neuroscience Graduate Program

3.3. Results Disseminated to Communities of Interest

Findings from this research study have been disseminated to the scientific research community through published manuscript (listed). In addition, findings on the impact of exercise eon brain health are used as a

foundation for describing these studies and their translation to the medical and patient community at seminars for patients and support groups.

3.4. Plans During the Next Reporting Period

In Year 2 we will:

- Continue with the glucose uptake mapping in lesioned and non-lesioned mice with and without exercise to identify regions of greatest activity.
- Utilizer FACS to identify genes and proteins in astrocytes whose expression is altered with exercise and 6-OHDA-lesioning.
- Determine the impact of administration of L-lactate on gene and protein expression in our rodent model of PD.
- Determine if blocking lactate transport leads to the attenuation of exercise-enhanced benefits in our mouse model of PD.
- Continue to examine the alterations in infiltrating monocytes observed with exercise in the brain of our mouse model of PD.
- Continue to collect blood from patients with PD to conduct analysis of immune components and correlate them with disease and fitness levels.

4. IMPACT

This application has immediate and long-term clinical and scientific impact. Studies from this application will (i) elucidate the role of glia in mediating exercise-induced neuroplasticity in PD and its models, (ii) support that changes in neuronal metabolism in conjunction with activation of astrocytes and microglia support improved synaptogenesis, leading to improved motor and cognitive behavior, and (iii) demonstrate how small energetic molecules like glucose and lactate in conjunction with components of the peripheral immune system (monocytes) link region-specific neuronal activation in the brain with non-neuronal cells (glia) at sites of circuitry activation. Understanding the mechanisms of exercise-induced neuroplasticity are critical to the development of strategies to treat patients suffering from degenerative brain disorders such as PD. Indeed, our studies in both animal models of PD and in patients with PD have led to widespread adoption of exercise and physical therapy as standard of care. The immediate impact of the studies in this application will shed additional mechanistic light on the benefits of exercise to reveal region specificity, allowing refinement of neurological physical therapy approaches. The long-term clinical impact will provide a framework for future clinical studies to determine if exercise (i) can modify disease progression, (ii) can impact immune components to promote synaptogenesis and restoration of motor and cognitive circuits, and (iii) whether benefits can be enhanced by including additional components of a healthy lifestyle, including diet, mindfulness, and stress management. Finally, it is possible that the data will reveal potential for the addition of supplemental pharmacological interventions designed to target astrocytes, microglia and components of the peripheral immune system), and interventions that modify metabolism.

Scientific Impact: Animal research over the past decade has shown that exercise and the way it is performed matters to neuro-rehabilitative outcomes, with changes in neuronal sprouting, restructuring of synapses and angiogenesis dependent. The current animal study provides a framework for understanding exercise-induced mechanisms of neuroplasticity at the regional level by examining synaptogenesis and metabolism and their influence on dopaminergic neurotransmission. An exciting aspect of this application is that it begins to investigate underlying mechanisms of exercise in animal models of PD and introduces astrocytes and microglia as important players in these processes including their impact on neuronal circuitry. Studies from this application will (i) elucidate the role of glia in mediating exercise-induced neuroplasticity in PD and its models, (ii) support that changes in neuronal metabolism in conjunction with activation of astrocytes and microglia support improved synaptogenesis leading to improved motor and cognitive behavior, and (iii) demonstrate how small energetic molecules like glucose and lactate in conjunction with components of the peripheral immune system (monocytes) link region-specific neuronal activation in the brain with non-neuronal cells (glia) at sites of circuitry activation. While the majority of the proposed studies are in young male animals, future studies can be designed to explore the impact of aging and sex in mediating the benefits of exercise in animal models. Also, benefits of exercise seen in our PD models may also show benefits in other models of disease and serve as an avenue to investigate these same phenomena in other human neurodegenerative disorders. Studies outlined in this application will begin to tease apart more specifically how non-neuronal components are impacted by

exercise may be driving differential biological changes in brain circuitry, and in doing so also provides needed insights toward biomarkers that may be critical for future clinical studies to monitor exercise benefits.

Clinical Impact on Patients and Health Care Performance: The proposed application has the potential to lead to improvements in the efficacy of care for individuals with cognitive and motor impairment in PD by more specifically identifying mechanisms underlying and impacting the exercise prescription. This application examines exercise in a novel way by recognizing critical gaps that once addressed will greatly improve the efficiency of health care delivery such as (i) defining the patient characteristics (immune health, diet) that will be directly impacted by exercise; (ii) establishing the specific molecular and metabolic characteristics that are critical for improving and evaluating the impact and benefits of exercise in patients with PD, and (iv) may provide a biomarker for disease progression and its modification. Understanding the mechanisms of exercise-induced neuroplasticity is critical to further develop important therapeutic modalities for patients suffering from degenerative brain disorders such as PD. Studies from our labs over the past 16 years in both animal models of PD and in patients suffering from PD have led to the wide-spread application of exercise and physical therapy as a component of the current standard of care. Improved quality of life with improved cognitive performance will reduce falls, reduce the burden on healthcare providers, and certainly reduce the economic burden. Findings from this application can be leveraged to begin to apply exercise as a viable evidence-based -treatment to modify other disorders of cognitive impairment and/or deficits in EF, including Alzheimer's disease, Huntington disease, schizophrenia, and traumatic brain injury. Studies in this application will provide important evidence-based data to allow neurologists and general internists to be able to prescribe a more precise form of exercise that targets cognition. Currently, physical therapy and exercise are not standard of care, and therefore not supported by most insurance policies. With information from this study, patients will be more empowered to take control of their personal treatment. The knowledge of a non-pharmacological and low-risk intervention falls within each individual's ability to control. Knowing they can truly impact their quality of life and disease progression, this will provide patients with a much-needed sense of self-empowerment and hope.

4.1. Impact on the Development of the Principal Disciplines of the Project

Studies in this research program are all underway. There are no technical or logistic issues to impede it progress. Findings from this program will demonstrate the important link between glia (astrocytes and microglia) and exercise-enhanced neuroplasticity in a rodent model of Parkinson's disease. We intend to demonstrate the important role played by astrocytes to regulate neuroplasticity especially through the transport of L-lactate that can act both as a metabolic substrate and a signaling molecular to strengthen synaptogenesis. We also aim to link microglia and peripheral monocytes as mediators of the immune response in playing a role in enhancing synaptogenesis and repair of neuronal circuits damaged in Parkinson's disease. The outcome measures of synaptic repair are demonstrated by recovery of both cognitive and motor behaviors in our models.

4.2. Impact on Other Disciplines

As pointed out in the Impact statements in this report the findings from this research program will impact our understanding of a wide spectrum of fields including neuroscience, physical therapy, disease progression in Parkinson's disease, and if such approaches can be implicated to alter disease progression. These studies will continue to implicate the importance of immunology in brain function as well as bringing together neuroscience, immunology, physical therapy, and clinical care.

4.3. Impact on Technology Transfer

Nothing to Report

4.4. Impact on Society Beyond Science and Technology

Findings in this research program will help guide our understanding of the role of exercise and physical therapy in treating neurodegenerative disorders including PD. For example, evidence medicine based on our outcome measures will provide additional support to guide clinicians, caregivers, and patients in the utility of exercise as an essential component of the first line of treatment and standard of care. It will also provide rationale for pharmaceutical and biotechnology companies to identify novel important therapeutic targets to enhance our findings and to find approaches for patients for which exercise may be challenging or difficult.

5. CHANGES / PROBLEMS

5.1. Changes in approach

Nothing to Report

5.2. Actual or Anticipated problems or delays and actions or plans to resolve

Due to COVID-19 outbreak the USC campus was closed to research personnel from March 13 to June 10. However, during this time all personnel were able to continue their responsibilities as outlined in the proposal. Breeding was allowed to continue such that there would be no loss of mice dedicated to these studies. However, some mice subjected to 6-OHDA lesioning just prior to the shutdown did not enter studies upon completion. We were able to utilize mice at 3 months post-lesion and match them to aged controls. The lab was allowed to reopen at 50% occupancy June 10^{th,} and this allowed proposed studies to commence. With careful planning and dedication of all researchers in this proposal we do not anticipate a significant delay other than possibly 3 or 4 months in the timeline. During this period, we were able to write and submit several manuscript supported by this application.

5.3. Changes that had a significant impact on Expenditures

Nothing to Report

5.4. Significant Changes in Use or Care of Human Subject, Vertebrate animal, Biohazards, or select Agents. (Outlined in the following sections)

5.4.1. Significant Changes in Use or Care of Human Subjects.

Nothing to Report

5.4.2. Significant Changes in Use or Care of Vertebrate animals.

Nothing to Report

5.4.3. Significant Changes in Biohazards.

Nothing to Report

5.4.4. Significant Changes in Select Agents.

Nothing to Report

6. PRODUCTS

6.1. Journal Publications

Lundquist, A.J., J. Parizher, G.M. Petzinger, and M.W. Jakowec, *Exercise induces region-specific remodeling of astrocyte morphology and reactive astrocyte gene expression patterns in male mice.* J Neurosci Res, 2019. **97**(9): p. 1081-1094.

Lundquist, A. J., T. J. Gallagher, G. M. Petzinger, and **M. W. Jakowec** (2020) Administration of L-Lactate to mice acts as a mimetic replicating exercise-enhanced changes in astrocytes. Submitted to Journal of Neuroscience Research. In Review

Wang, Z., I. Flores, E. K. Donahue, A. J. Lundquist, Y. Guo, G. M. Petzinger, **M. W. Jakowec**, and D. P. Holschneider (2020) Cognitive Flexibility Deficits in Rats with Dorsomedial Striatal 6-OHDA Lesions Tested Using a 3-Choice Serial Reaction Time Task with Reversal Learning. NeuroReport PMID: 32881776.

Caldwell, C. C, G. M. Petzinger, **M. W. Jakowec**, and E. Cadenas (2019) Treadmill Exercise Rescues Mitochondrial Function and Motor Behavior in a CAG_{140} Knock-In Advanced Huntington's Disease Mouse

Model. Chem Biol Interact. 2019 Nov 26; 315:108907. doi: 10.1016/j.cbi.2019.108907. [Epub ahead of print] PMID: 31778667

6.2. Conferences and Presentations

Nothing to report

6.3. Technologies or Techniques

Nothing to Report

6.4. Inventions, Patent Application, Licenses

Nothing to Report

6.5. Other Products

Nothing to Report

7. PARTICIPANTS & OTHER COLLABORATING ORGANIZATIONS

7.1. Individuals that Worked on the Project

Name: Michael Jakowec, Ph.D.
Project Role: PI
Research Identifier: N/A
Nearest person month worked: 2.4 Mo
Contribution to the project: No change. Project design, directing molecular, histology, and neuroanatomic studies.

Name: Daniel P. Holschneider, MD
Project Role: partnering co-I
Research Identifier: N/A
Nearest person month worked: 2.0 Mo
Contribution to the project: No change. Project design, project management, directing functional brain mapping studies, data analysis.

Name: Brett Lund, PhD
Project Role: co-I
Research Identifier: N/A
Nearest person month worked: 2.16 Mo
Contribution to the project: No change. Project design, project management, directing immune components, data analysis.

Name: Zhuo Wang, Ph.D.
Project Role: co-I
Research Identifier: N/A
Nearest person month worked: 4.2 Mo
Contribution to the project: No change. Stereotaxic lesioning, directing operant studies, functional brain mapping, data analysis.

Name: Giselle M. Petzinger, MD
Project Role: co-I
Research Identifier: N/A

Nearest person month worked: 0.36 Mo
Contribution to the project: No change. Project design, data analysis, interpretations, alternative approaches.

Name: Yumei Guo, MS
Project Role: Staff
Research Identifier: N/A
Nearest person month worked: 7.0 Mo
Contribution to the project: No change. Skilled and nonskilled exercising of animals, immunohistochemical staining (tyrosine hydroxylase).

Name: Adam Lundquist, BS
Project Role: Graduate Student
Research Identifier:
Nearest person month worked: 5.0 Mo
Contribution to the project: Western blotting, qRT-PCR, brain dissection, data analysis

Name: Erin Donahue, BS
Project Role: Graduate Student
Research Identifier:
Nearest person month worked: 5.0 Mo
Contribution to the project: Blood analysis, Animal behavior, Western blotting, qRT-PCR, brain dissection, data analysis

Name: Ilse Flores, BS
Project Role: Graduate student
Research Identifier:
Nearest person month worked: 1.5 Mo
Contribution to the project: immunohistochemistry, Golgi staining, sucrose preference testing, brain dissection

Name: Enrique Cadenas, Ph.D.
Project Role: Collaborator
Research Identifier: N/A
Nearest person month worked: 0.12 Mo
Contribution to the project: No change. Advisement on interpretation of molecular biologic studies

Name: Wendy Gilmore, Ph.D.
Project Role: Collaborator
Research Identifier: N/A
Nearest person month worked: 0.12 Mo
Contribution to the project: No change. Advisement on interpretation of immune studies

Name: Josh Nieman, Ph.D.
Project Role: Collaborator
Research Identifier: N/A
Nearest person month worked: 0.24 Mo
Contribution to the project: No change. Advisement on interpretation of immune studies

7.2. Changes in Active Support for PI or Senior Key Personnel

Nothing to Report regarding Key Personnel.

Note: The Graduate Student Ilse Flores was replaced by graduate student Adam Lundquist June 26, 2020.

7.3. Other Organizations Involved as Partners

Nothing to Report

8. SPECIAL REPORTING REQUIREMENTS

None

9. APPENDICES

Manuscripts in pdf Format

Chemico-Biological Interactions 315 (2020) 108907

Contents lists available at ScienceDirect

Chemico-Biological Interactions

journal homepage: www.elsevier.com/locate/chembioint

Treadmill exercise rescues mitochondrial function and motor behavior in the CAG_{140} knock-in mouse model of Huntington's disease

Charles C. Caldwell[a], Giselle M. Petzinger[b,c], Michael W. Jakowec[b,c,**], Enrique Cadenas[a,*]

[a] Pharmacology & Pharmaceutical Sciences, School of Pharmacy, University of Southern California, Los Angeles, CA, 90089, USA
[b] Department of Neurology, Keck School of Medicine, University of Southern California, Los Angeles, CA, 91007, USA
[c] Division of Biokinesiology and Physical Therapy, University of Southern California, Los Angeles, CA, 91107, USA

ARTICLE INFO

Keywords:
Huntington's disease
Long-term exercise training
Nitric oxide
Transglutaminase
Mitochondrial function
Metabolism
Neuroenergetics
Rotarod
Aconitase

ABSTRACT

Background: Huntington's disease (HD) is an autosomal dominant neurodegenerative disorder caused by polyglutamine (CAG) expansion in the Huntingtin (*HTT*) gene. The CAG_{140} knock-in (KI) mouse model recapitulates the progression of motor symptoms emerging at 12 months of age.
Objective: This study was aimed at assessing the effects of exercise, in the form of treadmill running, and examining its impact on motor behavior and markers of metabolism in the CAG_{140} KI mouse model of HD after motor symptoms have emerged.
Methods: CAG_{140} KI mice at 13–15 months of age were subjected to treadmill exercise 3 days per week for 1 h per day or remained sedentary. After 12 weeks of exercise brain tissues were analyzed for enzymatic activity including mitochondria Complexes I, II/III, and IV, transglutaminase, aconitase, pyruvate dehydrogenase, and phosphofructokinase1/2. In addition, the concentration was determined for nitrate/nitrite, pyruvate carboxylase, NAD^+/NADH, and glutamate as well as the ratio of mitochondria and nuclear DNA. Motor behavior was tested using the rotarod.
Results: Exercise resulted in increased [nitrite + nitrate] levels (surmised as nitric oxide), reduced transglutaminase activity, increased aconitase activity with increased tricarboxylic acid-generated reducing equivalents and mitochondrial oxidative phosphorylation complexes activity. Mitochondrial function was strengthened by increases in glycolysis, pyruvate dehydrogenase activity, and anaplerosis component represented by pyruvate carboxylase.
Conclusions: These changes in mitochondrial function were associated with improved motor performance on the rotarod test. These findings suggest that exercise may have beneficial effects on motor behavior by reversing deficits in mitochondrial function in a rodent model of HD.

1. Introduction

Huntington's disease (HD) is an autosomal dominant neurodegenerative disease that impacts 1 in 10,000 people. Patients phenotypically are characterized by progressive decline in cognitive and motor functions with neuropsychiatric disturbances leading ultimately to premature death 15–20 years after the onset of motor symptoms [1]. The disease is defined genetically by an excessive polyglutamine (CAG) expansion in the Huntingtin (*HTT*) gene on exon 1 of chromosome 4 resulting in a mutated form of the huntingtin (HTT) protein [2].

Therapeutic strategies for attenuating or reversing the progression of HD are still under development. Mounting evidence supports that cardiovascular exercise (physical activity) is associated with reduced risk of neurodegenerative diseases such as Alzheimer's disease and Parkinson's disease [3,4]. The application of exercise and its impact on neurodegenerative disorders over a lifetime is speculated to act in a neuroprotective fashion blocking the onset of disease including its genetic and toxicant initiators. Factors of lifestyle may also provide resilience, where cognitive and motor reserves in some individuals may fend off disease over their lifetime. On the other hand, mechanisms of resilience may be different than those engaged in either the prodromal or early stages of disease and may impact disease by modifying

Abbreviations: HD, Huntington's disease; NAD, nicotinamide adenine dinucleotide; NO, nitric oxidase; PC, pyruvate carboxylase; PFK1/2, phosphofructokinase 1/2; PDH, pyruvate dehydrogenase complex; TCA, tricarboxylic acid cycle; TG, transglutaminase

* Corresponding author. Pharmacology & Pharmaceutical Sciences, School of Pharmacy, University of Southern California, Los Angeles, CA, 90089.
** Corresponding author. Department of Neurology, Keck School of Medicine, University of Southern California, Los Angeles, CA, 91107.
E-mail addresses: Michael.Jakowec@med.usc.edu (M.W. Jakowec), cadenas@usc.edu (E. Cadenas).

https://doi.org/10.1016/j.cbi.2019.108907
Received 31 October 2019; Received in revised form 14 November 2019; Accepted 25 November 2019
Available online 26 November 2019
0009-2797/

progression in terms of severity, time course, and symptomology. Animal models of human neurological disorders provide an opportunity to investigate the impact of interventions such as exercise and begin to identify underlying mechanisms, both within the central nervous system (CNS) and the periphery, that may serve as novel therapeutic targets to treat patients.

A number of key molecules including nitric oxide (NO) play an important role in a variety of signal transduction pathways that are crucial for maintaining the physiologic functions of vascular, respiratory, immune, muscular, and nervous systems. Within the CNS, NO plays a major role in the regulation of cerebral blood flow and local brain metabolism, gene expression, memory function including receptor trafficking, neuroendocrine secretion, and synaptic plasticity [5]. While exercise has a wide spectrum of pleiotropic effects involving many biochemical targets, it is known to elevate levels of NO in the body especially muscle [6] as well as within the CNS [7,8]. Neuronal nitric oxide synthase (nNOS) activity and nNOS protein expression are reduced in HD possibly contributing to symptom progression in both animal models [9,10] and in patients [11]. Such findings suggest that the decrease in NO is a major contributing factor to HD-related cell death by a variety of mechanisms including excitotoxicity, the generation of reactive oxygen species (ROS), and activation of developmental cell death programs such as apoptosis [11]. Reversing the loss of NO activity may be neuroprotective as well as providing a means to restore or enhance functions compromised in disease. For example, several deficiencies of mitochondrial complex activities within the electron transport chain have been observed in preclinical and clinical HD [12–14]. Increased production of NO could be beneficial in mitochondrial enzymatic interactions. Specifically, NO donors at a linear rate could inactive tissue transglutaminase (TG), a mitochondrial protein that plays a critical role in mitochondrial homeostasis including the control of mitophagy and bioenergetics, shown to be elevated in HD [15]. The inactive TG can no longer use aconitase as a substrate and thus, preserve its function in the TCA cycle as a generator of reducing equivalents such as NADH. This improvement is seen downstream in the mitochondrial OXPHOS complex activity with increases in complexes I, II/III, and IV.

The purpose of this study was to explore a potential mechanisms by which chronic exercise impacts the metabolic and bioenergetic profile of aged HD mice focusing on mechanisms centered on the enhanced levels of brain [nitrite + nitrate] (surmised as NO) caused by exercise that results in changes in the metabolic profile elicited by initial modifications including TG activity. For these studies, we utilized the HD CAG_{140} Knock In (KI) mouse model which is characterized by 140 CAG repeats in exon 1 of the mouse huntingtin gene ortholog (hdh) and has been reported to demonstrate a protracted prodromal phase with motor features presenting after 12 months of age [16]. The CAG_{140} KI mouse is a model for investigating the mechanisms of exercise-induced NO production on disease modification and evaluating the functional outcomes linked to biochemical markers of brain bioenergetics. The impact of these metabolic changes was examined as a functional outcome that entails motor behavior in the rotarod test. Few studies have investigated the effects of exercise on HD models and even fewer have addressed the impact on aged HD animals [17,18].

2. Materials and Methods

2.1. Mice

For these studies we used knock-in mice that contained a chimeric mouse/human exon 1 with 140 CAG repeats inserted into the mouse gene by homologous targeting [16]. The CAG_{140} KI mice were maintained in-house using lines descended from heterozygous pairing. The founder mice for the colony were a gift of Drs. Michael Levine and Carlos Cepeda (UCLA) with permission from Dr. Scott Zeitlin (University of Virginia) through a Material Transfer Agreement. Mice were backcrossed onto the C57BL/6J background annually to maintain vigor. Mouse genotypes from tail biopsies were determined using PCR (Transnetyx, Inc., Cordova, TN). The protracted prodromal phase with motor features is present in the HD CAG_{140} KI mouse model after 12 months of age. The CAG140 KI mouse line has a life expectancy of about 2 years. Mice 13–15 months of age were used and represent moderate to advanced HD. Mice were randomly assigned to one of 2 groups (i) CAG_{140}KI, $n = 8$ (3 males and 5 females) and (ii) CAG_{140}KI + exercise, $n = 8$ (3 males and 5 females). No differences between males and females HD mice have been reported; hence groups were collapsed for analysis. Mice were group housed with a reverse light cycle (lights off from 7 a.m. to 7 p.m.) and were allowed access to food (rodent chow manufactured by Purina Inc.) and water *ad libitum*. Experimental procedures were approved by the University of Southern California's Institutional Animal Care and Use Committee (IACUC) and conducted in accordance with the National Research Council Guide for the Care and Use of Laboratory Animals (DHEW Publication 80–23, 2011, Office of Laboratory Animal Welfare, DRR/NIH, Bethesda, MD). All efforts were made to minimize animal suffering and to reduce the number of animals used to achieve statistical significance.

2.2. Exercise regimen

Treadmill running was initiated in CAG_{140} KI mice at 13–15 months of age, performed on a Model EXER-6M Motorized Treadmill (Columbus Instruments, Columbus, Ohio). The treadmill exercise protocol was conducted based on previous publications with modifications [19,20]. Briefly, on day 1 of week 1, mice in the exercise group ran at a speed of 8.0 ± 0.5 m/min for 40 min and closely monitored for any adverse reaction to the treadmill, inability to run, or failure to learn the task. Exercise continued at a velocity of 10.0 ± 1.5 m/min 3 times per week for a 12-week period. Treadmill speed was gradually increased to 20 ± 1.5 m/min by the final month. A non-noxious stimulus (metal beaded curtain) was used as a tactile incentive to prevent animals from drifting back on the treadmill. All mice were weighed at the end of each week and closely assessed for adverse reactions including stress; there were no abnormalities in weight. Treadmill running is not stressful based on the evaluation of anxiety, depression, and corticosterone levels [21]. All mice tolerated the exercise regimen, with no dropouts.

2.3. Rotarod test for motor behavior

Behavioral testing was carried out after completion of the exercise regimen and consisted of motor performance using the accelerating rotarod. Outcome was measured by latency to fall (in seconds). Mice were given 10 min to acclimate to the behavior room environment on the day of the test. The rotarod was set to its base speed as mice were assigned to their respective lanes. At t = 0s, the rotarod began the acceleration phase reaching peak velocity at t = 24 s before decelerating. At t = 48 s, the rotarod switched directions and repeated the cycle. Endpoint criteria for the rotarod test were: (i) mouse falling off the cylinder onto the platform; (ii) mouse completing three revolutions via clutching onto the cylinder pad; or (iii) mouse showing any signs of pain or distress. For criteria 1 and 2, the time was recorded, and the mouse was given a rest period of 5 min with access to food and water. This was repeated for a total of 6 trials. For criteria 3, the mouse would be removed from the study completely. No mice were removed from the rotarod test. For each mouse, times for the first two trials were removed so rotarod data would accurately reflect the ability to perform the test. The average time across trials was calculated for each mouse. A two-factor ANOVA with replication was performed to determine significance.

2.4. Mitochondrial isolation and mitochondrial complex activities

For all subsequent analyses whole brain was utilized. Briefly, mice

were quickly decapitated, and brain removed fresh while kept cold on wet ice. The forebrain, excluding the cerebellum, was isolated and utilized for subsequent enzymatic and mitochondrial analyses. Brain mitochondria was isolated by a Percoll gradient as previously described [22]. The resulting mitochondrial samples were used immediately or stored at −80 °C for later protein and enzymatic assays. During mitochondrial purification, aliquots were collected and evaluated for confirmation of mitochondrial purity and integrity. Isolated brain mitochondria were plated in Abcam Mitoscience complex activity assays. Complex I activity was expressed as $OD\lambda_{450nm}$ as NADH oxidation (ab109721), Complex II/III was expressed as $OD\lambda_{550nm}$ as cytochrome C reduction (ab109905), and complex IV as $OD\lambda_{550nm}$ as cytochrome *c* oxidation (ab109911).

2.5. Enzyme activities

Transglutaminase activity was measured using the Abcam Transglutaminase Activity Assay Kit (ab204700) measured colorimetrically at 525 nm. The limit of quantification of this assay is ~10 μU in cell/tissue lysates. Aconitase activity was measured using the Cayman Aconitase Assay Kit (cat. N° 705502); the reactions were monitored by measuring the increase in absorbance at 340 nm associated with the formation of NADH proportional to aconitase activity. Pyruvate Dehydrogenase (PDH) activity was measured in whole brain homogenate by the Abcam PDH enzyme activity microplate assay (ab109902), which captures fully functional PDH. Activity is determined by the rate of reduction of NAD^+ to NADH linked to a reporter dye that can be detected at 450 nm. The Abcam phosphofructokinase Activity (PFK) assay kit (ab155898) measured PFK1 and PFK2 and activities were measured in whole brain homogenates and the color product detected at 450 nm.

Nitrate and nitrite concentration was measured in brain homogenates with the Cayman Chemical Nitrate/Nitrite Assay Kit (cat. N° 780001) and photometric measurement of the absorbance due to the azochromophore corresponding to nitrate concentration. Pyruvate carboxylase (PC) concentration was measured using the Cloud-Clone Corp. PC immunosorbent assay kit (Product serial# 6ECC39CD3D). Color product was measured at 450 nm. NAD^+ and NADH concentration was measured using NAD/NADH Assay Kit (ab65348) which measures intracellular nucleotides NAD^+, NADH, and their ratio. Glutamate concentration was measured in whole brain and isolated brain mitochondria using the Abcam Glutamate Assay ELISA Kit (ab83389) that recognizes glutamate as a specific substrate forming a color product at 450 nm.

Mitochondrial biogenesis was expressed as the ratio of COXII/gamma-Globin corresponding to mitochondrial (mtDNA) and nuclear DNA (nDNA), respectively. Primers were developed by Integrated DNA Technologies. Primer sequences (5′-3′) COXII F:GCCGACTAAATCAAG CAACA R:CAATGGGCATAAA GCTATGG gamma-Globin; F:GAAG CGA TTCTAGGGAGCAG R:GGAG CAGCGATTCTGAGTAGA.

2.6. Activities of c-JUN N-Terminal kinase (JNK) and serine/threonine kinase Akt

JNK activity was measured in whole brain homogenates using the Abcam JNK1/2 (pT183/Y185) +Total JNK1/2 ELISA kit (abcam176662) following the manufacturer's instructions. The kit employs an affinity tag labeled capture antibody coated in the wells of the plate. A reporter conjugated detector antibody immunocaptures the analytes within the sample and a stop solution generates a signal detected at 450 nm. Activity was determined by the ratio of Phospho~JNK/JNK. AKT activity was measured in whole brain homogenate using the Abcam AKT1/2/3 (pS473) + AKT Total ELISA kit (abcam176657) following the manufacturer's instructions. The kit employs an affinity tag labeled capture antibody coated in the wells of the plate and a reporter conjugated detector antibody that immunocaptures the analyte within the sample and stop solution generating a signal detected at 450 nm. Activity was determined by the ratio of Phospho~AKT/AKT.

2.7. Data analysis

Data are reported as means ± SEM of at least three experimental replicates. Group size (*n*) is eight unless otherwise stated for specific method. Statistical significance between means was determined by Student's two-tailed *t*-test of paired data. The level of statistical significance is indicated in the respective figures ($*p < 0.05$, $**p < 0.01$). Two-way ANOVA between the sedentary group and exercised group of HD mice was used for the rotarod test. Post-hoc analysis using Student-Neuman Keuls with statistical significance considered if $p < 0.05$.

3. Results

3.1. Exercise generated markers of nitric oxide

We found that exercise increased [NO_2^- + NO_3^-] levels (surmised as NO) in the brain by 48% when compared to the sedentary group (Fig. 1A). Total nitrite and nitrate [NO_2^- + NO_3^-] were measured in brain homogenates of the HD mouse model in both the sedentary group (483 ± 110 μM) and the exercise group (714 ± 32 μM) ($p < 0.05$).

3.2. Exercise decreases transglutaminase (TG) activity

Since NO inhibits TG cross-linking activity by S-nitrosylation of Cys^{277} in the catalytic core of the enzyme, we examined TG expression in HD mice with and without exercise [23]. We found that TG activity in isolated brain mitochondria was decreased 52% in the exercise group (0.399 ± 0.087 μmol/min/mg protein) compared to the sedentary group (0.800 ± 0.141 μmol/min/mg protein) ($p < 0.05$) (Fig. 1B). TG activity in whole brain homogenates of the sedentary (0.240 ± 0.024 μmol/min/mg protein) and exercise (0.184 ± 0.011 μmol/min/mg protein) groups, showed a decrease of approximately 24%, which did not reach statistical significance, probably because the effect was diluted by other cellular proteins since the majority of TG activity resides within mitochondria [24]. Since TG protein level and activity are highly expressed in liver [25] we examined the systemic effects of exercise. We found that TG activity was also decreased with exercise (1.241 ± 0.091 μmol/min/mg protein) compared to the sedentary (2.622 ± 0.442 μmol/min/mg protein) group ($p < 0.05$).

3.3. Aconitase activity and TCA reducing equivalents

Since aconitase is a substrate for TG and has been shown to be altered in HD, we examined if changes in TG expression and activity also resulted in changes in aconitase activity [24]. We found that exercise increased brain mitochondrial aconitase activity by 22% comparing the sedentary group (13.92 ± 0.78 μmol/min/mg protein) with the exercise group (17.02 ± 1.05 μmol/min/mg protein) ($p < 0.05$) (Fig. 1C). This suggests that the decrease in TG activity observed in brain and liver has minimized the crosslinking with aconitase thereby rescuing aconitase activity.

Several steps in the TCA cycle generate the reduced form of nicotinamide adenine dinucleotide (NADH) that serves as a reducing agent to donate electrons in oxidative phosphorylation. We found that NAD^+ was increased 6-fold in the exercise group (0.710 ± 0.187 μM) compared to the sedentary group (0.117 ± 0.0729 μM) ($p < 0.05$) (Fig. 1D). NADH levels also increased by 22% in the exercise group but this did not reach statistical significance: sedentary (1.918 ± 0.297 μM) versus exercise (2.330 ± 0.051 μM) (Fig. 1D). The significant increase in NAD^+ suggests a higher rate of NADH

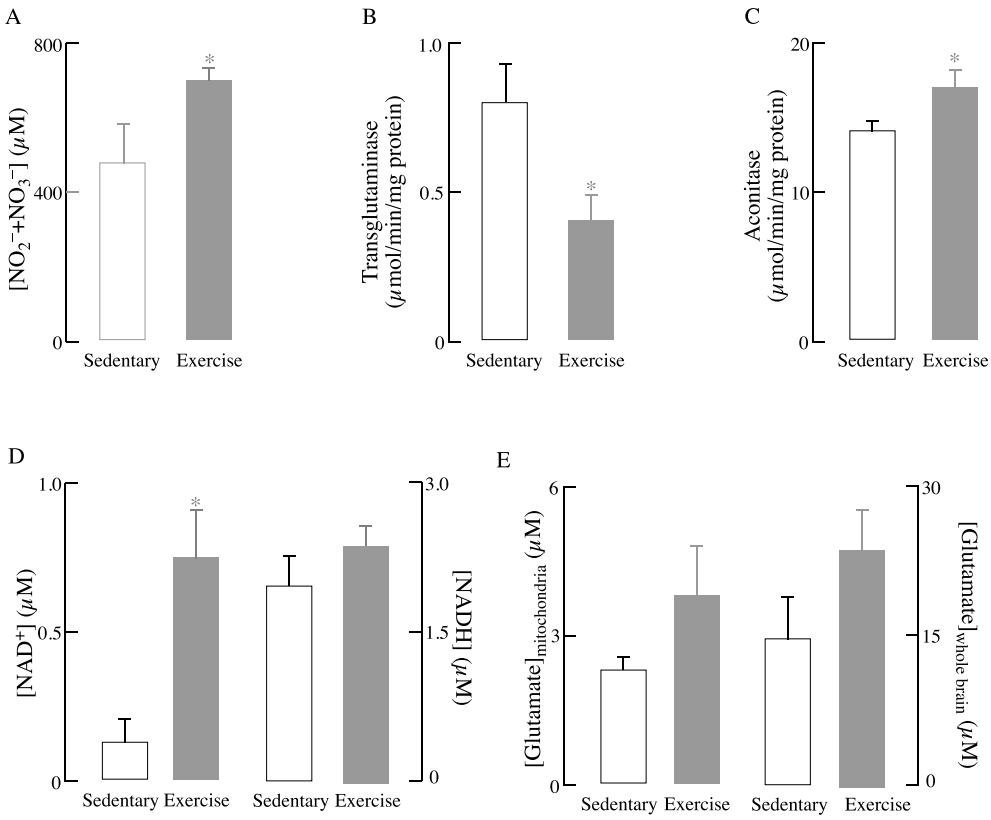

Fig. 1. *Effect of Treadmill Exercise on Metabolic Parameters*. (A) [NO_2^- + NO_3^-] levels were measured in the whole brain homogenate of the HD mouse model. (B) Transglutaminase activity was measured in isolated brain mitochondria. (C) Aconitase activity was measured in isolated brain mitochondria. (D) NAD^+ and NADH concentrations. (E) Glutamate levels in mitochondria and whole brain homogenate. Experimental conditions as described in the Materials and Methods section. $n = 8$; *$p < 0.05$.

utilization due to enhanced mitochondrial complex activities (see below and Fig. 2A–C).

The neurotransmitter glutamate is generated from α-ketoglutarate in the TCA cycle, and its impaired production and transport have been documented in HD [26]. We found that glutamate levels measured in whole brain homogenates increased 60% (sedentary (17.7 ± 4.9 μM) versus exercise (28.4 ± 4.9 μM)) and in isolated brain mitochondria increased 68% (sedentary (2.25 ± 0.25 μM) versus exercise (3.78 ± 1.07 μM)) (Fig. 1E), but did not reach statistical significance.

3.4. Mitochondrial complex activities

Since an increase in NAD + levels can be linked to increased mitochondrial complex activity, we determined the effect of exercise on the activity of Complexes I, II/III and IV (Fig. 1D) relative to sedentary mice: Complex I increased 41% (Fig. 2A) (sedentary (1.93 ± 0.14 mOD/min/mg protein) versus exercise (2.725 ± 0.20 mOD/min/mg protein) ($p < 0.01$); Complexes II/III increased 31% (Fig. 2B) (sedentary (1.24 ± 0.25 mOD/min/mg protein) versus exercise (1.62 ± 0.24 mOD/min/mg protein) ($p < 0.05$), and Complex IV increased 58% (Fig. 2C) (sedentary (1.11 ± 0.07 mOD/min/mg protein) versus exercise (1.77 ± 0.23 mOD/min/mg protein) ($p < 0.01$). The increased flow of reducing equivalents across the complexes suggests a higher rate of energy production in the form of proton gradient generated ATP.

The potential contribution of mitochondrial biogenesis was assessed by examining the mtDNA/nDNA ratio. While there was a trend for increased ratio with exercise (Fig. 2D): sedentary ($2.20 \pm 0.573 \times 10^{-4}$) versus exercise ($3.03 \pm 0.815 \times 10^{-4}$), this did not reach statistical significance.

3.5. Glycolysis regulation and upstream fuel production for TCA

Phosphofructokinase (PFK) is the key regulator of glycolysis leading to pyruvate formation in the cytosol and its further mitochondrial metabolism upon oxidative decarboxylation by the pyruvate dehydrogenase complex. This is consistent with previous reports on NO augmenting glycolysis in astrocytes through activation of PFK2 [27]. Total PFK activity (combination of PFK1 and PFK2), converting fructose-6-phosphate to fructose-(1/2),6-diphosphate was increased by 17% in the exercise group (3.486 ± 0.131 μmol/min/mg protein) as compared to sedentary (2.98 ± 0.135 μmol/min/mg protein) ($p < 0.05$) (Fig. 3A).

The pyruvate dehydrogenase (PDH) complex converts pyruvate to acetyl-CoA through oxidative decarboxylation allowing it to react with oxaloacetate to form citrate in the TCA cycle. We found that PDH complex activity was increased by 18% in the exercise (3.68 ± 0.104 μmol/min/mg protein) group versus sedentary (3.12 ± 0.227 μmol/min/mg protein) group ($p < 0.01$) (Fig. 3B).

Pyruvate carboxylase (PC) converts pyruvate to oxaloacetate, the acceptor of acetyl-CoA in the TCA cycle. Pyruvate carboxylase is expressed in astrocytes, and astrocytes are the sole *de novo* synthesizers of glutamate from glucose in the CNS [28]. Exercise increased pyruvate carboxylase concentration by 64% (4.16 ± 0.23 ng/mg protein) compared to sedentary (2.53 ± 0.19 ng/mg protein) ($p < 0.05$) (Fig. 3C).

3.6. JNK and Akt activity

Insulin signaling plays a pivotal role in peripheral tissues and the CNS where it participates in neuronal survival, synaptic plasticity, memory, and learning [29,30]. Insulin signaling is regulated by the stress-responsive Jun-N-terminal kinase (JNK) and both signaling processes interact to regulate metabolic homeostasis. The Akt pathway mediates some of the effects of insulin signaling in brain. Akt activity was increased by 22% in the exercise group expressed as the ratio of phospho~Akt/Akt; (sedentary 0.045 ± 0.0032, exercise 0.055 ± 0.0016), p < 0.05 (Fig. 4A), whereas JNK activity was decreased by 27% in the exercise group measured as a ratio phospho~JNK/JNK; (sedentary 2.93 ± 0.24, exercise 2.13 ± 0.19),

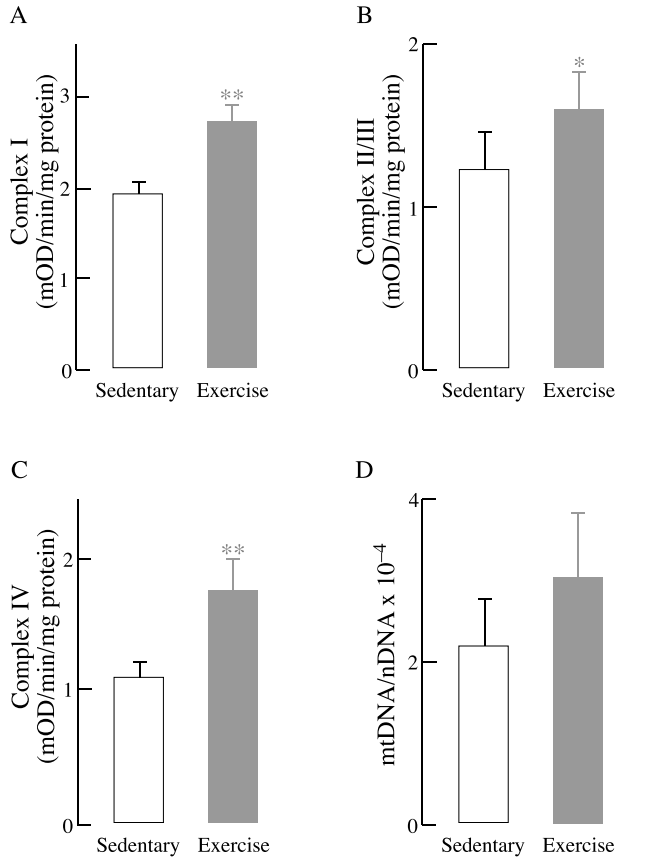

Fig. 2. *Effect of Treadmill Exercise on Mitochondrial Electron Transfer Complexes and Mitochondrial Biogenesis.* (A) Complex I; (B) Complex II/III; (C) Complex IV; (D) mitochondrial biogenesis expressed as mtDNA/nDNA values. Experimental conditions as described in the Materials and Methods section. $n = 8$; $^{*}p < 0.05$, $^{**}p < 0.01$.

$p < 0.05$ (Fig. 4B). Hence, exercise results in stimulation of the Akt pathway of insulin signaling and inhibition of the JNK pathway (Fig. 4C).

3.7. Motor behavior on the rotarod

The motor behavior in HD mice was evaluated on the accelerating rotarod using latency to fall (expressed as seconds, s). Exercise (37.0 ± 8.6 s) significantly improved latency to fall in HD mice by 73% compared to the sedentary (21.3 ± 3.5 s) ($p < 0.05$) group (Fig. 5).

4. Discussion

Exercise, incorporating components of skill and aerobic, is emerging as an important component of the standard of care in a number of neurological disorders including PD and mild cognitive impairment (MCI) [31,32]. In HD a small number of clinical trials in patients have demonstrated feasibility and some mild but transient symptomatic improvement [33,34]. We have previously shown that exercise, in the form of intensive treadmill running, initiated during the prodromal phase of disease (at 2–6 months of age) in the CAG_{140} KI mouse model modifies disease progression manifesting in improvement in a number of behaviors including anxiety, depression, and motor [20]. In addition, the time course of the emergence of HTT protein aggregate pathology was attenuate. Others have also reported the beneficial effects of exercise in rodent models of HD [35–37]. Reports of early lifestyle behaviors that incorporate physical activity may impact disease progression in humans by delaying or altering the onset of symptoms [38–40]. Despite encouraging findings, the underlying mechanisms by which exercise may impact disease progression and symptomology remain unknown, especially in neurodegenerative disorders such as HD.

In both the pre-symptomatic and symptomatic phases of HD there is evidence of deficits in neuroenergetics including mitochondrial dysfunction manifesting in a reduction in ATP production, excessive generation of ROS, and failure to efficiently buffer calcium [41]. Impairment in mitochondrial function can have devastating impact on neuronal function especially in synaptic neurotransmission, circuit connectivity, and the maintenance of neuroenergetic homeostasis. It is becoming evident that synaptic dysfunction manifests early in disease and progresses during the prodromal phase, years before typical motor behaviors of HD emerge [42,43]. Deficits in energy metabolism may in fact precede neuropathology and the loss of cells observed at autopsy [44].

The purpose of this study was to explore the potential impact of exercise, in the form of intensive running on a motorized treadmill, on markers of HD disease in a progressive mouse model at an age when typical motor symptoms emerge. In the CAG_{140} KI mouse model, motor symptoms begin to manifest at 12–14 months of age and slowly progress, thus allowing a window of opportunity by which an intervention, such as exercise, can be applied. While the potential molecular targets in energy production are numerous and complex, we focused on specific markers of metabolism and mitochondrial function known to be impacted in HD. In these studies we focused on NO due to its key role in regulating metabolism and the facts it is known to be dysfunctional in HD [11] and its expression be elevated through exercise [8,45].

We summarize graphically our working model based on our findings in the HD mouse model in Fig. 6. Exercise leads to the generation of NO, which is stored as nitrosothiols and entails Akt activation of eNOS as a major mechanism [46–48]. One function of NO is to inhibit TG cross-

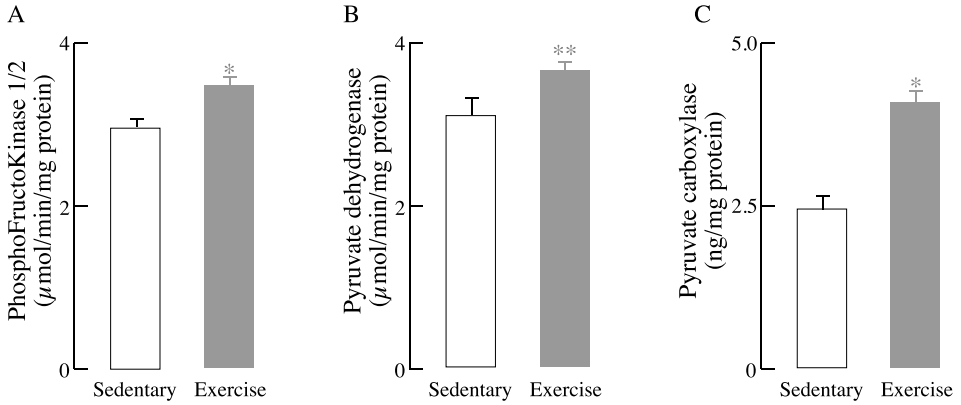

Fig. 3. *Effect of Exercise on Glucose and Pyruvate Metabolism.* (A) PFK1/2 activity; (B) Pyruvate dehydrogenase (PDH) activity. (C) Pyruvate carboxylase content. Experimental conditions as described in the Materials and Methods section. $n = 8$; $^{*}p < 0.05$, $^{**}p < 0.01$.

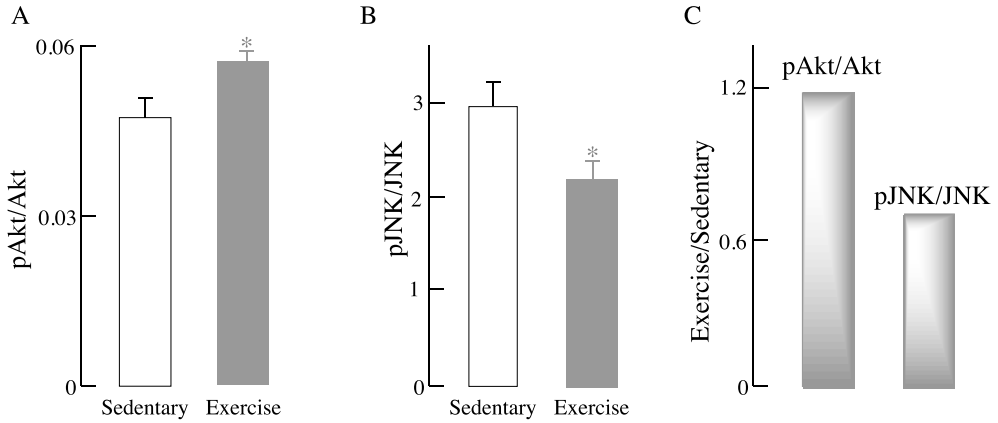

Fig. 4. *Effect of Exercise on Akt and JNK Expression.* Experimental conditions as described in the Materials and Methods section. $n = 8$; $^{*}p < 0.05$, $^{**}p < 0.01$.

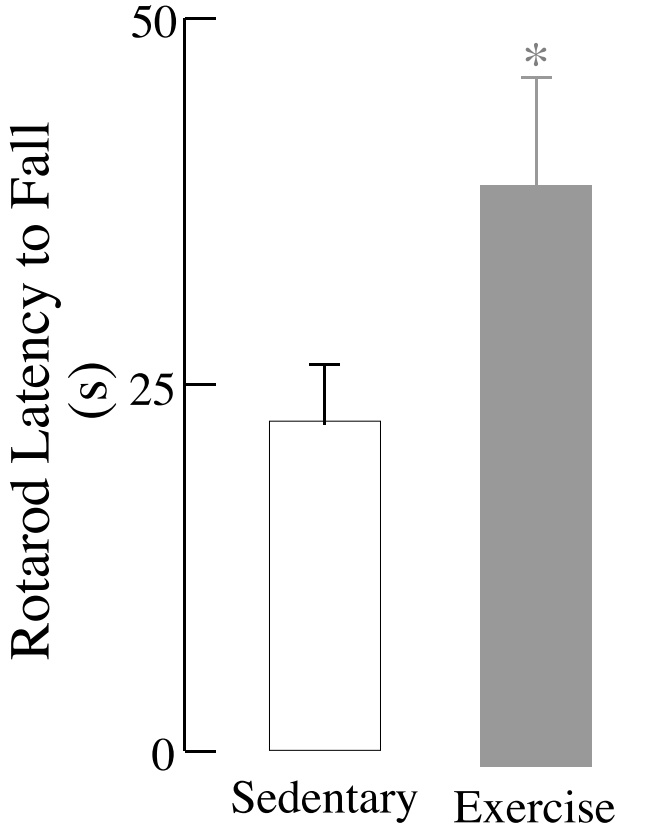

Fig. 5. *Motor Behavior as Assessed by Rotarod Test.* Rotarod latency to fall, expressed in sec. Behavioral testing as described in the Materials and Methods section. $n = 8$; $^{*}p < 0.05$.

linking activity by S-nitrosylation of Cys_{277} in the catalytic core of the enzyme [23]. Typically, TG catalyzes Ca^{2+}-dependent protein deamidation, transamidation, and cross-linking activities through addition of the ϵ-amino group of a lysyl residue to the carboxamide moiety of a glutaminyl residues to form an isopeptide bond (cross-link) and ammonia [49,50]. The majority of TG-driven cross-linking occurs in mitochondria [23,51]. TG activity has been shown to be elevated while aconitase activity is decreased in pre-clinical rodent models and CSF and postmortem brain samples of HD patients [52–55] and is involved in the pathogenesis of mitochondrial dysfunction in HD due to the formation of high molecular weight aggregates of aconitase through these cross-linking reactions [50,56]. Although a complete understanding of why TG activity is elevated in HD and other neurodegenerative diseases is unknown, several mechanisms have been proposed [24,57,58]. TG may promote protein aggregates resulting in the generation of amyloid plaques in AD, nuclear inclusions in HD, and Lewy bodies in PD that may enhance cytotoxicity in this disorder [24,58–60]. Additionally, TG may sensitize cells to apoptosis thus promoting cell death [25,61]. Evidence supporting the role of TG in HD originates from a TG knockout R6/1 HD mouse model that reported reduction in neuronal death, improved behavior, and prolonged survival [62]. In our studies, we observed decreased TG activity in brain mitochondria with exercise in HD mice. We also observed a systemic effect of exercise with decreased TG activity in the liver; however, the impact of such changes on CNS targets has yet to be established.

Aconitase catalyzes the isomerization of citrate to isocitrate in the TCA cycle. The aberrant activity of TG in HD is associated with mitochondrial dysfunction, in part due to aconitase inactivation by cross-linking [24]. Currently, it is unclear whether aconitase acts as an acyl acceptor, donor, or both, and unclear as to which mitochondrial proteins aconitase is bound as second substrates including itself. The increase of brain $[NO_2^- + NO_3^-]$ following treadmill training supports the notion that the observed decrease in brain mitochondrial TG activity is potentially a consequence of its inhibition by increased NO, thus preventing its crosslinking inactivation of aconitase. It is unlikely that peroxynitrite [63] or superoxide anion [64] are involved in aconitase inhibition because they elicit an irreversible inactivation of the iron-sulfur cluster upon loss of labile iron in the enzyme [65]. Thus, the likely mechanism is that exercise induces an inverse relationship in which aconitase activity is preserved through NO inactivation of TG in brain mitochondria. Exercise significantly improved aconitase activity in the HD mouse model, which impacted downstream levels of reducing equivalents (i.e. NADH and NAD^+). These data confirm earlier reports of inhibition of TG subjected to a NO flow from a NO-donor such as S-nitroso-N-acetylpenicillamine (SNAP) [15].

The preservation of aconitase activity further improves the generation of reducing equivalents in the TCA cycle. NAD^+ was significantly increased while NADH was not in exercised HD mice, which was interpreted as the kinetic control exerted by the high electron flow through respiratory complexes I, II/III, and IV. Although deficiencies of all mitochondrial complexes have been reported in preclinical and clinical HD, the majority of these are seen in complex II and III [12–14,54,56]. However, the effect of exercise seems to affect complexes I to IV of the respiratory chain. The neurotransmitter glutamate has also been associated with metabolic dysfunction in HD [66], albeit the substantial increase elicited by exercise was not statistically significant. Supporting a high formation of reducing equivalents in the TCA cycle are (i) faster glycolysis by conversion of glucose to pyruvate upon increased PFK1/2 activity; (ii) increased delivery of acetyl-CoA to the cycle upon increased PDH activity; and (iii) an increased anaplerotic mechanism sustained by way of pyruvate carboxylase levels. PFK and PDH as well as glucose uptake and GLUT transporter

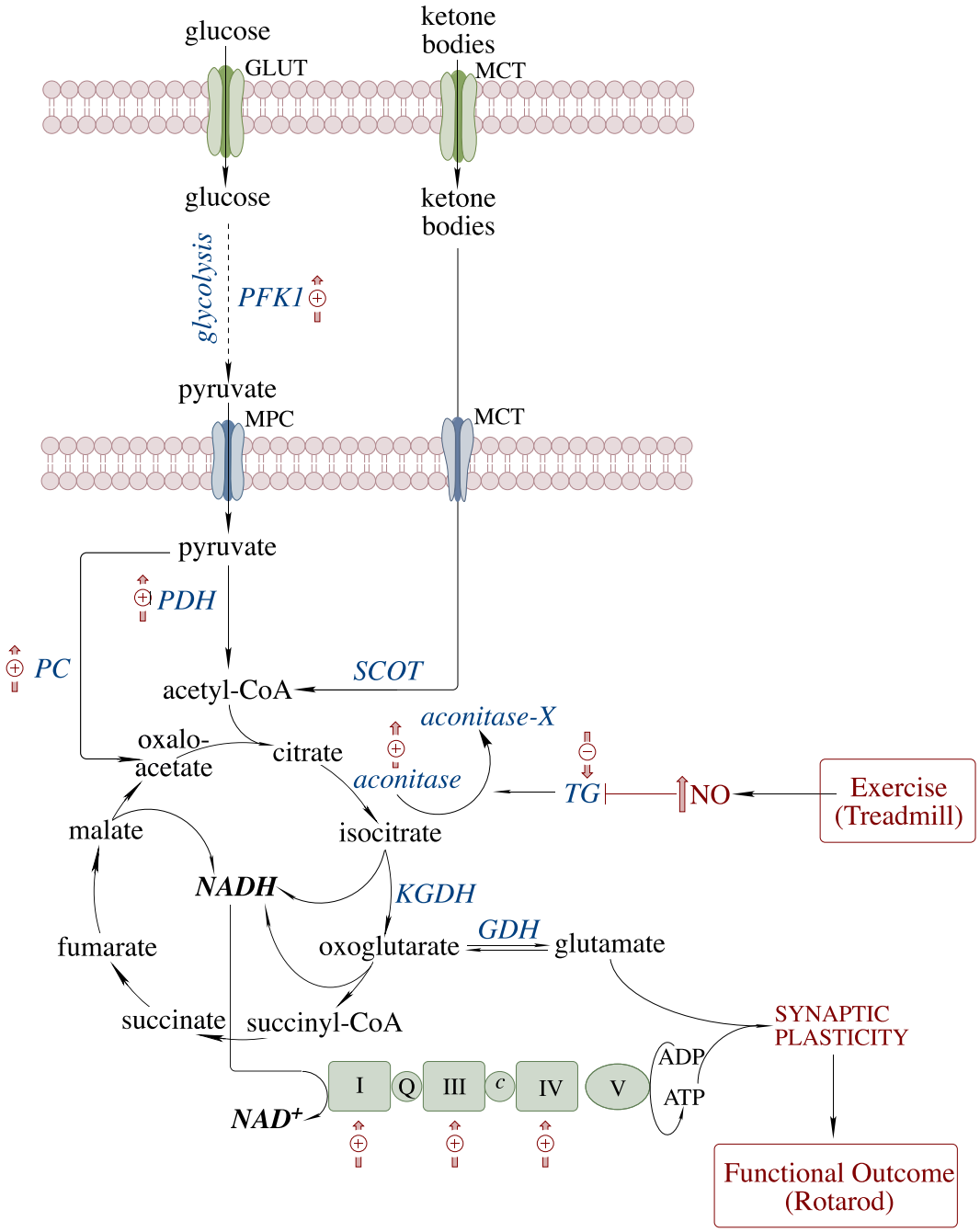

Fig. 6. *Effects of Treadmill Exercise on Metabolic Parameters.* The figure summarizes the findings in this study. Positive effects of treadmill training (resulting in brain [NO_2^- + NO_3^-] are indicated by a (+) arrow. Inhibition by a (−) arrow. MPC, mitochondrial pyruvate carrier; MCT, monocarboxylate transporter; PFK1/2, phosphofructokinase 1 and 2. PDH, pyruvate dehydrogenase; SCOT, succinyl-CoA transferase; TG, transglutaminase.

expression are impaired in HD human brain in caudate, putamen, and globus pallidus and in the striatum of R6/2 HD mouse model [54].

It is well-established that exercise impacts positively glucose transporter expression and insulin signaling through phosphorylation of Akt in skeletal muscle [67,68]. Akt insulin signaling facilitates the translocation of GLUT 3/4 in brain to the plasma membrane, promotes glycolysis, and enhances mitochondrial function through Akt translocation into mitochondria [69]. Insulin signaling plays a pivotal role not only in peripheral tissues, but also the CNS where it participates in neuronal survival, synaptic plasticity, memory and learning [29,30]. Insulin signaling is also regulated by the stress-responsive Jun-N-terminal kinase (JNK) and both signaling processes interact to regulate metabolic homeostasis. Findings from this study showed that Akt activity was increased and JNK activity was decreased with exercise. These data may confirm previous reports that endogenous NO negatively regulates JNK activation by S-nitrosylation [70]. Likewise, the significance of Akt/JNK homeostasis in brain aging and HD has been reported [71–73].

There are some limitations of these studies. Whole brain homogenates were used for analysis due to limitations in the number of aged HD mice, thus not allowing delineation of changes in metabolic markers in either a circuit specific or cell specific manner. For example, we found that pyruvate carboxylase (PC), which converts pyruvate to oxaloacetate, the acceptor of acetyl-CoA in the TCA cycle is elevated with exercise. Pyruvate carboxylase is expressed in astrocytes, and astrocytes are the sole *de novo* synthesizers of glutamate from glucose in the CNS

[28]. Astrocytes may also be playing other roles as a consequence of exercise including metabolism and synaptogenesis as we have recently demonstrated through treadmill running in mice [74]. While we examined motor behavior in these studies to show the benefits of exercise, we have not yet experimentally linked NO with behavioral outcomes. Future studies blocking or enhancing NO expression will address this issue.

In conclusion, our findings support the beneficial effects of exercise in a rodent model of HD even during the period of onset of motor symptoms. We summarize a working model for the findings in our study as shown in Fig. 6. This metabolic platform entailing NO-derived inhibition of TG activity and concomitant rescue of aconitase activity, increase in glycolysis and mitochondrial oxidative metabolism, that impinge and modulate energy metabolism. These pathways attempt to provide mechanistic insights between the initial input (treadmill exercise) and the functional outcome (improved motor behavior on the rotarod) mediated by the increase in brain NO [NO_2^- + NO_3^-]. While the impact of exercise may target a wide spectrum of molecular components, a limited number of targets such as NO may prove pivotal in mediating a cascade of effects including pathophysiology and energy metabolism all potentially impacting synaptic connectivity. The goal is to identify these critical components and to develop optimal interventions targeting both pharmacological therapeutic modalities as well as the parameters of exercise that are most effective. The increased expression and activity of protein deacetylases, sirtuins, are well-established consequences of physical exercise [75–78]. Although sirtuins affect several cellular pathways, their involvement as drivers of mitochondrial biogenesis is a salient feature: sirtuin activity and AMPK are required to activate the co-activator of mitochondrial biogenesis, PGC1α, which, in turn induces the expression of several transcription factors engaged in mitochondrial biogenesis [79]. Although we cannot rule out an involvement of sirtuins in this study, the mDNA/nDNA values shown in Fig. 2D (reflecting mitochondrial biogenesis) were not statistically significant, thus tempering sirtuin involvement in the beneficial effects of exercise reported here.

Author statement

Charles Caldwell: Investigation, Methodology, Validation, Resources, Formal analysis.

Giselle Petzinger: Formal analysis.

Michael Jakowec: Conceptualization, Writing – review & editing.

Enrique Cadenas: Conceptualization, supervision, project administration, writing, review & editing.

Declaration of competing interest

The authors declare that they have no known competing financial interests or personal relationships that could have appeared to influence the work reported in this paper.

Acknowledgements

We would like to acknowledge the support of the U.S. Army NETRP (Grant N° W81XWH18-1-0666), the Confidence Foundation, and the Plotkin Family Foundation. A special thanks to Friends of the USC Parkinson's Disease Research Group including George and Mary Lou Boone, Walter and Susan Doniger, Anthony McLaren and the Climb Above Parkinson's, and the family of Don Gonzalez Barrera.

Appendix A. Supplementary data

Supplementary data to this article can be found online at https://doi.org/10.1016/j.cbi.2019.108907.

References

[1] F.O. Walker, Huntington's disease, Lancet 369 (2007) 218–228.
[2] P. McColgan, S.J. Tabrizi, Huntington's disease: a clinical review, Eur. J. Neurol. 25 (2018) 24–34.
[3] H. Ohman, N. Savikko, T.E. Strandberg, H. Kautiainen, M.M. Raivio, M.L. Laakkonen, et al., Effects of exercise on cognition: the Finnish Alzheimer disease exercise trial: a randomized, controlled trial, J. Am. Geriatr. Soc. 64 (2016) 731–738.
[4] H. Chen, S.M. Zhang, M.A. Schwarzschild, M.A. Hernan, A. Ascherio, Physical activity and the risk of Parkinson disease, Neurology 64 (2005) 664–669.
[5] A. Philippu, Nitric oxide: a universal modulator of brain function, Curr. Med. Chem. 23 (2016) 2643–2652.
[6] B.A. Kingwell, Nitric oxide as a metabolic regulator during exercise: effects of training in health and disease, Clin. Exp. Pharmacol. Physiol. 27 (2000) 239–250.
[7] A. Pietrelli, J.J. Lopez-Costa, R. Goni, E.M. Lopez, A. Brusco, N. Basso, Effects of moderate and chronic exercise on the nitrergic system and behavioral parameters in rats, Brain Res. 1389 (2011) 71–82.
[8] M.J. Chen, A.S. Ivy, A.A. Russo-Neustadt, Nitric oxide synthesis is required for exercise-induced increases in hippocampal BDNF and phosphatidylinositol 3' kinase expression, Brain Res. Bull. 68 (2006) 257–268.
[9] F.E. Padovan-Neto, L. Jurkowski, C. Murray, G.E. Stutzmann, M. Kwan, A. Ghavami, et al., Age- and sex-related changes in cortical and striatal nitric oxide synthase in the Q175 mouse model of Huntington's disease, Nitric Oxide 83 (2019) 40–50.
[10] F. Perez-Severiano, B. Escalante, P. Vergara, C. Rios, J. Segovia, Age-dependent changes in nitric oxide synthase activity and protein expression in striata of mice transgenic for the Huntington's disease mutation, Brain Res. 951 (2002) 36–42.
[11] A.W. Deckel, Nitric oxide and nitric oxide synthase in Huntington's disease, J. Neurosci. Res. 64 (2001) 99–107.
[12] S.E. Browne, A.C. Bowling, U. MacGarvey, M.J. Baik, S.C. Berger, M.M. Muqit, et al., Oxidative damage and metabolic dysfunction in Huntington's disease: selective vulnerability of the basal ganglia, Ann. Neurol. 41 (1997) 646–653.
[13] M. Gu, M.T. Gash, V.M. Mann, F. Javoy-Agid, J.M. Cooper, A.H. Schapira, Mitochondrial defect in Huntington's disease caudate nucleus, Ann. Neurol. 39 (1996) 385–389.
[14] A. Johri, A. Chandra, M.F. Beal, PGC-1alpha, mitochondrial dysfunction, and Huntington's disease, Free Radic. Biol. Med. 62 (2013) 37–46.
[15] F. Bernassola, A. Rossi, G. Melino, Regulation of transglutaminases by nitric oxide, Ann. N. Y. Acad. Sci. 887 (1999) 83–91.
[16] L.B. Menalled, J.D. Sison, I. Dragatsis, S. Zeitlin, M.F. Chesselet, Time course of early motor and neuropathological anomalies in a knock-in mouse model of Huntington's disease with 140 CAG repeats, J. Comp. Neurol. 465 (2003) 11–26.
[17] C. Cepeda, D.M. Cummings, M.A. Hickey, M. Kleiman-Weiner, J.Y. Chen, J.B. Watson, et al., Rescuing the corticostriatal synaptic disconnection in the R6/2 mouse model of Huntington's disease: exercise, adenosine receptors and ampakines, PLoS Curr. 2 (2010) RRN1182.
[18] E.A. Herbst, G.P. Holloway, Exercise training normalizes mitochondrial respiratory capacity within the striatum of the R6/1 model of Huntington's disease, Neuroscience 303 (2015) 515–523.
[19] B.E. Fisher, G.M. Petzinger, K. Nixon, E. Hogg, S. Bremmer, C.K. Meshul, et al., Exercise-induced behavioral recovery and neuroplasticity in the 1-methyl-4-phenyl-1,2,3,6-tetrahydropyridine-lesioned mouse basal ganglia, J. Neurosci. Res. 77 (2004) 378–390.
[20] D.P. Stefanko, V.D. Shah, W.K. Yamasaki, G.M. Petzinger, M.W. Jakowec, Treadmill exercise delays the onset of non-motor behaviors and striatal pathology in the CAG140 knock-in mouse model of Huntington's disease, Neurobiol. Dis. 105 (2017) 15–32.
[21] L.M. Gorton, M.G. Vuckovic, N. Vertelkina, G.M. Petzinger, M.W. Jakowec, R.I. Wood, Exercise effects on motor and affective behavior and catecholamine neurochemistry in the MPTP-lesioned mouse, Behav. Brain Res. 213 (2010) 253–262.
[22] R.W. Irwin, J. Yao, R.T. Hamilton, E. Cadenas, R.D. Brinton, J. Nilsen, Progesterone and estrogen regulate oxidative metabolism in brain mitochondria, Endocrinology 149 (2008) 3167–3175.
[23] S.K. Jandu, A.K. Webb, A. Pak, B. Sevinc, D. Nyhan, A.M. Belkin, et al., Nitric oxide regulates tissue transglutaminase localization and function in the vasculature, Amino Acids 44 (2013) 261–269.
[24] S.Y. Kim, L. Marekov, P. Bubber, S.E. Browne, I. Stavrovskaya, J. Lee, et al., Mitochondrial aconitase is a transglutaminase 2 substrate: transglutamination is a probable mechanism contributing to high-molecular-weight aggregates of aconitase and loss of aconitase activity in Huntington disease brain, Neurochem. Res. 30 (2005) 1245–1255.
[25] M. Piacentini, M. D'Eletto, M.G. Farrace, C. Rodolfo, F. Del Nonno, G. Ippolito, et al., Characterization of distinct sub-cellular location of transglutaminase type II: changes in intracellular distribution in physiological and pathological states, Cell Tissue Res. 358 (2014) 793–805.
[26] G.V. Rebec, Corticostriatal network dysfunction in Huntington's disease: deficits in neural processing, glutamate transport, and ascorbate release, CNS Neurosci. Ther. 24 (2018) 281–291.
[27] A. Almeida, S. Moncada, J.P. Bolanos, Nitric oxide switches on glycolysis through the AMP protein kinase and 6-phosphofructo-2-kinase pathway, Nat. Cell Biol. 6 (2004) 45–51.
[28] A. Verkhratsky, M. Nedergaard, Physiology of astroglia, Physiol. Rev. 98 (2018) 239–389.

[29] S. Craft, G.S. Watson, Insulin and neurodegenerative disease: shared and specific mechanisms, Lancet Neurol. 3 (2004) 169–178.
[30] L.P. van der Heide, G.M. Ramakers, M.P. Smidt, Insulin signaling in the central nervous system: learning to survive, Prog. Neurobiol. 79 (2006) 205–221.
[31] M.W. Jakowec, Z. Wang, D. Holschneider, J. Beeler, G.M. Petzinger, Engaging cognitive circuits to promote motor recovery in degenerative disorders. exercise as a learning modality, J. Hum. Kinet. 52 (2016) 35–51.
[32] G.M. Petzinger, B.E. Fisher, S. McEwen, J.A. Beeler, J.P. Walsh, M.W. Jakowec, Exercise-enhanced neuroplasticity targeting motor and cognitive circuitry in Parkinson's disease, Lancet Neurol. 12 (2013) 716–726.
[33] L. Quinn, K. Hamana, M. Kelson, H. Dawes, J. Collett, J. Townson, et al., A randomized, controlled trial of a multi-modal exercise intervention in Huntington's disease, Park. Relat. Disord. 31 (2016) 46–52.
[34] N. Fritz, A.K. Rao, D. Kegelmeyer, A. Kloos, M. Busse, L. Hartel, et al., Physical therapy and exercise interventions in Huntington's disease: a mixed methods systematic review, J. Huntingt. Dis. 6 (2017) 217–236.
[35] A. van Dellen, P.M. Cordery, T.L. Spires, C. Blakemore, A.J. Hannan, Wheel running from a juvenile age delays onset of specific motor deficits but does not alter protein aggregate density in a mouse model of Huntington's disease, BMC Neurosci. 9 (2008) 34.
[36] T. Renoir, T.Y. Pang, M.S. Zajac, G. Chan, X. Du, L. Leang, et al., Treatment of depressive-like behaviour in Huntington's disease mice by chronic sertraline and exercise, Br. J. Pharmacol. 165 (2012) 1375–1389.
[37] T.Y. Pang, N.C. Stam, J. Nithianantharajah, M.L. Howard, A.J. Hannan, Differential effects of voluntary physical exercise on behavioral and brain-derived neurotrophic factor expression deficits in Huntington's disease transgenic mice, Neuroscience 141 (2006) 569–584.
[38] T.M. Cruickshank, J.A. Thompson, D.J. Dominguez, A.P. Reyes, M. Bynevelt, N. Georgiou-Karistianis, et al., The effect of multidisciplinary rehabilitation on brain structure and cognition in Huntington's disease: an exploratory study, Brain Behav. 5 (2015) e00312.
[39] N. Georgiou, J.L. Bradshaw, E. Chiu, A. Tudor, L. O'Gorman, J.G. Phillips, Differential clinical and motor control function in a pair of monozygotic twins with Huntington's disease, Mov. Disord. 14 (1999) 320–325.
[40] S.M. Mueller, J.A. Petersen, H.H. Jung, Exercise in Huntington's Disease: Current State and Clinical Significance. Tremor and Other Hyperkinetic Movements (New York, NY), vol. 9, (2019), p. 601.
[41] F. Mochel, R.G. Haller, Energy deficit in Huntington disease: why it matters, J. Clin. Investig. 121 (2011) 493–499.
[42] A. Feigin, K.L. Leenders, J.R. Moeller, J. Missimer, G. Kuenig, P. Spetsieris, et al., Metabolic network abnormalities in early Huntington's disease: an [(18)F]FDG PET study, J. Nucl. Med. 42 (2001) 1591–1595.
[43] A.V. Panov, C.A. Gutekunst, B.R. Leavitt, M.R. Hayden, J.R. Burke, W.J. Strittmatter, et al., Early mitochondrial calcium defects in Huntington's disease are a direct effect of polyglutamines, Nat. Neurosci. 5 (2002) 731–736.
[44] C. Saft, J. Zange, J. Andrich, K. Muller, K. Lindenberg, B. Landwehrmeyer, et al., Mitochondrial impairment in patients and asymptomatic mutation carriers of Huntington's disease, Mov. Disord. 20 (2005) 674–679.
[45] A.C. Lacerda, U. Marubayashi, C.H. Balthazar, C.C. Coimbra, Evidence that brain nitric oxide inhibition increases metabolic cost of exercise, reducing running performance in rats, Neurosci. Lett. 393 (2006) 260–263.
[46] J.W. Calvert, M.E. Condit, J.P. Aragon, C.K. Nicholson, B.F. Moody, R.L. Hood, et al., Exercise protects against myocardial ischemia-reperfusion injury via stimulation of beta(3)-adrenergic receptors and increased nitric oxide signaling: role of nitrite and nitrosothiols, Circ. Res. 108 (2011) 1448–1458.
[47] B.A. Kingwell, G.L. Jennings, A.M. Dart, Exercise and endothelial function, Circulation 102 (2000) E179.
[48] F. Sessa, G. Messina, R. Russo, M. Salerno, C. Castruccio Castracani, A. Distefano, et al., Consequences on aging process and human wellness of generation of nitrogen and oxygen species during strenuous exercise, Aging Male (2018) 1–9.
[49] J.J. Gorman, J.E. Folk, Transglutaminase amine substrates for photochemical labeling and cleavable cross-linking of proteins, J. Biol. Chem. 255 (1980) 1175–1180.
[50] M.V. Nurminskaya, A.M. Belkin, Cellular functions of tissue transglutaminase, Int. Rev. Cell Mol. Biol. 294 (2012) 1–97.
[51] S. Altuntas, M. D'Eletto, F. Rossin, L. Diaz Hidalgo, M.G. Farrace, L. Falasca, et al., Transglutaminase type 2, mitochondria and Huntington's disease: menage a trois, Mitochondrion 19 (2014) 97–104.
[52] M.V. Karpuj, H. Garren, H. Slunt, D.L. Price, J. Gusella, M.W. Becher, et al., Transglutaminase aggregates huntingtin into nonamyloidogenic polymers, and its enzymatic activity increases in Huntington's disease brain nuclei, Proc. Natl. Acad. Sci. U. S. A. 96 (1999) 7388–7393.
[53] M. Lesort, W. Chun, G.V. Johnson, R.J. Ferrante, Tissue transglutaminase is increased in Huntington's disease brain, J. Neurochem. 73 (1999) 2018–2027.
[54] J.M. Dubinsky, Towards an understanding of energy impairment in Huntington's disease brain, J. Huntingt. Dis. 6 (2017) 267–302.
[55] T.M. Jeitner, W.R. Matson, J.E. Folk, J.P. Blass, A.J. Cooper, Increased levels of gamma-glutamylamines in Huntington disease CSF, J. Neurochem. 106 (2008) 37–44.
[56] C. Carmo, L. Naia, C. Lopes, A.C. Rego, Mitochondrial dysfunction in Huntington's disease, Adv. Exp. Med. Biol. 1049 (2018) 59–83.
[57] B.A. Citron, Z. Suo, K. SantaCruz, P.J. Davies, F. Qin, B.W. Festoff, Protein cross-linking, tissue transglutaminase, alternative splicing and neurodegeneration, Neurochem. Int. 40 (2002) 69–78.
[58] G.M. Zainelli, N.L. Dudek, C.A. Ross, S.Y. Kim, N.A. Muma, Mutant huntingtin protein: a substrate for transglutaminase 1, 2, and 3, J. Neuropathol. Exp. Neurol. 64 (2005) 58–65.
[59] W. Andre, I. Nondier, M. Valensi, F. Guillonneau, C. Federici, G. Hoffner, et al., Identification of brain substrates of transglutaminase by functional proteomics supports its role in neurodegenerative diseases, Neurobiol. Dis. 101 (2017) 40–58.
[60] H. Grosso, J.M. Woo, K.W. Lee, J.Y. Im, E. Masliah, E. Junn, et al., Transglutaminase 2 exacerbates alpha-synuclein toxicity in mice and yeast, FASEB J. 28 (2014) 4280–4291.
[61] Q. Ruan, R.A. Quintanilla, G.V. Johnson, Type 2 transglutaminase differentially modulates striatal cell death in the presence of wild type or mutant huntingtin, J. Neurochem. 102 (2007) 25–36.
[62] P.G. Mastroberardino, C. Iannicola, R. Nardacci, F. Bernassola, V. De Laurenzi, G. Melino, et al., 'Tissue' transglutaminase ablation reduces neuronal death and prolongs survival in a mouse model of Huntington's disease, Cell Death Differ. 9 (2002) 873–880.
[63] F. Schopfer, N. Riobo, M.C. Carreras, B. Alvarez, R. Radi, A. Boveris, et al., Oxidation of ubiquinol by peroxynitrite: implications for protection of mitochondria against nitrosative damage, Biochem. J. 349 (2000) 35–42.
[64] A. Hausladen, I. Fridovich, Superoxide and peroxynitrite inactivate aconitases, but nitric oxide does not, J. Biol. Chem. 269 (1994) 29405–29408.
[65] D. Han, R. Canali, J. Garcia, R. Aguilera, T.K. Gallaher, E. Cadenas, Sites and mechanisms of aconitase inactivation by peroxynitrite: modulation by citrate and glutathione, Biochemistry 44 (2005) 11986–11996.
[66] G.V. Rebec, Dysregulation of corticostriatal ascorbate release and glutamate uptake in transgenic models of Huntington's disease, Antioxidants Redox Signal. 19 (2013) 2115–2128.
[67] E.B. Arias, J. Kim, K. Funai, G.D. Cartee, Prior exercise increases phosphorylation of Akt substrate of 160 kDa (AS160) in rat skeletal muscle, Am. J. Physiol. Endocrinol. Metab. 292 (2007) E1191–E1200.
[68] M.D. Bruss, E.B. Arias, G.E. Lienhard, G.D. Cartee, Increased phosphorylation of Akt substrate of 160 kDa (AS160) in rat skeletal muscle in response to insulin or contractile activity, Diabetes 54 (2005) 41–50.
[69] X. Yin, M. Manczak, P.H. Reddy, Mitochondria-targeted molecules MitoQ and SS31 reduce mutant huntingtin-induced mitochondrial toxicity and synaptic damage in Huntington's disease, Hum. Mol. Genet. 25 (2016) 1739–1753.
[70] H.S. Park, S.H. Huh, M.S. Kim, S.H. Lee, E.J. Choi, Nitric oxide negatively regulates c-Jun N-terminal kinase/stress-activated protein kinase by means of S-nitrosylation, Proc. Natl. Acad. Sci. U. S. A. 97 (2000) 14382–14387.
[71] T. Jiang, F. Yin, J. Yao, R.D. Brinton, E. Cadenas, Lipoic acid restores age-associated impairment of brain energy metabolism through the modulation of Akt/JNK signaling and PGC1alpha transcriptional pathway, Aging Cell 12 (2013) 1021–1031.
[72] E. Colin, E. Regulier, V. Perrin, A. Durr, A. Brice, P. Aebischer, et al., Akt is altered in an animal model of Huntington's disease and in patients, Eur. J. Neurosci. 21 (2005) 1478–1488.
[73] F. Yin, A. Boveris, E. Cadenas, Mitochondrial energy metabolism and redox signaling in brain aging and neurodegeneration, Antioxidants Redox Signal. 20 (2014) 353–371.
[74] A.J. Lundquist, J. Parizher, G.M. Petzinger, M.W. Jakowec, Exercise induces region-specific remodeling of astrocyte morphology and reactive astrocyte gene expression patterns in male mice, J. Neurosci. Res. 97 (2019) 1081–1094.
[75] Z. Radak, Z. Zhao, E. Koltai, H. Ohno, M. Atalay, Oxygen consumption and usage during physical exercise: the balance between oxidative stress and ROS-dependent adaptive signaling, Antioxidants Redox Signal. 18 (2013) 1208–1246.
[76] K. Vargas-Ortiz, V. Pérez-Vázquez, M. Macías-Certantes, Exercise and sirtuins: a way to mitochondrial health in skeletal muscle, Int. J. Mol. Sci. 20 (2019) E2717.
[77] P. Kaliman, M. Párrizas, J.F. Lalanza, A. Camins, R.M. Escorihuela, M. Pallas, Neurophysiological and epigenetic effects of physical exercise on the aging process, Ageing Res. Rev. 10 (2011) 475–486.
[78] S. Bayod, J. del Valle, J.F. Lalanza, S. Sanchez-Roige, B. de Luxán-Delgado, A. Coto-Montes, A.M. Canudas, A. Camins, R.M. Escorihuela, M. Pallas, Long-term physical exercise induces changes in sirtuin 1 pathway and oxidative parameters in adult rat tissue, Exp. Gerontol. 47 (2012) 925–935 2012.
[79] M.N. Sack, T. Finkel, Mitochondrial metabolism, sirtuins, and aging, Cold Spring Harb Perspect. Biol. 4 (2012) a013102.

Cognitive flexibility deficits in rats with dorsomedial striatal 6-hydroxydopamine lesions tested using a three-choice serial reaction time task with reversal learning

Zhuo Wang[a], Ilse Flores[b], Erin K. Donahue[b], Adam J. Lundquist[b], Yumei Guo[a], Giselle M. Petzinger[b,c], Michael W. Jakowec[b,c] and Daniel P. Holschneider[a,b,c,d]

Lesions of the dorsomedial striatum elicit deficits in cognitive flexibility that are an early feature of Parkinson's disease (PD), and presumably reflect alterations in frontostriatal processing. The current study aimed to examine deficits in cognitive flexibility in rats with bilateral 6-hydroxydopamine lesions in the dorsomedial striatum. While deficits in cognitive flexibility have previously been examined in rodent PD models using the cross-maze, T-maze, and a food-digging task, the current study is the first to examine such deficits using a 3-choice serial reaction time task (3-CSRT) with reversal learning (3-CSRT-R). Although the rate of acquisition in 3-CSRT was slower in lesioned compared to control rats, lesioned animals were able to acquire a level of accuracy comparable to that of control animals following 4 weeks of training. In contrast, substantial and persistent deficits were apparent during the reversal learning phase. Our results demonstrate that deficits in cognitive flexibility can be robustly unmasked by reversal learning in the 3-CSRT-R paradigm, which can be a useful test for evaluating effects of dorsomedial striatal deafferentation and interventions. *NeuroReport* **31: 1055–1064**

NeuroReport 2020, **31**:1055–1064

Keywords: animal model, cognition, executive function, frontostriatal, mild cognitive impairment, operant learning, Parkinson's disease, striatum

[a]Department of Psychiatry and Behavioral Sciences, University of Southern California, [b]Graduate Program in Neurosciences, University of Southern California, Departments of [c]Neurology and [d]Biomedical Engineering, University of Southern California, Los Angeles, California, USA

Correspondence to Daniel P. Holschneider, MD, Department of Psychiatry and Behavioral Sciences, University of Southern California, 1975 Zonal Avenue, KAM 400, MC9037, Los Angeles, CA 90089-9037, USA
Tel: +1 323 442 1536; fax: +1 323 442 1587; e-mail: holschne@usc.edu

Received 15 May 2020 **Accepted** 22 June 2020

Introduction

Deficits in cognition, ranging from mild cognitive impairment (MCI) to dementia, are debilitating nonmotor symptoms in Parkinson's disease (PD) [1]. Prior even to the appearance of motor symptoms, patients may manifest an impairment of executive function. Executive dysfunction in PD can elicit deficits in attentional control, cognitive inhibition, inhibitory control, working memory, and cognitive flexibility, all of which can impair a patient's ability to plan, organize, initiate, and regulate goal-directed behavior. This can lead, even in early phases of the illness, to difficulty in multitasking, initiating new tasks, and switching tasks. While the etiology remains to be fully understood, the frontostriatal circuits, dopaminergic and cholinergic systems have been implicated in executive dysfunction [2].

Early diagnosis and intervention at the stage of MCI are believed to be critical for treatment. Animal models and behavioral tests that allow investigation of PD-related cognitive deficits are key to mechanistic research and preclinical testing of new treatments. However, studies in this area have been relatively few compared to research on motor deficits. A challenge is that cognitive tests in animals often rely on motor functions and motor impairment in many animal models of PD can therefore be a confound. Recent preclinical PD research using an animal model has explored the dorsomedial aspect of the striatum, a brain region associated with behavioral flexibility and cognitive switching [3]. Cognitive tests using touch screens that presumably require only limited locomotor activities have also been utilized with PD animal models [4].

The five-choice serial reaction time task (5-CSRT), modeled after clinical tests, has been broadly used to study operant learning, impulse control, and visual attention in rodents [5–7]. Tsutsui-Kimura *et al.* [8] reported a three-choice variation (3-CSRT) to shorten the training time for rats to reach learning criteria. The current study applied 3-CSRT with reversal learning (3-CSRT-R) to test cognitive flexibility in rats with 6-hydroxydopamine (6-OHDA) lesion to the bilateral dorsomedial striatum. Whereas past research has generally used lever press in the 5-CSRT, it has been shown that nose poke is an easier response to learn in rats [9]. We therefore chose nose poke, which has been used in more recent 5-CSRT studies [6,7]. In addition, sufficient time was allowed (stimulus duration) for completion of the nose poke choice. These choices were made to lower the task difficulty so

 DOI: 10.1097/WNR.0000000000001509

that lesioned animals could rapidly learn the task to a similar level as controls prior to the initiation of reversal learning in which a rule change required cognitive switching. Thereby, cognitive flexibility could be investigated largely in separation from other possible cognitive deficits in the initial ability to acquire operant learning, attention, and impulse control.

Methods

Animals

Experiments were conducted under a protocol approved by the Institutional Animal Care and Use Committee of the University of Southern California, an institution approved by the Association for Assessment and Accreditation of Laboratory Animal Care, as well as by the Animal Use and Care Review Office of the US Department of the Army, and in compliance with the National Institutes of Health Guide for the Care and Use of Laboratory Animals. Male Wistar rats were purchased from Envigo (Placentia, California, USA) at age 8–9 weeks. Animals were housed under standard vivaria conditions in pairs on a 12 h light/12 h dark cycle (dark cycle 6 p.m. to 6 a.m.). A total of 38 rats were used. The main cohort of animals underwent 3-CSRT-R operant training as shown in Fig. 1a (lesioned rats, n = 6; controls, n = 6). Some lesioned animals in this cohort were also evaluated in overnight locomotor activities (n = 4), rotarod running (n = 2), sucrose preference (n = 2), and tyrosine-hydroxylase (TH) immunostaining (n = 4). In addition, 26 animals (lesioned n = 15, controls n = 11) from a pilot study were used to examine the effects of lesion on overnight locomotor activity (n = 9 lesioned), rotarod running (n = 6 lesioned, n = 8 controls), sucrose preference (n = 6 lesioned, n = 6 controls), and TH staining (n = 2 lesioned).

Animal model and stereotaxic surgical procedure

The 6-OHDA basal ganglia lesion model is a widely accepted model of dopaminergic deafferentation, and parallels many pathophysiologic features of the human disorder [10]. Animals were about 10 weeks old at the time of surgery. The procedure was as described before with changes in the injection sites [11]. To prevent any noradrenergic effects of the toxin, animals received desipramine (25 mg/kg in 2 ml/kg bodyweight in saline, i. p.; Sigma-Aldrich Co., St. Louis, Missouri, USA) before the start of surgery. They were then placed under isoflurane anesthesia (1.5% in 30% oxygen and 70% nitrous oxide) in a stereotaxic apparatus (David KOPF Instruments, Tujunga, California, USA) and received injection of 6-OHDA (Sigma-Aldrich Co.) at four sites targeting the dorsomedial striatum bilaterally (AP: +1.5, ML: ±2.2, DV: –5.2 mm, and AP: +0.3, ML: ±2.8, DV: –5.0 mm, relative to the bregma), which is the primary striatal sector targeted by the medial prefrontal cortex (anterior cingulate, prelimbic area) [12]. Injection of 10 µg of 6-OHDA dissolved in 2 µl of 0.1% L-ascorbic acid/saline was made at each site through a 10 µl Hamilton 1701 microsyringe (Hamilton Company, Reno, Nevada, USA) fitted with a

Fig. 1

3-CSRT	Stim Dur (s)	Limited Hold (s)	ITI (s)	TO (s)	Days
Pretraining a,b	n/a	n/a	n/a	n/a	1 (twice)
Pretraining c	∞	∞	2	n/a	2
Training Level 1	30	30	2	2	3
Training Level 2	15	15	2	2	3
Training Level 3	5	10	2	2	10
3-CSRT Reversal					
Pretraining aR	n/a	n/a	n/a	n/a	1 (twice)
Pretraining cR	∞	∞	2	n/a	5
Training Level 1R	30	30	2	2	10
Training Level 2R	15	15	2	2	5
Training Level 3R	5	10	2	2	15

Experimental protocol for operant training. (a) Timeline of experiment. (b) 3-CSRT and reversal learning. (c) Progressive training schedule. 3-CSRT, 3-choice serial reaction time task.

30-gauge, blunted needle, at 0.4 µl/min controlled by a Micro4 microsyringe pump controller (World Precision Instruments, Sarasota, Florida, USA). After injection, the needle was left in place for 5 minutes before being slowly retracted (1 mm/min). To allow comparison to normal 3-CSRT learning, naïve rats were used for controls. Carprofen (2 mg in 5 g tablet, p. o.; Bio-Serv, Flemington, New Jersey, USA) was administered for 1 day preoperatively and for 2 days postoperatively for analgesia. Following lesioning, animals were left to recover for 2 weeks prior to initiating the 3-CSRT training.

Tyrosine hydroxylase immunostaining

TH immunostaining data were collected from n = 6 lesioned animals about 16 weeks after 6-OHDA lesioning. Rats were humanely anesthetized and subjected to transcardial perfusion with 100 ml of ice-cold saline followed by 250 ml of ice-cold 4% PFA/PBS. Brains were removed, transferred to the same fixative for 24 h, and then immersed in 20% sucrose for 48 h. After sinking, brains were flash-frozen, mounted and cut at 25 µm thickness on a cryostat microtome in the coronal orientation throughout the entire anterior-posterior extent of the brain. Selective sections representing levels of the brain spanning the site of 6-OHDA in both the striatum and midbrain were subjected to TH-immunostaining. Sections were rinsed with tris-buffered saline (TBS) at room temperature (RT) for 30 minutes, and quenched with 3% H_2O_2 for 10 minutes at RT. After rinsing in TBS, slides were washed in TBS +0.2% Triton-X 100 (TBST-0.2%) for 60 minutes at room temperature, then blocked with 4% NHS/TBST-0.2% and incubated overnight at 4°C in primary antibody solution (1:2500 anti-tyrosine hydroxylase, clone LNC1; Millipore, Billerica, Massachusetts, USA) in 2% NHS/TBST-0.2%. Sections were visualized using secondary antibody solution (biotinylated anti-mouse IgG, Vectastain Elite ABC kit) 1:1000 in 2% NHS/TBST-0.05%, 60 minutes at RT. After rinsing with TBS, sections were placed in ABC Reagent for 60 min at RT. Staining was developed with 3,3′-diaminobenzidine (Vector Labs DAB Peroxidase Substrate Kit, Burlingame, California, USA), until optimal contrast on sections was achieved. Sections were then mounted, dried overnight, and dehydrated before being coverslipped.

Images of tissues were made using an Olympus BX-50 microscope at low magnification, and the lesion size of the striatum was estimated bilaterally in the digitized, thresholded images of each rat by manual tracing using ImageJ 1.52k (Wayne Rasband, National Institutes of Health). Certain anatomical landmarks were used in the selection of striatal sections to demarcate rostral (bregma +2.28 to +1.28 mm, representative level +1.80 mm, genu of the corpus callosum with lateral appearance of the anterior commissures), mid (bregma +1.28 to +0.36 mm, representative level 0.72 mm, medially located anterior commissure), and caudal levels (bregma +0.24 to −0.48 mm, representative level 0.00 mm, posterior tail of the anterior commissure). Lesioned striatal areas were evaluated as a percentage of bilateral total striatal area.

Spontaneous overnight locomotor activity

Overnight locomotor activity of the animals (n = 13) was recorded prior to 6-OHDA lesioning and 2 weeks thereafter. Recordings were performed in the vivarium during the dark cycle (6 p.m. to 6 a.m.). Animals were individually placed into clear plastic filtertop cages (46 cm length × 25 cm width × 22 cm height) with fresh direct bedding. During the recording period, animals were given a water gel cup for fluid intake but no food chow. Activity counts of each rats were recorded in the horizontal and vertical planes in time bins of 15 minutes by an infrared beam break system (Opto-M3, 160 Hz beam scan rate, 2.5 cm sensor spacing, 16 × 16 sensor grid; Columbus Instruments, Columbus, Ohio, USA) mounted around their cages.

Accelerating rotarod test

The effects of lesioning on coordination, balance and strength were evaluated on rotarod, a rotating cylinder treadmill with a diameter of 7.3 cm [11]. Data were collected from animals (n = 8 lesioned, n = 8 controls) after the completion of operant training and with ad-lib food access. Rats were familiarized with the rotarod (Columbus Instruments) at 2.3 m/min for 3 minutes twice the day before testing. Rats were run using an acceleration paradigm (initial speed: 5 rpm = 1.15 m/min, acceleration rate: 6 rotations/min^2 = 1.38 m/min^2, two trials/day, 30-minute intertrial interval for 2 days) until they fell onto a padded surface or reached the 5 minutes cutoff time (maximum speed: 35 rpm = 8.02 m/min). The outcome variable was the latency to fall averaged over four trials.

Sucrose preference test

We examined the effects of lesioning on sucrose preference to investigate anhedonia, which could emerge in toxin-induced models and therefore impact the motivation for reward in 3-CSRT. Data were collected from animals (n = 8 lesioned, n = 6 controls) after the completion of operant training and with ad-lib access to food. The protocol used was similar to those we have previously published [13]. To minimize neophobia, rats were exposed to the sucrose solution overnight for 2 days. The water bottle in each home-cage was replaced with two 50-ml bottles fitted with ball-point drinking spouts containing 2% sucrose. On the day of testing, rats were water-deprived for approximately 9 h. At the onset of the dark phase, rats were individually housed overnight with access to two bottles, one containing 2% sucrose and the other water. Each filled bottle was weighed before and after the sucrose preference test, with fluid consumption measured by the difference. The location of the sucrose bottle (to the right or left side of the cage) was alternated to minimize side

preferences. Sucrose preference was calculated as a percentage of total fluid intake, that is, 100 × volume sucrose intake/(volume of sucrose + volume water).

Food restriction

Food restriction was started 2 weeks after lesion surgery and maintained throughout the experiment. Animals were brought to 85% of their baseline bodyweight in 1 week and were allowed to gain 5 g in body weight per week thereafter, with ad libitum access to water. Animals were fed after behavioral training. Body weights were recorded Monday–Friday, with meal size (Rodent Diet #5001; LabDiet, St. Louis, Missouri, USA) individually adjusted on a daily basis.

Three-choice serial reaction time task with reversal learning

We modified the well-established 5-CSRT protocol and its 3-CSRT variation (Tsutsui-Kimura *et al.*, 2009) (Fig. 1a). (1) Animals were trained through three difficulty levels with progressively shortened stimulus durations. While most 5-CSRT protocols train the animal at each difficulty level for a variable number of days until the animal reaches certain performance criteria, we chose to control the number of training days for each level across animals to facilitate between-group comparison. (2) The final stimulus duration was set at 5 seconds, reflecting a moderate level of difficulty. This was selected based on pilot data showing that 6-OHDA lesioned animals can reach a performance level comparable to that of control animals at this difficulty level. Differences in reversal learning can thus be interpreted as differences in cognitive flexibility, rather than as differences in operant learning per se. (3) During the reversal phase of training, the rule was switched from rewarding nose poke into a lit aperture to rewarding nose poke into a dark aperture.

Training was started 1 week following the initiation of food restriction and was always performed between 8 a.m. and 1 p.m. Each operant cage (MedAssociates, St. Albans, Vermont, USA) consisted of a sound-attenuating cubicle (63 cm width, 46 cm depth, 61 cm height) with a fan which was always turned on during testing, modular test chamber (33 cm width, 25 cm depth, 33 cm height) with grid floor, house light, three-bay nose poke wall, pellet dispenser on the wall opposite the nose poke bays, pellet trough receptacle, receptacle light, head entry detector, smart controller, and infrared camera (Birdhouse Spy Cam, West Linn, Oregon, USA) for real-time viewing of animals on a TV monitor. Cages were operated by MED-PC software using a personal computer. Pellet dispensers were loaded with dustless sucrose pellets (45 mg/pellet, #F0025; Bio-Serv). Behavioral training was implemented with a fixed ratio FR1 schedule response-reward task (up to 90 trials or 30 min/day, 5 days/week). The walls, nose poke apertures, food receptacle, and grid floor were wiped with 70% isopropyl alcohol between animals.

Habituation and shaping of behavior

Rats were familiarized with the test chamber and sugar pellets prior to training. Nose poke and reward retrieval behavior were shaped in pretraining. In pretraining '*a*', 10 sugar pellets were put in each nose poke aperture and pellet receptacle, and the animal was allowed to explore the test chamber and retrieve the pellets for 15 minutes. In pretraining '*b*', the animal was kept in the test chamber for 10 minutes, while a sugar pellet was dispensed into the receptacle every 20 seconds with the receptacle light turned on. The receptacle light was turned off 2 seconds after detection of a head entry (reward retrieval). Pretraining '*a*' and '*b*' were repeated once during the same day. In pretraining '*c*', the animal was trained to associate nose poking into a lit aperture with receiving a single sugar pellet reward into the receptacle. Each daily session lasted 30 minutes or until the animal received 90 rewards. For each trial, the light in a pseudorandomly chosen nose poke aperture was turned on (stimulus). When a nose poke was detected in the lit aperture (correct nose poke), the aperture light was turned off, and the light in the pellet receptacle was turned on with a sugar pellet dispensed (reward). The receptacle light was turned off 2 seconds after detection of a head entry. After a 2-second inter-trial interval (ITI), the next trial was started.

Three-choice serial reaction time task training

During the regular phase of 3-CSRT training, the animal was trained following a progressive schedule (Fig. 1b and c). The animal was trained to make a correct nose poke in response to a relatively short stimulus duration. Each single daily session lasted 30 minutes or until 90 trials were reached. At the start of each trial, the chamber light was turned on and a randomly selected stimulus was started. The stimulus stayed on for a set duration or until a nose poke (correct or incorrect) was detected. The animal received a food reward following a correct nose poke within the set limited hold duration, which was set to be the same as the stimulus duration or slightly longer for short stimulus durations. Following reward retrieval and ITI, the next trial was started. If an incorrect nose poke was detected, the animal was punished with a time out (TO), during which the chamber light was turned off for 2 seconds. If no nose poke was detected within the limited hold duration, an omission was recorded, and the animal punished with a TO. After each TO, the chamber light was turned on, and after an ITI, the next trial was started. If a nose poke was detected during the ITI, a premature response was recorded without incrementing the trial number, and the animal punished with a TO. Any nose pokes following a correct response and before reward retrieval were recorded as perseverative responses.

Reversal training

During the reversal phase of 3-CSRT-R training (Fig. 1b and c), the stimulus was switched from a lit aperture

among dark apertures to a dark aperture among lit apertures. The animal was trained progressively to learn to nose poke the dark aperture to receive reward. The current task, while not a classical reversal task [14,15] that usually involves two stimuli and two locations, incorporated essential elements of reversal learning [16], with the addition of a third location that aided in avoiding solving the discrimination using simple configural learning strategies [16,17]. Pretraining cR (Fig. 1c), in which the animal was rewarded until it made a correct nose poke (into a dark hole) without any timeout punishment, was critical to initial acquisition of the reversal task. This modification was necessitated by an increase in the task difficulty and to avoid diminishing the animal's motivation to complete the task.

Analysis of the operant behavior included [7]:

(1) nose poke accuracy = (number of correct responses)/(number of correct + number of incorrect responses) × 100%, a primary measure of operant learning;
(2) omissions rate = (number of omissions)/(number of trials completed), a measure of attention;
(3) premature responses, a measure of impulsivity;
(4) perseverative rate = (number of perseverative responses)/(number of correct responses), a measure of compulsive behavior;
(5) correct nose poke latency = average time from onset of stimulus to a correct response, a measure of attention and cognitive processing speed;
(6) reward retrieval latency = average time from correct response to retrieval of sugar pellet, a measure of motivation.

It is important to note that sensorimotor functions contribute critically to the operant training performance. Therefore, interpretation of the above variables should take into consideration possible lesion-induced sensorimotor dysfunctions.

Statistical analysis

Data are presented as the mean ± SEM and analyzed using GraphPad Prism (version 8.3.0; GraphPad Software, San Diego, California, USA). All data were subjected to the Shapiro–Wilk test for normality. The following data transformations were applied to improve normality and homogeneity of variance: arcsine for nose poke accuracy, logarithm for nose poke latency, reciprocal for reward latency, square root for premature responses and perseverative rate. 3-CSRT data were analyzed using a two-way analysis of variance (ANOVA) with repeated measures for each training level, with lesion and time as the two factors, and with Holm–Sidak's post-hoc multiple comparisons test. Data for individual days that failed the normality test were excluded from ANOVA and analyzed separately using the Mann–Whitney test. Data were subjected to Bartlett's test for homogeneity of variance for each training level. Data that failed the Bartlett's test were analyzed using unpaired Student's or Welch's *t*-test (based on Levene's test for equal variance) to compare 6-OHDA lesioned and control group on individual days instead of ANOVA. Overnight activity data were analyzed using paired Student's *t*-test. Accelerating rotarod and sucrose preference data were analyzed using unpaired Student's *t*-test. $P < 0.05$ was considered statistically significant.

Results

Lesion verification

TH immunostaining confirmed that the dopamine-depletion lesion was mainly limited to the dorsomedial aspect of the striatum, a region of the basal ganglia central to cognitive processing. Figure 2a shows representative brain slices at three bregma levels designated as rostral, mid, and caudal with reduced TH immunoreactivity in the dorsomedial striatum. Lesioned area was quantified as a percentage of total striatal area bilaterally: rostral (26.21 ± 6.23%), mid (32.89 ± 3.18%), and caudal (34.92 ± 2.43%) (Fig. 2b). There was also loss of TH-immunoreactive cells in the substantia nigra pars compacta (Fig. 2d compared to Fig. 2c).

Lesion spared motor functions and sucrose preference

Overnight activity measurement in home cage showed no significant differences in horizontal activity counts 2 weeks after 6-OHDA lesioning (15 077 ± 1296 counts, $n = 13$) compared to baseline (18 223 ± 1815 counts, $P = 0.074$, paired Student's *t*-test), and in vertical activity counts (4870 ± 1129 counts) compared to baseline (6033 ± 1531 counts, $P = 0.52$; Fig. 3a). There was also no significant lesioning effect on the maximum velocity during any 15-minute intervals (data not shown). In the accelerating rotarod test, no significant differences were evident in latency to fall between control (169 ± 15 seconds, $n = 8$) and lesioned animals (161 ± 22 seconds, $n = 8$, $P = 0.77$, unpaired Student's *t*-test; Fig. 3b). Analysis of sucrose preference (Fig. 3c) revealed that 6-OHDA lesioned animals (74.76 ± 4.60%, $n = 8$) did not differ from controls (78.76 ± 6.06%, $n = 6$, $P = 0.20$, unpaired Student's *t*-test).

Lesion induced deficits in cognitive flexibility

During the acquisition phase of 3-CSRT (levels L1, L2, and L3), both lesioned and control rats showed improvement in nose poke accuracy and shortening of correct nose poke latency (Fig. 4). Lesioned rats compared to controls showed: (1) statistically significant lower nose poke accuracy (L1: $F_{1,10} = 26.39$, $P = 0.0004$; L2: $F_{1,10} = 40.68$, $P < 0.0001$; L3: $F_{1,10} = 23.47$, $P = 0.0007$. Main lesion effect, two-way ANOVA repeated measure) that diminished towards the end of L3 ($P = 0.16$ for day 9 and day 10 of L3, Holm–Sidak post-hoc test; Fig. 4a); (2) no significant differences in omission rate ($P > 0.05$, Mann–Whitney test), but statistically significant differences in variance (Levene's test; Fig. 4b); (3) no significant differences in nose poke latency (L1: $F_{1,10} = 4.121$, $P = 0.070$; L2: $F_{1,10} = 3.58$, $P = 0.088$; L3: $F_{1,10} = 1.942$, $P = 0.19$. Main

Fig. 2

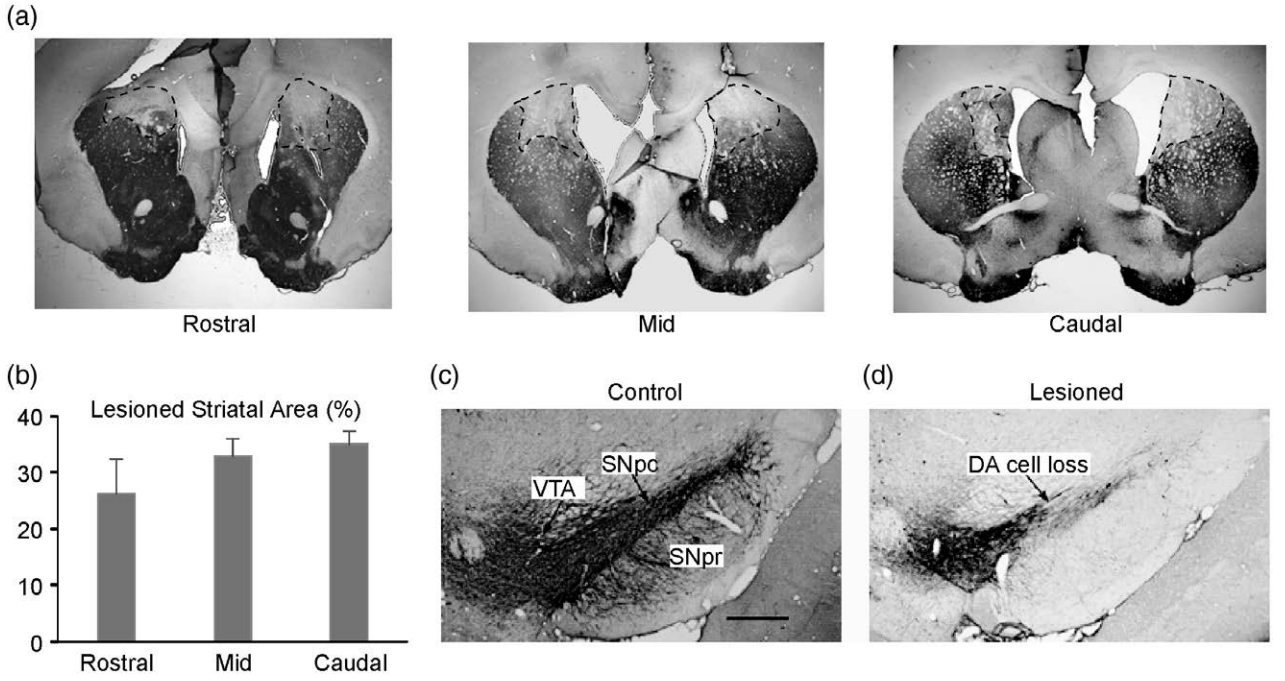

Immunostaining for tyrosine hydroxylase to determine the degree and anatomical site of lesion. (a) Representative images of coronal sections reveal bilateral loss in TH immunoreactivity in the dorsomedial striatum (rostral: bregma + 1.80 mm, mid: +0.72 mm, caudal: +0.00 mm). (b) Lesioned striatal areas were quantified as percent of bilateral striatal area at rostral, mid, and caudal levels ($n = 6$). (c and d) Representative images showing lesion-induced loss in TH immunoreactivity in the substantia nigra pars compacta (bregma − 5.28 mm). Scale bar = 0.5 mm. TH, tyrosine-hydroxylase.

Fig. 3

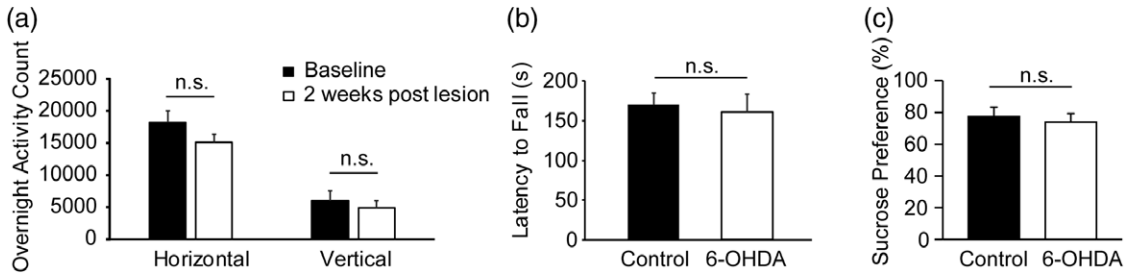

Lesion largely spared motor functions and sucrose preference. (a) Overnight locomotor activity before and 2 weeks after 6-OHDA lesioning ($n = 13$, horizontal $P = 0.074$, vertical $P = 0.52$, unpaired Student's t-test). (b) Accelerating rotarod test showed no significant differences in mean latency to fall between lesioned ($n = 8$) and control rats ($n = 8$, $P = 0.77$). (c) Analysis of sucrose preference revealed no significant differences between lesioned ($n = 8$) and control rats ($n = 6$, $P = 0.20$, unpaired Student's t-test). 6-OHDA, 6-hydroxydopamine.

lesion effect, ANOVA; Fig. 4c); (4) statistically significant greater reward retrieval latency (L1: $P < 0.005$, Student's t-test; L2: $F_{1,10} = 17.71$, $P = 0.0018$, ANOVA; L3: $P < 0.05$, t-test and Mann–Whitney test; Fig. 4d); (5) no differences in premature responses (Fig. 4e) and fecal pellet count (Fig. 4g); and (6) statistically higher perseverative rate in L1 ($F_{1,10} = 17.71$, $P = 0.033$, main lesion effect, ANOVA) and day 1 of L2 ($P = 0.043$, Mann–Whitney) that diminished in L3 ($F_{1,10} = 2.024$, $P = 0.19$, main lesion effect, ANOVA; Fig. 4f).

At the start of the 3-CSRT-R, when the rule for correct (rewarded) response was switched from nose poking a lit aperture to nose poking a dark aperture, both lesioned and control rats showed a sudden drop in performance with decreased nose poke accuracy to the same extent, increased correct nose poke latency, and increased premature responses. Both groups showed improvement in these parameters with continued training. Control rats improved nose poke accuracy to a plateau of about 75%, while lesioned animals only improved accuracy modestly

Fig. 4

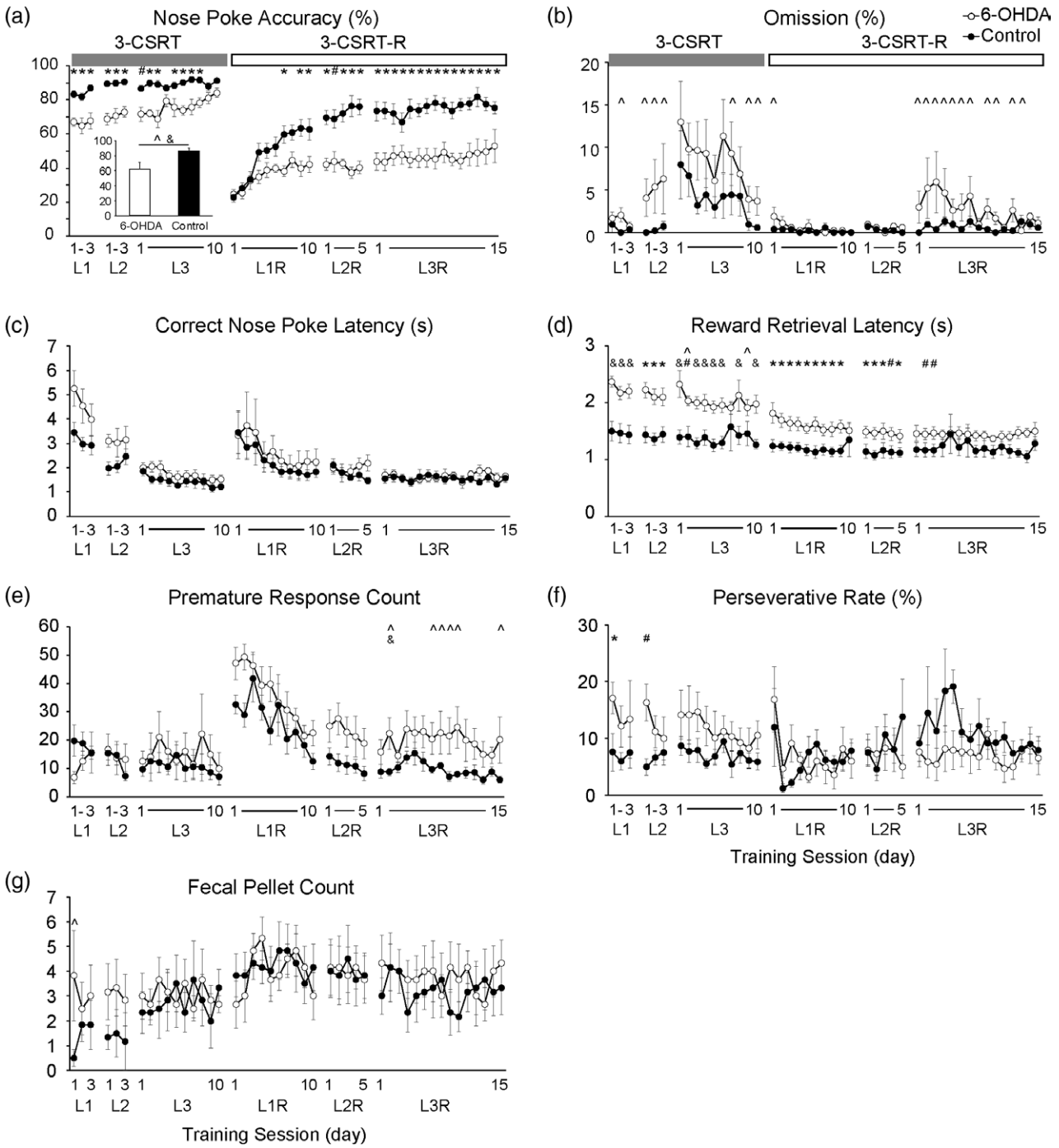

Differences in 3-CSRT acquisition and reversal learning (3-CSRT-R) in 6-OHDA lesioned animals ($n = 6$) compared to controls ($n = 6$). (a) While 6-OHDA animals were moderately impaired in 3-CSRT acquisition with lower nose poke accuracy, profound deficits were noted during the reversal phase compared to controls. Inset shows average nose poke accuracy over the last 5 days of L3R (level 3, reversal) normalized by the mean of last 5 days of L3 (level 3). The normalize accuracy was significantly lower in 6-OHDA animals ($P < 0.05$, Welch's *t*-test). (b) Omission rate. (c) Correct nose poke latency. (d) Reward retrieval latency was longer in 6-OHDA animals compared to controls. (e) Premature responses. (f) Perseverative rate. (g) Fecal pellet count. $P < 0.05$, 6-OHDA vs. control groups: *Holm–Sidak post-hoc test, two-way ANOVA repeated measure; #Mann–Whitney test; &Student's or Welch's *t*-test; and ^Levene's test for homogeneity of variance. 3-CSRT, 3-choice serial reaction time task; 6-OHDA, 6-hydroxydopamine; ANOVA, analysis of variance.

to a plateau of about 50%. There were statistically significant differences between the two groups (Fig. 4a, L1R: $F_{1,10}$ = 6.451, P = 0.029; L2R: $F_{1,10}$ = 29.26, P = 0.0003; L3R: $F_{1,10}$ = 16.28, P = 0.0024; main lesion effect, ANOVA). Figure 4a inset shows average nose poke accuracy over the last 5 days of L3R normalized by the mean of the last 5 days of L3. The normalized accuracy was significantly lower in 6-OHDA animals (P = 0.041, Welch's t-test). Lesioned compared to control rats continued to demonstrate significantly greater reward retrieval latency up to day 3 of L3R (Fig. 4d, L1R: $F_{1,10}$ = 11.16, P = 0.0075; L2R: $F_{1,10}$ = 6.69, P = 0.027; L3R: $F_{1,10}$ = 4.843, P = 0.052; main lesion effect, ANOVA; days 2 and 3 of L3R, $P < 0.05$, Mann–Whitney). There were no significant differences in premature responses (Fig. 4e, L1R: $F_{1,10}$ = 3.241, P = 0.10; L2R: $F_{1,10}$ = 4.602, P = 0.058, main lesion effect, ANOVA), except on day 2 of L3R (P = 0.037, Welch's t-test), but significant differences in variance (L3R, Levene's test). Also noted were significant differences in variance in omission rate between the lesioned and control rats (Fig. 4b, Levene's test). No between-group differences were noted in correct nose poke latency, perseverative rate, and fecal pellet count.

Discussion

We modified the well-established 5-CSRT paradigm to a 3-CSRT task with nose poke and reversal learning to test cognitive flexibility in animals with 6-OHDA lesion to the dorsomedial striatum. Lesioned animals compared to controls showed robust and persistent deficits in reversal learning, despite having previously learned the task to an equivalent extent, and in the absence of anhedonia and general deficits in motor functions.

Acquisition of three-choice serial reaction time task

The CSRT paradigm is an operant learning task widely used to study attention and impulse control in rodents [6]. The task requires a consecutive series of information processing, decision making, and actions, including waiting for the stimulus and inhibition of premature responses during the inter-trial interval → attention to the stimulus → recall of prior successful responses → choice of nose poke response → nose poke → recall of reward retrieval → decision to initiate reward retrieval → reward retrieval. Control rats quickly learned the 3-CSRT task and reached a plateau of about 90% accuracy. Lesioned rats, while showing deficits in the initial phase of training, were able to reach a comparable level of accuracy (84.24 ± 2.64%) after 4 weeks of training. During the acquisition of the 3-CSRT, there were no significant group differences in premature responses. This suggests that during acquisition there was little evidence for a group difference in impulsive behavior. It is important to note that the animals were not challenged with longer ITIs to test impulsivity more vigorously. The lesioned animals compared to controls did not show significant differences in means, but did show statistically significant differences in variance during the later portion of 3-CSRT-R, suggesting a mild lesion-induced deficit in attention.

Lesioned compared to control rats demonstrated a significantly greater reaction time for reward retrieval. Although motor deficits could in principle contribute to group differences seen in reward retrieval latency and omission rate, several lines of evidence argued against general motor impairment. Lesion did not induce significant differences in spontaneous locomotor activity or in general motor strength, balance and coordination as measured using the accelerating rotarod test. Of importance, the correct nose poke latency following the first week of initial learning was almost identical between the two groups. This suggests that after the first week, lesioned compared to control animals showed comparable levels of attention, speed for information processing and decision making, and speed to nose poke action. Likewise, no lesion effect was noted in the appetitive preference for sucrose reward using the sucrose preference test. This suggests that differences in reward retrieval latency (or omissions rate) likely reflect a slowing of cognitive processing of reward expectation and mildly impaired attention, rather than general motor dysfunction, lack of motivation, or severe attention deficit. The number of fecal pellets counted during the learning phase showed no group differences, suggesting no lesion effect on anxiety-like behavior during the cognitive challenges in 3-CSRT. Our study did not assess possible lesion effects on the somatosensory perception which if present chronically could have modulated our behavioral responses.

Reversal learning in three-choice serial reaction time task

The reversal learning phase was initiated at a time point when lesioned and control animals had reached similar levels of accuracy. During the initial stage of reversal learning, both lesioned and control rats showed a sudden drop in nose poke accuracy to the same extent. However, with continued training of only a few sessions, control rats rapidly improved their performance, reaching a plateau of about 80% accuracy, while lesioned animals only improved modestly and reached a plateau of about 50% accuracy. We further normalized the average accuracy over the last 5 days of reversal learning (L3R) by the mean of accuracy over the last 5 days of regular training (L3), to control any possible lesion-related deficits in motor and cognitive functions. The normalized 3-CSRT-R accuracy remained significant lower in lesioned (61.83 ± 8.78%) compared to control animals (86.00 ± 4.28%) (Fig. 4a, inset). Thus, the 3-CSRT-R task unmasked lesion-induced deficits in cognitive flexibility.

Deficits in reversal learning can be impacted by 'perseverant' responses, that is, the inappropriate maintenance of responses previously associated with either reward

(learned-reward response) and/or with non-reward (learned-nonreward responses) [18]. The exact contribution of persistent learned-reward or learned-nonreward responses in the lesioned animals, and the role these might play in inhibiting new learning of the reversal task is unclear. There was a nonsignificant trend of greater premature responses and omission rate in lesioned compared to control animals, as well as significant differences in variance, suggesting mild impairment in impulse control and attention.

Our findings suggest that learning is substantially more rapid in the 3-CSRT and 3-CSRT-R nose-poke tasks than has been typically reported with either the 5-CSRT and 5-CSRT-R lever-press task [19,20], the 5-CSRT touchscreen task [17], or the 5-CSRT nose-poke task [6,7]. In part, such difference may be related to the fact that nose-poke responses occur at a higher baseline rate compared to those of lever pressing or touchscreen responses. Significant lesion effect in nose poke accuracy was achieved with a relatively small number of animals (n = 6/group), possibly a reflection of smaller variability in a behavior well within the natural repertoire of the animal.

Of note, De Bruin *et al.* [21] previously applied a variant of the 5-CSRT lever as a 2-CSRT lever-pressing task, a paradigm later adapted by Homberg et al. to a two-choice nose-poke paradigm (2-CSRT) [22]. The latter, using a fixed-ratio FR3 schedule of reinforcement in nonlesioned rats, demonstrated learning acquisition in 25 training sessions of 50 trials per session, and reversal-learning to criterion performance in three sessions. This shortened duration for reversal training is consistent with the notion that reversal learning decreases in difficulty as the number of holes available for nose poke decreases. While the shortening of training time is desirable, the lower level of task difficulty may decrease the sensitivity to detect deficits in executive function. Therefore, experimental design, and the choice of 5-CSRT or 3-CSRT should be based upon the anticipated magnitude of the deficit.

Dorsomedial striatal lesions

An early feature of PD is deficits in cognitive flexibility, an aspect of executive functions, which involve cognitive processes of set-shifting, working memory, and information processing. Dopamine loss in PD patients is predominant in the posterior putamen, a region associated with the control of habitual behavior. It has been proposed that executive dysfunction, may result as patients become overly reliant on the goal-directed mode of action control that is mediated by comparatively preserved processing in the rostromedial striatum [23]. While not identical to PD, the 6-OHDA lesioning of dopaminergic neurons of the nigrostriatal system reproduces many of its features [10]. Dopaminergic lesions in the dorsomedial striatum of rodents are critical for successfully observing impaired reversal learning [3,24,25]. Past work has shown that the formation of the critical action-outcome associations mediating goal-directed learning are localized to the dorsomedial striatum, whereas the sensorimotor connections that control the performance of habitual actions or procedural learning are localized to the dorsolateral striatum [26]. In patients and in the animal models, such deficits presumably reflect alterations in frontostriatal processing [12]. Our TH immunostaining results showed that lesions were primarily localized in the mid-caudal levels of the striatum, and appropriately limited to the dorsomedial quadrant of the striatum. Retrograde dopaminergic cell losses were also apparent bilaterally in the substantia nigra. While in 6-OHDA rodent model deficits in cognitive flexibility have previously been examined using the cross-maze [3], T-maze [27], and a food-digging task [28], the current study is the first to examine such deficits during the reversal phase of a choice serial reaction time task. Our results demonstrate that dramatic and persistent deficits in cognitive flexibility can be robustly detected in the 3-CSRT-R nose-poke paradigm 2 weeks after initiation of the change of rule. While differences in experimental design and criteria for determining 'learning', as well as rodent strains may affect the final duration of experimentation, our findings underscore the practicality of using a 3-CSRT-R nose poke paradigm in evaluating cognitive flexibility. We propose that use of the 3-CSRT-R in rats with bilateral dorsomedial striatal lesions may be a useful model for future testing of treatments aimed at improving executive dysfunction in PD.

Acknowledgements

This work was supported by grants from the US Department of Defense (Army, CDMRP) grant no. W81XWH18-1-0666 (D.P.H.) and grant no. W81XWH19-1-0443 (M.W.J.).

Conflicts of interest

There are no conflicts of interest.

References

1 Dubois B, Pillon B. Cognitive deficits in Parkinson's disease. *J Neurol* 1997; **244**:2–8.
2 Halliday GM, Leverenz JB, Schneider JS, Adler CH. The neurobiological basis of cognitive impairment in Parkinson's disease. *Mov Disord* 2014; **29**:634–650.
3 Grospe GM, Baker PM, Ragozzino ME. Cognitive flexibility deficits following 6-OHDA lesions of the rat dorsomedial striatum. *Neuroscience* 2018; **374**:80–90.
4 Kwak C, Lim CS, Kaang BK. Assessments of cognitive abilities in a mouse model of Parkinson's disease with a touch screen test. *Behav Brain Res* 2016; **301**:63–71.
5 Carli M, Robbins TW, Evenden JL, Everitt BJ. Effects of lesions to ascending noradrenergic neurones on performance of a 5-choice serial reaction task in rats; implications for theories of dorsal noradrenergic bundle function based on selective attention and arousal. *Behav Brain Res* 1983; **9**:361–380.
6 Bari A, Dalley JW, Robbins TW. The application of the 5-choice serial reaction time task for the assessment of visual attentional processes and impulse control in rats. *Nat Protoc* 2008; **3**:759–767.
7 Asinof SK, Paine TA. The 5-choice serial reaction time task: a task of attention and impulse control for rodents. *J Vis Exp* 2014:e51574.

8 Tsutsui-Kimura I, Ohmura Y, Izumi T, Yamaguchi T, Yoshida T, Yoshioka M. The effects of serotonin and/or noradrenaline reuptake inhibitors on impulsive-like action assessed by the three-choice serial reaction time task: a simple and valid model of impulsive action using rats. *Behav Pharmacol* 2009; **20**:474–483.

9 Schindler CW, Thorndike EB, Goldberg SR. Acquisition of a nose-poke response in rats as an operant. *Bulletin Psychonomic Society* 1993; **31**:291–294.

10 Cenci MA, Whishaw IQ, Schallert T. Animal models of neurological deficits: how relevant is the rat? *Nat Rev Neurosci* 2002; **3**:574–579.

11 Wang Z, Myers KG, Guo Y, Ocampo MA, Pang RD, Jakowec MW, Holschneider DP. Functional reorganization of motor and limbic circuits after exercise training in a rat model of bilateral parkinsonism. *PLoS One* 2013; **8**:e80058.

12 Voorn P, Vanderschuren LJ, Groenewegen HJ, Robbins TW, Pennartz CM. Putting a spin on the dorsal-ventral divide of the striatum. *Trends Neurosci* 2004; **27**:468–474.

13 Gorton LM, Vuckovic MG, Vertelkina N, Petzinger GM, Jakowec MW, Wood RI. Exercise effects on motor and affective behavior and catecholamine neurochemistry in the MPTP-lesioned mouse. *Behav Brain Res* 2010; **213**:253–262.

14 Fellows LK, Farah MJ. Ventromedial frontal cortex mediates affective shifting in humans: evidence from a reversal learning paradigm. *Brain* 2003; **126**:1830–1837.

15 Schoenbaum G, Chiba AA, Gallagher M. Changes in functional connectivity in orbitofrontal cortex and basolateral amygdala during learning and reversal training. *J Neurosci* 2000; **20**:5179–5189.

16 Izquierdo A, Brigman JL, Radke AK, Rudebeck PH, Holmes A. The neural basis of reversal learning: An updated perspective. *Neuroscience* 2017; **345**:12–26.

17 Mar AC, Horner AE, Nilsson SR, Alsiö J, Kent BA, Kim CH, *et al*. The touchscreen operant platform for assessing executive function in rats and mice. *Nat Protoc* 2013; **8**:1985–2005.

18 Nilsson SR, Alsiö J, Somerville EM, Clifton PG. The rat's not for turning: dissociating the psychological components of cognitive inflexibility. *Neurosci Biobehav Rev* 2015; **56**:1–14.

19 Higgs S, Deacon RM, Rawlins JN. Effects of scopolamine on a novel choice serial reaction time task. *Eur J Neurosci* 2000; **12**: 1781–1788.

20 Lê AD, Lê Dzung A, Funk D, Harding S, Juzytsch W, Li Z, Fletcher PJ. Intramedian raphe nucleus (MRN) infusions of muscimol, a GABA-A receptor agonist, reinstate alcohol seeking in rats: role of impulsivity and reward. *Psychopharmacology (Berl)* 2008; **195**:605–615.

21 De Bruin JP, Feenstra MG, Broersen LM, Van Leeuwen M, Arens C, De Vries S, Joosten RN. Role of the prefrontal cortex of the rat in learning and decision making: effects of transient inactivation. *Prog Brain Res* 2000; **126**:103–113.

22 Homberg JR, Pattij T, Janssen MC, Ronken E, De Boer SF, Schoffelmeer AN, Cuppen E. Serotonin transporter deficiency in rats improves inhibitory control but not behavioural flexibility. *Eur J Neurosci* 2007; **26**: 2066–2073.

23 Redgrave P, Rodriguez M, Smith Y, Rodriguez-Oroz MC, Lehericy S, Bergman H, *et al*. Goal-directed and habitual control in the basal ganglia: implications for Parkinson's disease. *Nat Rev Neurosci* 2010; **11**:760–772.

24 Baker PM, Ragozzino ME. Contralateral disconnection of the rat prelimbic cortex and dorsomedial striatum impairs cue-guided behavioral switching. *Learn Mem* 2014; **21**:368–379.

25 O'Neill M, Brown VJ. The effect of striatal dopamine depletion and the adenosine A2A antagonist KW-6002 on reversal learning in rats. *Neurobiol Learn Mem* 2007; **88**:75–81.

26 Balleine BW, Liljeholm M, Ostlund SB. The integrative function of the basal ganglia in instrumental conditioning. *Behav Brain Res* 2009; **199**:43–52.

27 Haik KL, Shear DA, Hargrove C, Patton J, Mazei-Robison M, Sandstrom MI, Dunbar GL. 7-nitroindazole attenuates 6-hydroxydopamine-induced spatial learning deficits and dopamine neuron loss in a presymptomatic animal model of Parkinson's disease. *Exp Clin Psychopharmacol* 2008; **16**:178–189.

28 Tait DS, Phillips JM, Blackwell AD, Brown VJ. Effects of lesions of the subthalamic nucleus/zona incerta area and dorsomedial striatum on attentional set-shifting in the rat. *Neuroscience* 2017; **345**:287–296.

Intensive treadmill exercise increases expression of hypoxia-inducible factor 1α and its downstream transcript targets: a potential role in neuroplasticity

Matthew R. Halliday[a], Dishan Abeydeera[a], Adam J. Lundquist[a], Giselle M. Petzinger[a,b] and Michael W. Jakowec[a,b]

Exercise and other forms of physical activity lead to the activation of specific motor and cognitive circuits within the mammalian brain. These activated neuronal circuits are subjected to increased metabolic demand and must respond to transient but significant reduction in available oxygen. The transcription factor hypoxia-inducible factor 1α (HIF-1α) is a regulatory mediator of a wide spectrum of genes involved in metabolism, synaptogenesis, and blood flow. The purpose of this study was to begin to explore the potential relationship between exercise in the form of running on a motorized treadmill and the activation of genes involved in exercise-dependent neuroplasticity to begin to elucidate the underlying molecular mechanisms involved. Mice were subjected to treadmill exercise and striatal tissues analyzed with a commercial microarray designed to identify transcripts whose expression is altered by exposure to hypoxia, a condition occurring in cells under a high metabolic demand. Several candidate genes were identified, and a subset involved in metabolism and angiogenesis were selected to elucidate their temporal and regional patterns of expression with exercise. Transcript analysis included *Hif1a* (hypoxia-inducible factor 1α), *Ldha* (lactate dehydrogenase A), *Slc2a1* (glucose transporter 1), *Slc16a1* (monocarboxylate transporter 1), *Slc16a7* (monocarboxylate transporter 2), and *Vegf* (vascular endothelial growth factor). Overall these results indicate that several genes involved in the elevated metabolic response with exercise are consistent with increased expression of HIF-1α suggesting a regulatory role for HIF-1α in exercise-enhanced neuroplasticity. Furthermore, these increases in gene expression appear regionally specific; occurring with brain regions we have previously shown to be sites for increased cerebral blood flow with activity. Such findings are beginning to lay down a working hypothesis that specific forms of exercise lead to circuit specific neuronal activation and can identify a potentially novel therapeutic approach to target dysfunctional behaviors subserved by such circuitry. *NeuroReport* 30:619–627

NeuroReport 2019, **30**:619–627

Keywords: hypoxia-inducible factor 1α protein, neuroplasticity, physical activity

[a]Department of Neurology and [b]Division of Biokinesiology and Physical Therapy, University of Southern California, Los Angeles, California, USA

Correspondence to Michael W. Jakowec, PhD, Department of Neurology, University of Southern California, 1333 San Pablo Street, MCA-241, Los Angeles, CA 90033, USA
Tel: +1 323 442 3367; fax: +1 323 442 1055;
e-mail: mjakowec@surgery.usc.edu

Received 4 February 2019 **accepted** 5 March 2019

Introduction

Exercise and physical activity are critical in maintaining healthy motor and cognitive circuitry. Not only is exercise important for normal healthy aging but studies from our research group have shown that exercise can serve as a means to enhance neuroplasticity and restore motor and cognitive behavioral deficits in both patients and in animal models of neurodegenerative disorders including Parkinson's disease (PD) and Huntington's disease [1–3]. A major gap in knowledge is an understanding of the underlying molecular mechanisms by which exercise leads to the enhancement of neuroplasticity and the strengthening of brain circuitry. For example, using animal models of PD under conditions of high intensity exercise, we have documented changes in corticostriatal plasticity based on a wide range of techniques including molecular, histological, morphological, electrophysiological, and behavioral outcome measures [2,4–7].

Under conditions of high neuronal activity, neurons and glia undergo significant metabolic changes with respect to the utilization of glucose and lactate and the generation of ATP [8]. It is hypothesized that prolonged metabolic demands in these neuronal circuits lead to downstream activation and expression of genes and proteins involved in synaptogenesis and angiogenesis and the consequential consolidation of these circuits and permanency of the underlying behaviors. Metabolic demands impact the availability of oxygen and elevate the expression of factors in response to transient hypoxia. One such responsive mediator is hypoxia-inducible factor 1α (HIF-1α), a transcription factor induced by a number of cellular parameters including hypoxia, neuronal activity, and reactive oxygen species [9]. HIF-1α activates a transcript cascade that includes a wide spectrum of specific mRNAs including those encoding proteins involved

0959-4965 DOI: 10.1097/WNR.0000000000001239

Fig. 1

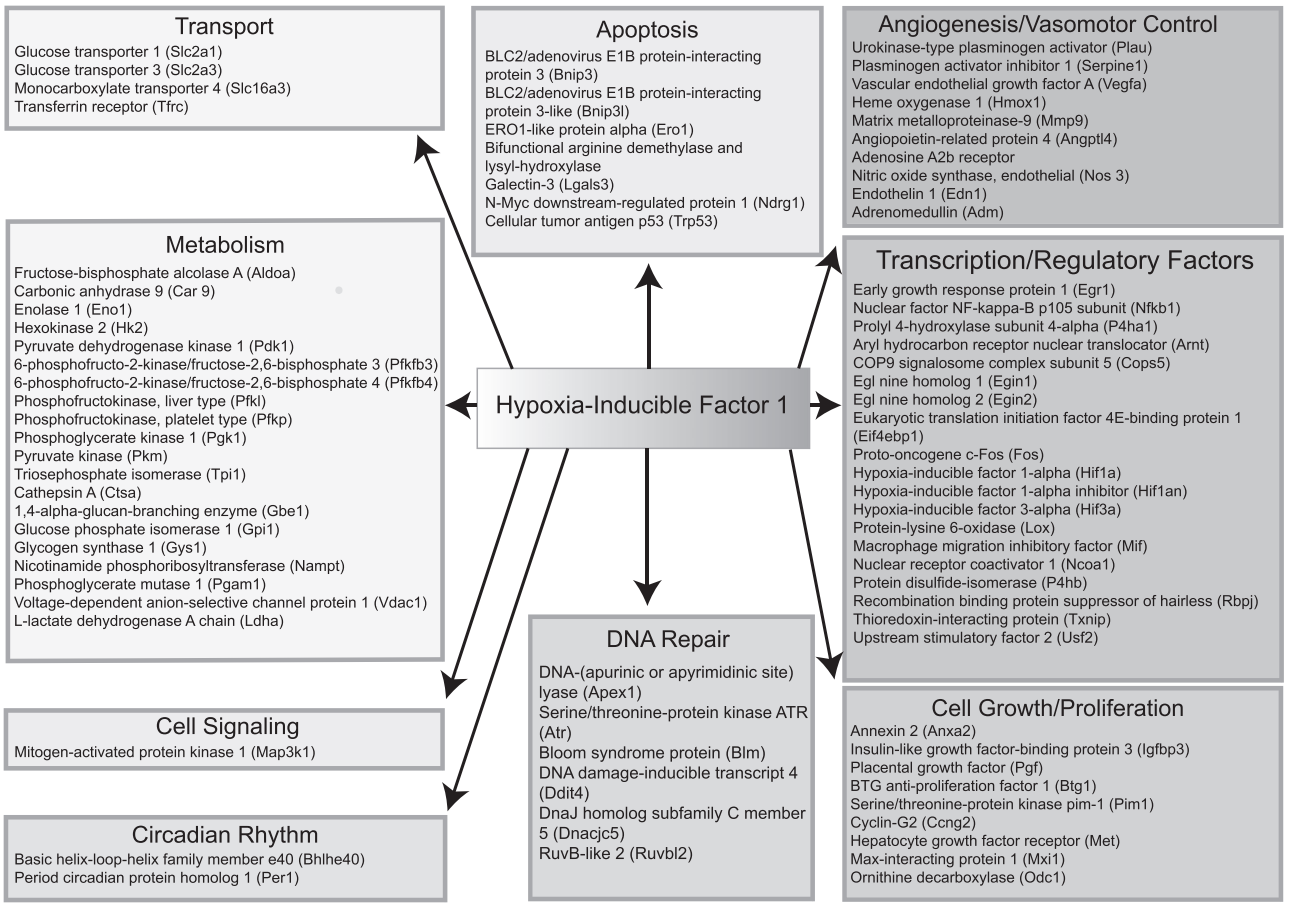

Transcript analysis using the Qiagen Hypoxia Signaling Pathway RT2 Profiler PCR Array. Shown are the arbitrary classifications of the 84 transcripts screened in this microarray. These classifications include genes playing a role in angiogenesis, transcription, cell growth, DNA repair, apoptosis, molecular transport, metabolism, cell signaling, and circadian rhythm. This figure serves to show the range of transcripts explored. This microarray is derived from transcripts whose expression is elevated under conditions of reduced oxygen (hypoxia) and is not designed to be tissue specific.

in metabolism, angiogenesis, synaptogenesis, and morphology. In Fig. 1, we highlight some of the distinct groups of transcripts explored in these analyses showing the diverse targets in HIF-1α regulated gene expression.

Studies from Holschneider and colleagues have investigated the changes that occur in regional cerebral blood flow (rCBF) with exercise in both normal rodents and models of neurodegenerative disorders [10,11]. Findings have shown that exercise leads to selective activation of rCBF in rodents engaged in exercise on a motorized treadmill or motorized running wheel. For example, significant activation is seen within a number of distinctive regions including the frontal cortex, dorsal striatum (STR), motor cortex, and vermis of the cerebellum. Other regions of the brain either show no change or a reduction in rCBF. Using rCBF changes as a guide, we hypothesize that these same regions with increased rCBF also show increased neuroplasticity. This is supported by molecular studies where the dorsal STR and prefrontal cortex (PFC) show activation of specific subunits of glutamate receptors of the AMPA subtype as well as electrophysiological parameters of plasticity (spontaneous excitatory postsynaptic current sEPSCs) and morphological changes with the restoration of dendritic spine density [5,6]. The association between changes in rCBF, and between molecular and morphological supports a hypothesis that exercise mediates circuit specific changes in neuroplasticity. In these studies, we focused on STR, the primary region of the basal ganglia involved in motor control, and expanded our exploration to include the PFC, where increased rCBF has been documented with exercise, and the ectorhinal cortex (ERC), a region of the brain where changes in rCBF in our exercise regimen is not observed.

The purpose of this study was to begin to identify the molecular mechanisms by which exercise, in the form of running on a motorized treadmill, leads to the activation of genes involved in metabolic and synaptic functions

that mediate neuroplasticity. We initiated this exploratory study using a commercially available microarray approach targeting a subset of genes mediate by the activation of HIF-1α in normal mice. We then validated a number of transcripts including HIF-1α in both a time course and a region-specific fashion based on anatomical regions of the brain where we have previously documented changes in rCBF and synaptogenesis. Our findings support the important role of metabolic changes within the brain with exercise that are consistent with circuit specific activation of brain connectivity.

Materials and methods

Animals

For all experiments conducted in this study, a total of 37 young adult (8–10 weeks) male C57BL/6J mice (Jackson Laboratory, Bar Harbor, Maine, USA) were used. Mice were housed five to a cage and acclimated to a 12 h shift in light/dark cycle (off at 07 : 00 h and on at 14 : 00 h) and exercise occurred during the normal awake period (typically between 09 : 00 and 12 : 00 h). For the initial quantitative PCR (qPCR) array screening, animals were randomly divided into five groups: (i) no exercise (NE), (ii) 1-day exercise (1DE), (iii) 3-day exercise (3DE), (iv) 5-day exercise (5DE), and (v) 10-day exercise (10DE). For subsequent qPCR validations, only NE, 1DE, and 5DE groups were analyzed ($n = 3$/group). For regional and temporal analysis of selected genes of interest animals were randomly divided into five groups ($n = 5$/group): (i) NE, (ii) 1DE, (iii) 5DE, (iv) 10DE, and (v) 5DE followed by 5 days of rest (5DR), For subsequent qPCR validations, only NE, 1DE, and 5DE groups were analyzed ($n = 3$/group). Mice were housed five to a cage and acclimated to a 12-h light/dark cycle. All experiments were conducted in accordance with the NIH Guide for the Care and Use of Laboratory Animals (NIH Publication No. 80–23, revised 1996) and were approved by the University of Southern California Institutional Animal Care and Use Committee.

Exercise regimen

The treadmill exercise protocol was conducted as previously described [2]. Briefly, prior to group randomization, all mice were challenged to maintain a forward position on the 45 cm treadmill belt (Columbus Instruments, Columbus, Ohio, USA) for 5 min at 5.0 m/min to ensure exercise competency. A metal bead curtain was used as a tactile incentive to encourage mice to maintain a forward position on the treadmill throughout the duration of the exercise session. Mice were exercised 1 h per day, 5 days per week. To control for any NE effects of treadmill running (handling, novel environment, noise, and vibration), NE animals were exposed to the treadmill apparatus without running for a time period equivalent to that of the exercise groups alternating between simply placing the cage of mice on the apparatus with the treadmill running (noise exposure) or placing NE mice in the treadmill apparatus with the treadmill stationary (environment exposure). Exercise mice started at an initial velocity of 10.0 ± 2.5 m/min that was incrementally increased to a maximum velocity of 18.5 ± 1.5 m/min by the second week. All animals were able to complete the exercise regimen successfully.

Preparation of tissues

To explore the temporal and regional patterns of expression of HIF-1α-dependent genes of interest, we analyzed their pattern of expression not only in the STR (circuits involved in motor behavior) but also in tissues from the PFC, which includes brain regions involved in cognition and consisting of the cingulate cortex, prelimbic cortex, and infralimbic cortex, and the ERC, a region of the brain involved in visual information processing. These tissue selections were based on brain regions where we have previously observed exercise-dependent elevation in regional rCBF (STR and PFC) or no change in rCBF (ERC) [12]. Tissues were collected from groups with NE, 1DE, 5DE, and 10DE. In addition, tissues were collected from a group of mice subjected to 5DE + 5DR to examine any retention of transcript expression changes. Mice were killed by cervical dislocation for fresh tissue collection. For microarray analysis, dorsal STR tissue was dissected in a block from a coronal slice: (i) Bregma +1.20 to +0.60 mm, (ii) 2.5 mm lateral from midline, (iii) dorsal–ventral, inferior to the corpus callosum and superior to the anterior commissure. All exercise samples were collected immediately after the animals' last training session. Brain tissue was dissected on ice and stored in RNAlater RNA Stabilization Reagent (Qiagen, Germantown, Maryland, USA) for later use. For qRT-PCR analysis of specific brain regions, fresh tissue was rapidly microdissected in blocks from (i) PFC consisting of the cingulate cortex, prelimbic cortex, and infralimbic cortex of the mouse (Bregma +2.0 to +1.4 mm anteroposterior, rostral to corpus callosum; ±1 mm mediolateral from midline to the corpus callosum, and −1.5 to −3.0 mm dorsoventral); (ii) STR (Bregma +1.2 to −0.2 mm anteroposterior, including tissue bordered ventrally by the anterior commissure, dorsally by the corpus callosum, medially by the lateral ventricle, and ±2.5 mm laterally from the midline); and (iii) ERC (Bregma −2.0 to −3.0 mm anteroposterior, laterally bounded by the edge of the cortex and extending 1 mm medially to the edge of the STR, and −3.0 to −3.5 mm dorsoventral) Tissues were placed in RNAlater Stabilization Solution (Qiagen, Germantown, Maryland, USA) and stored at 4°C overnight.

Microarray analysis and quantitative PCR of target transcripts

RNA was isolated and purified using a RNeasy Mini Kit (Qiagen, Hilden, Germany) strictly adhering to the manufacturer's suggested protocol. RNA concentration and purity were analyzed at a 1 : 10 dilution using a BioPhotometer (Eppendorf, Hamburg, Germany). The ratio between the absorbance at 260 and 280 nm was used to evaluate purity;

we assumed ratios between 1.8 and 2.0 to be pure. cDNA synthesis was performed using a QuantiTect Reverse Transcription Kit (Qiagen, Hilden, Germany) and the reaction product was stored at − 20°C for downstream qPCR applications. Gene expression data shown in Table 1 were generated using the Hypoxia Signaling Pathway RT2 Profiler PCR Array (cat. No. PAMM-032Z; Qiagen, Germantown, Maryland, USA) strictly following the manufacturer's suggested protocol. Samples were processed on an Eppendorf realplex2 Mastercycler and analyzed using realplex software (Eppendorf). Following our initial qPCR array screening analysis, gene expression of *Car9* (carbonic anhydrase 9) (5′-TGCTCCAAGTGTCTGCTCAG, 3′-CAGGTGCATCCTCTTCACTGG); *Hif1a* (5′-ACCTTCATCGGAAACTCCAAAG, 3′-CTGTTAGGCTGGGAAAAGTTAGG); *Ldha* (lactate dehydrogenase A) (5′-TGTCTCCAGCAAAGACTACTGT, 3′-GACTGTACTTGACAATGTTGGGA); *Slc2a1* (glucose transporter 1) (5′-CAGTTCGGCTATAACACTGGTG, 3′-GCCCCCGACAGAGAAGATG); and *Vegfa* (vascular endothelial growth factor) (5′-GCACATAGAGAGAATGAGCTTCC, 3′-CTCCGCTCTGAACAAGGCT) were analyzed with the SYBR Green PCR Kit (Qiagen, Hilden, Germany). All qPCR data was analyzed using the $2^{-\Delta\Delta C_t}$ method.

Statistical methods

All data are reported as mean ± SEM. The *F*-test was conducted to verify that the samples were normally distributed and have homogenous variances. The variances of the respective samples compared between the groups were statistically similar. For multiple comparisons, a one-way analysis of variance followed by Tukey's post-hoc test was used. A value of *P* less than 0.05 was considered statistically significant. Statistical significance is reported comparing groups to the NE group. Precise *P* values are reported when appropriate. Trends in expression changes are reported even if not statistically significant. All data were analyzed using GraphPad Prism 6.0 software (GraphPad Software, La Jolla, California, USA).

Results

The Qiagen Hypoxia Microarray examined 84 different transcripts from a wide spectrum of functional classifications. Figure 1 shows an arbitrary classification of these gene targets based on the most common function of proteins expressed by these transcripts. Microarray analysis shows significant changes, both increased and decreased, in a number of HIF-1α-dependent targets. Several transcript targets showed no change in expression. These outcomes in gene expression are listed in Table 1.

Figure 2 shows data from the time course analysis of transcript expression in STR tissue comparing NE with exercise days for 1DE or 5DE of HIF-1α (*Hif1a* gene) and a small subset of HIF-1α-dependent transcription targets including *Car9* (hypoxia-dependent marker), *Ldha*, *Slc2a1*, and *Vegf*. All transcripts showed increase in expression. Only the *Hif1a* showed a trend toward a statistically significant increase in expression at 1DE (1.38-fold) but there was a statistically significant increases at 5DE [1.74-fold, $F_{(2,6)} = 9.731$, $P = 0.0131$]. This transcript returned to near sedentary levels by 10DE (Table 1). Although there was a trend for increased expression in the other transcripts at 1 day they did not reach statistical significance because of small number and some variability, but greatest increases were seen at 5DE (*Car9*, 1.56-fold increase; *Ldha*, 1.33-fold increase; *Slc2a1*, 1.69-fold increase, and *Vegf*, 1.53-fold increase). Correlation analysis against Hif1a are shown in Fig. 2c (Car9), e (Ldha), g (Slc2a1), and i (Vegf). All correlations were positive.

These tissue selections were based on regions where we have previously observed exercise-dependent elevation in regional rCBF in the STR and PFC or no change in rCBF (ERC) [12]. Tissues were collected from groups with NE, 1DE, 5DE, and 10DE. In addition, tissues were collected from a group of mice subjected to 5DE + 5DR to examine any retention of transcript expression changes.

To explore the temporal and regional patterns of expression of HIF-1α-dependent genes of interest, we also analyzed their pattern of expression in the STR, then PFC and ERC. These data are shown in Fig. 3. We observed a statistically significant increase in expression of *Hif1a* transcript in the STR [$F_{(4,20)} = 17.28$, $P < 0.001$] at 5DE (1.65-fold) as well as in the PFC [$F_{(4,20)} = 9.650$, $P < 0.001$] at 5DE (1.82-fold) (Fig. 3a and b). There was a trend for an increased expression at 1DE (1.22-fold) in the PFC. Expression returned to baseline in the 10DE and 5DE + 5DR groups. The ERC did not show a statistically significant change in *Hif1a* expression (Fig. 3c) except there was a decrease in the 5DE + 5DR group of 0.79-fold [$F_{(4,20)} = 3.028$, $P = 0.042$].

Ldha gene expression was similar to previously observed in the microarray analysis. There was a statistically significant increase in expression at 5DE (1.28-fold) and 10DE (1.20-fold) in the STR [$F_{(4,20)} = 3.347$, $P = 0.030$] (Fig. 3e). In the PFC, there was a trend for increased expression at 5DE (1.26-fold) and returning to baseline at 10DE but this did not reach statistical significance [$F_{(4,20)} = 1.234$, $P = 0.328$] (Fig. 3d). There was no change in the level of *Ldha* transcript expression in the ERC (Fig. 3f).

Slc2a1 was similar to previously observed with increased expression at 5DE in both the STR and PFC. In the STR there was a trend for increased expression at 5DE (1.29-fold) and 10DE (1.59-fold) but this did not reach statistical significance [$F_{(4,20)} = 1.332$, $P = 0.292$] (Fig. 3h). In the PFC, there was a trend for increased expression at both 5DE (1.55-fold) and 10DE (1.50-fold) but this did not reach statistical significance [$F_{(4,20)} = 2.352$, $P = 0.089$] (Fig. 3g). In the ERC only the 10DE group

Table 1 Treadmill exercise activates a wide range of hypoxia-inducible factor 1α-related oxygen-sensitive genes

		Fold-change regulation				
Gene symbol	Protein	NE	1DE	3DE	5DE	10DE
Adm	Adrenomedullin	**1.00**	**1.64↑**	**3.78↑**	**1.42↑**	**1.69↑**
Adora2b	Adenosine A2b receptor	1.00	0.99	1.06	*0.63↓*	*0.63↓*
Aldoa	Fructose-bisphosphate aldolase A	1.00	0.85	*0.72↓*	*0.70↓*	*0.59↓*
Angpt4l	Angiopoietin-related protein 4	1.00	**3.01↑**	**2.45↑**	**2.35↑**	1.18
Ankrd37	Ankyrin repeat domain 37	1.00	0.88	1.06	*0.75↓*	*0.70↓*
Anxa2	Annexin 2	1.00	**1.57↑**	**1.29↑**	**1.54↑**	1.07
Apex1	DNA-(apurinic or apyrimidinic site) lyase	1.00	**1.29↑**	**1.36↑**	1.03	0.85
Arnt	Aryl hydrocarbon receptor nuclear translocator	1.00	1.08	1.01	0.82	*0.80↓*
Atr	Serine/threonine-protein kinase ATR	1.00	**2.30↑**	*0.59↓*	**0.44↓**	0.92
Bhlhe40	Basic helix–loop–helix family member e40	1.00	**1.36↑**	**1.39↑**	*0.65↓*	*0.69↓*
Blm	Bloom syndrome protein	1.00	1.02	0.95	1.04	*0.80↓*
Bnip3	BLC2/adenovirus E1B protein-interacting protein 3	1.00	1.14	0.97	*0.75↓*	1.00
Bnip3l	BLC2/adenovirus E1B protein-interacting protein 3-like	1.00	1.05	*0.76↓*	0.81	*0.75↓*
Btg1	BTG antiproliferation factor 1	1.00	**1.60↑**	*1.23↑*	*1.29↑*	1.04
Car9	Carbonic anhydrase 9	1.00	*1.21↑*	*1.34↑*	**1.56↑**	1.14
Ccng2	Cyclin-G2	1.00	0.98	1.00	0.88	*0.76↓*
Cops5	COP9 signalosome complex subunit 5	1.00	0.97	**1.29↑**	1.18	0.90
Ctsa	Cathepsin A	1.00	1.14	**1.21↑**	1.01	1.09
Ddit4	DNA damage-inducible transcript 4	1.00	**2.19↑**	**2.36↑**	**1.89↑**	*1.40↑*
Dnajc5	DnaJ homolog subfamily C member 5	1.00	*1.25↑*	0.90	*0.73↓*	0.81
Edn1	Endothelin 1	1.00	*0.73↓*	**0.42↓**	*0.69↓*	**0.49↓**
Egln1	Egl nine homolog 1	1.00	1.09	0.96	1.04	*0.80↓*
Egln2	Egl nine homolog 2	1.00	*1.20↑*	*1.43↑*	1.12	0.85
Egr1	Early growth response protein 1	1.00	1.01	0.88	0.82	0.82
Eif4ebp1	Eukaryotic translation initiation factor 4E-binding protein 1	1.00	1.12	**1.69↑**	1.17	1.04
Eno1	Enolase 1	1.00	0.94	1.19	0.94	1.04
Ero1	ERO1-like protein α	1.00	*1.39↑*	1.13	1.19	0.90
Fos	Proto-oncogene c-Fos	1.00	**3.76↑**	**1.79↑**	**1.78↑**	*1.42↑*
Gbe1	1,4-α-glucan-branching enzyme	1.00	*0.61↓*	*0.59↓*	*0.62↓*	**0.45↓**
Gpi1	Glucose phosphate isomerase 1	1.00	1.18	0.95	1.01	0.91
Gys1	Glycogen synthase 1	1.00	1.14	*1.32↓*	*1.39↑*	*1.29↓*
Hif1a	Hypoxia-inducible factor 1α	1.00	*1.38↑*	*1.41↑*	**1.74↑**	0.82
Hif1an	Hypoxia-inducible factor 1α inhibitor	1.00	0.92	0.94	*0.80↓*	0.94
Hif3a	Hypoxia-inducible factor 3α	1.00	1.11	1.01	1.07	1.10
Hk2	Hexokinase 2	1.00	*1.29↑*	1.06	0.86	0.98
Hmox1	Heme oxygenase 1	1.00	1.06	1.11	0.88	0.90
Ier3	Radiation-inducible immediate-early gene IEX1	1.00	1.06	0.91	0.90	1.00
Igfbp3	Insulin-like growth factor-binding protein 3	1.00	*1.38↑*	**2.00↑**	**1.61↑**	1.17
Jmjd6	Bifunctional arginine demethylase and lysyl-hydroxylase JMJD6	1.00	*1.27↑*	*1.25↑*	*1.34↑*	1.01
Ldha	L-lactate dehydrogenase A chain	1.00	1.17	1.18	*1.33↑*	1.01
Lgals3	Galectin-3	1.00	**2.33↑**	**3.18↑**	**3.32↑**	*1.45↑*
Lox	Protein-lysine 6-oxidase	1.00	**2.23↑**	**1.77↑**	**2.60↑**	1.07
Map3k1	Mitogen-activated protein kinase 1	1.00	1.13	*0.66↓*	*0.76↓*	*0.54↓*
Met	Hepatocyte growth factor receptor	1.00	**1.88↑**	1.16	0.95	0.91
Mif	Macrophage migration inhibitory factor	1.00	1.08	1.17	1.18	0.95
Mmp9	Matrix metalloproteinase-9	1.00	**1.75↑**	1.16	**1.93↑**	1.00
Mxi1	Max-interacting protein 1	1.00	1.07	0.99	0.81	0.85
Nampt	Nicotinamide phosphoribosyltransferase	1.00	*1.44↑*	1.01	1.15	0.82
Ncoa1	Nuclear receptor coactivator 1	1.00	0.86	0.94	1.02	0.90
Ndrg1	*N*-Myc downstream-regulated protein 1	1.00	*1.29↑*	1.03	1.18	0.95
Nfkb1	Nuclear factor NF-kappa-B p105 subunit	1.00	1.09	0.90	1.05	*0.78↓*
Nos3	Nitric oxide synthase, endothelial	1.00	*1.29↑*	*1.47↑*	0.89	*1.40↑*
Odc1	Ornithine decarboxylase	1.00	*1.24↑*	1.09	0.97	0.92
P4ha1	Prolyl 4-hydroxylase subunit 4α	1.00	1.16	1.05	1.10	0.93
P4hb	Protein disulfide-isomerase	1.00	1.16	*1.28↑*	0.81	*0.75↓*
Pdk1	Pyruvate dehydrogenase kinase 1	1.00	0.93	1.01	*0.78↓*	*0.54↓*
Per1	Period circadian protein homolog 1	1.00	**1.58↑**	**1.62↑**	1.11	0.97
Pfkfb3	6-phosphofructo-2-kinase/fructose-2,6-bisphosphate 3	1.00	**1.60↑**	1.14	0.97	1.06
Pfkfb4	6-phosphofructo-2-kinase/fructose-2,6-bisphosphate 4	1.00	0.92	0.81	0.95	*0.76↓*
Pfkl	Phosphofructokinase, liver type	1.00	0.92	0.95	0.95	0.90
Pfkp	Phosphofructokinase, platelet type	1.00	0.98	0.90	0.88	0.82
Pgam1	Phosphoglycerate mutase 1	1.00	0.90	1.03	1.13	0.95
Pgf	Placental growth factor	1.00	1.06	*1.40↑*	0.91	0.90
Pgk1	Phosphoglycerate kinase 1	1.00	*1.31↑*	*1.21↑*	1.14	0.95
Pim1	Serine/threonine-protein kinase pim1	1.00	*1.23↑*	**1.56↑**	1.06	1.16
Pkm	Pyruvate kinase	1.00	*1.38↑*	**1.57↑**	1.06	0.91
Plau	Urokinase-type plasminogen activator	1.00	**0.47↓**	**0.37↓**	**0.43↓**	**0.30↓**
Rbpj	Recombination binding protein suppressor of hairless	1.00	*1.45↑*	*1.21↑*	1.01	1.04
Ruvbl2	RuvB-like 2	1.00	0.99	0.82	0.89	0.95
Serpine1	Plasminogen activator inhibitor 1	1.00	**1.66↑**	*1.43↑*	*1.38↑*	0.86
Slc16a3	Monocarboxylate transporter 4	1.00	0.92	1.11	*1.21↑*	0.96

Table 1 (*continued*)

		Fold-change regulation				
Gene symbol	Protein	NE	1DE	3DE	5DE	10DE
Slc2a1	Glucose transporter 1	1.00	1.16	*1.47*↑	**1.69**↑	1.05
Slc2a3	Glucose transporter 3	1.00	1.14	1.13	1.07	0.93
Tfrc	Transferrin receptor	1.00	*1.26*↑	0.97	0.85	0.88
Tpi1	Triosephosphate isomerase	1.00	1.17	0.92	0.90	0.96
Trp53	Cellular tumor antigen p53	1.00	1.03	0.91	0.82	*0.80*↓
Txnip	Thioredoxin-interacting protein	1.00	**2.64**↑	**1.88**↑	**2.53**↑	*1.44*↑
Usf2	Upstream stimulatory factor 2	1.00	*1.30*↑	1.09	0.88	0.99
Vdac1	Voltage-dependent anion-selective channel protein 1	1.00	*1.26*↑	**1.77**↑	*1.45*↑	0.93
Vegfa	Vascular endothelial growth factor A	1.00	*1.23*↑	*1.30*↑	**1.53**↑	1.06

Microarray results of mouse Hypoxia Signaling Profiler PCR Array. Transcripts from the Hypoxia Signaling Pathway RT2 Profiler PCR Array are tabulated in alphabetical order of gene name. Changes relative to the NE group were based on arbitrary criteria of fold changes. Increased transcript expression is indicated with italics and upwards arrow (↑) for a 1.20- to 1.49-fold increase and bold text and upwards arrow (↑) for an increases of greater than 1.50-fold. Reduced transcript expression is indicated with italics and a downwards arrow (↓) for a decrease between 0.80- and 0.51-fold and bold text and a downwards arrow (↓) for a decrease between 0.3 and 0.49-fold. A range of 0.81- to 1.19-fold change was considered as no change in transcript expression. Results from this microarray analysis were used to select a subset of transcript for temporal and region-specific expression analysis with exercise. Transcripts for further analysis included *hif1a*, *Car9*, *Ldha*, *Slc2a1*, *Slc16a1*, *Slc16a7*, and *Vegfa*.
1DE, 1-day exercise; 3DE, 3-day exercise; 5DE, 5-day exercise; 10DE, 10-day exercise; NE, no exercise.

(1.51-fold) showed a statistically significant increase in expression of *Slc2a1* (Fig. 3i) [$F_{(4,20)} = 2.792$, $P = 0.043$].

Slc16a1 showed a statistically significant increase in transcript expression at the 5DE (1.32-fold), 10DE (1.47-fold), and 5DE + 5DR (1.45-fold) groups [$F_{(4,20)} = 8.82$, $P = 0.001$] in the STR and at 5DE (1.37-fold) and 5DE + 5DR (1.69-fold) groups in the PFC [$F_{(4,20)} = 9.312$, $P < 0.001$] (Fig. 3j and k). In the ERC, there was a statistically significant increase in the 10DE group (2.06-fold) and the 5DE + 5DR group (2.00-fold) [$F_{(4,20)} = 2.792$, $P = 0.054$] (Fig. 3l).

Slc16a7 transcript showed a statistically significant increase in expression at only the 5DE group (1.28-fold) in the [$F_{(4,20)} = 4.089$, $P < 0.014$] (Fig. 3n). There was no change in the level of *Slc16a7* transcript expression in the PFC [$F_{(4,20)} = 0.962$, $P = 0.450$) (Fig. 3m) or ERC [$F_{(4,20)} = 0.685$, $P = 0.611$] (Fig. 3o).

Vegf transcript showed a statistically significant increase in expression in the STR at 1DE (1.44-fold) and 5DE (1.81-fold) [$F_{(4,20)} = 10.53$, $P < 0.001$] returning to near baseline at 10DE (Fig. 3q). There was no statistically significant change in *Vegf* transcript expression in the PFC [$F_{(4,20)} = 1.208$, $P = 0.331$] (Fig. 3p) and ERC [$F_{(4,20)} = 0.458$, $P = 0.766$] (Fig. 3r).

Discussion

Evidence is accumulating that different forms of exercise engage specific anatomical regions and circuits. This is elegantly displayed in recent reports by Holschneider and colleagues where they utilized the tracer [^{14}C]-iodoantipyrine with functional brain mapping and showed that in both normal rodents and in models of disease different forms of exercise can alter rCBF with increased blood flow observed in regions of the brain whose circuits are engaged in specific motor behaviors [10–14]. For example, comparing skilled versus aerobic forms of exercise on a motorized running wheel (Lafayette Instrument, Lafayette, Indiana, USA) implicated the activation of the frontal cortex, dorsal STR, motor cortex, and cerebellar vermis with increased rCBF.

The transcription factor HIF-1α plays a critical role in response to metabolic demands in the brain. In its inactive form, HIF-1α resides within the cytoplasm as part of a multimeric protein complex. Initially identified as a global regulatory component in cancer cells to better understand metabolic homeostasis, HIF-1α has emerged as a potentially important component in neurons in maintaining homeostasis and responding to stressful conditions or injury. Activation occurs in response to a number of molecular perturbations including reduced oxygen (hypoxia), increased reactive oxygen species, elevated levels of metabolites and small molecules including glutamate and potassium [9]. HIF-1α targets a large catalog of genes several subsets that may be differentially expressed based on cell phenotype, specificity of the molecular triggers, and activation of cofactors that may influence expression. Although the precise trigger for HIF-1α activation by exercise in specific neuronal circuits is not known, it is likely because of a combination of these factors all of which are elevated with activity. As increased neuronal activity is associated with increased metabolic demand and subsequent hypoxic conditions as oxygen stores are utilized, we set out to explore if such a mechanism may be engaged in a circuit specific manner with exercise.

The major findings from these studies are that within the normal rodent brain, exercise in the form of running on a motorized treadmill, leads to the early activation of the transcriptional factor HIF-1α and several of its reported targets. In addition, we found that this exercise-dependent activation of HIF-1α-dependent targets occurs in a fashion that supports a temporal and region-specific mode of action rather than simply global activation throughout the brain. Specifically, within regions of the brain that display

Fig. 2

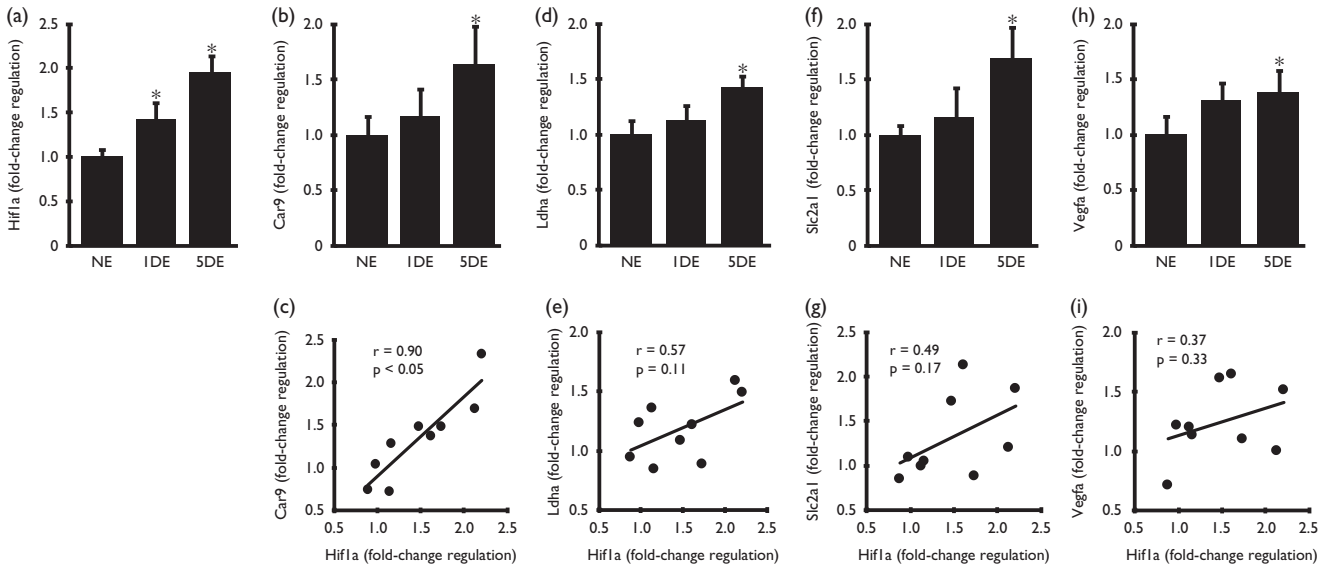

Exercise leads to the activation of hypoxia-inducible factor 1α (HIF-1α) and several of its downstream transcript targets. Results from quantitative RT-PCR in (a) show the increased expression of HIF-1α after 1-day exercise (1DE) and 5-day exercise (5DE) compared with no exercise (NE) groups in the dorsal striatum. Other transcriptional targets examined by quantitative RT-PCR also show elevated expression as well as positive correlation compared with HIF-1α including *Car9* (carbonic anhydrase 9) (b, c), *Ldha* (lactate dehydrogenase A) (d, e), *Slc2a1* (glucose transporter 1) (f, g), and *Vegfa* (vascular endothelial growth factor) (h, i). $^*P < 0.05$, significance. $N = 3$ mice per group.

elevation of rCBF with exercise, including the STR and PFC, we observe an association in the expression of several HIF-1α-dependent transcripts. Within regions of the brain where exercise-induced rCBF elevation is not observed such as the ERC, we do not observe such changes in transcript activation. Although this survey is limited in scope to a small number of brain regions, it does, however, support the hypothesis that exercise leads to the activation of a limited number of neuronal circuits and colocalize with increased neuroplasticity. This is consistent with previous studies showing that in rodent models of dopamine-depletion with exercise we observe changes in the dorsal including increased synaptic spine density on medium spiny neurons [5], increased evoked dopamine release and reduced dopamine decay [4], altered glutamatergic neurotransmission including subunit expression and evoked excitatory postsynaptic currents and potentials [6,7], as well as restoration of the depletion of the dopamine D2 receptor [15,16].

Although narrow in scope, this study serves as starting point to begin to understand the mechanisms by which exercise influences circuit specific neuroplasticity. The *Car9* gene encodes carbonic anhydrase, an enzyme that catalyzes the conversion of carbon dioxide (CO_2) and water (H_2O) to carbonic acid (HCO_3^-) and a proton (H^+). This enzyme is sensitive to hypoxia and its expression is dependent on HIF-1α [17]. For these studies it served as a reliable marker to validate the potential link between exercise and hypoxia as an activator of transcript expression. The *Ldha* gene encodes the enzyme lactate dehydrogenase that catalyzes the interconversion of lactate and pyruvate with one potential role in converting astrocytic sources of lactate to pyruvate in neurons for inclusion into the tricarboxylic cycle [18]. The *Slc2a1* gene encodes the glucose transporter type 1 that is distributed in a wide spectrum of tissues including the endothelial cells responsible for the blood–brain barrier and whose expression is elevated with increased cellular glucose metabolism [19]. The *Vegf* gene encodes the signaling protein VEGF whose induction under conditions of hypoxia leads to the promotion of vascularization and increased blood flow [20]. Elevated VEGF protein has been shown to occur with exercise and is region specific, occurring within activated sites within the brain including the hippocampus [21]. Together, the pattern of expression of these four transcripts provide support of the hypothesis that specific forms of behavioral activity, such as treadmill running, leads to the activation of specific neuronal circuits in restricted regions of the brain that subserve motor behavior.

The benefits of exercise on generalized cardiovascular fitness and health are undeniable both for their short-term neurological effects on improving cognition and long-term impact providing protection from degenerative disorders including Alzheimer's disease and PD [22,23]. The neuroprotective mechanisms, while largely unknown, have focused on elevated expression and distribution of neurotrophic factors especially brain-derived neurotrophic factor,

Fig. 3

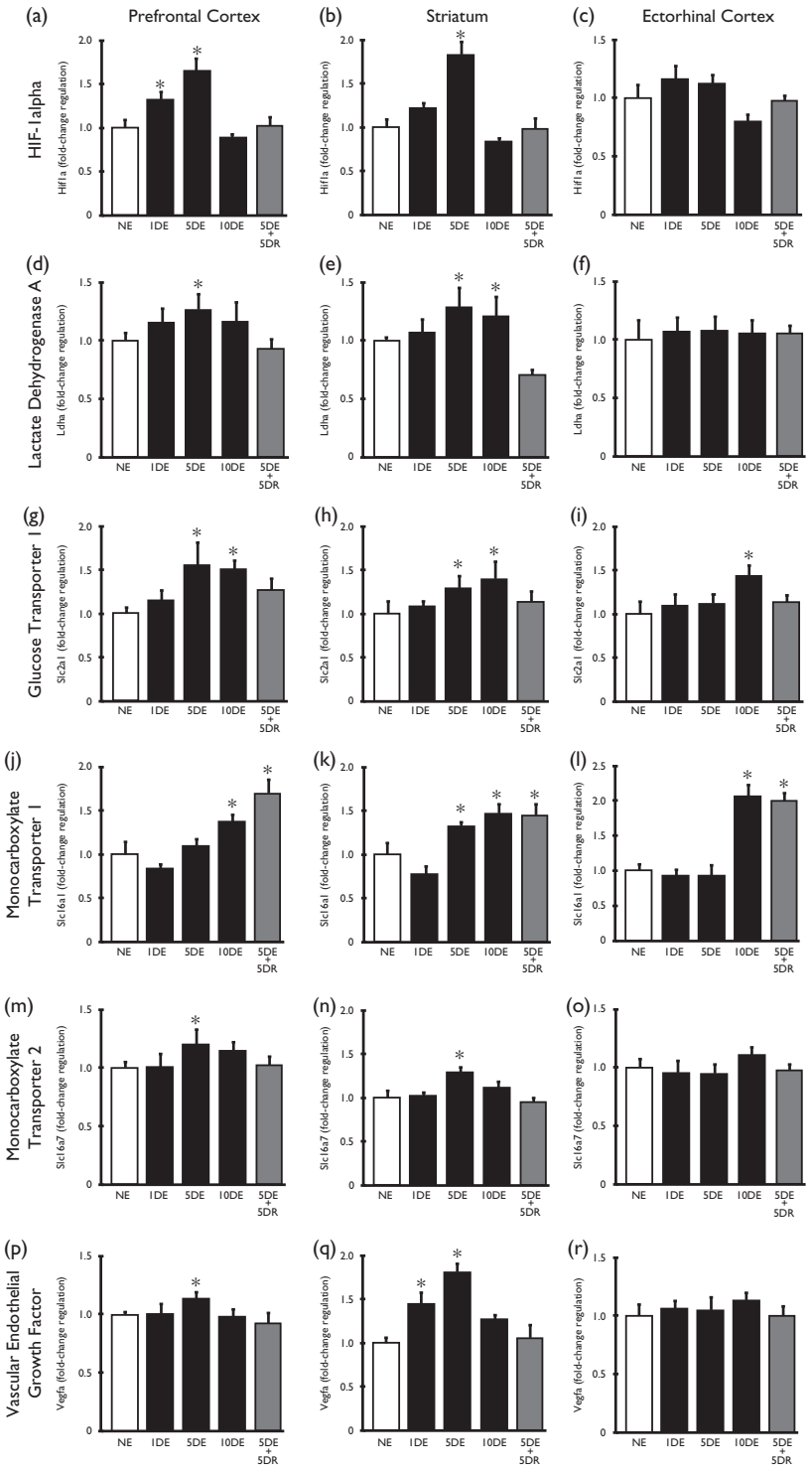

Exercise leads to temporal and regional differences in the pattern of expression of hypoxia-inducible factor 1α (HIF-1α) and in a subset of its transcription targets. Tissues from the prefrontal cortex, striatum, and ectorhinal cortex were collected and analyzed for gene expression by quantitative RT-PCR in groups with no exercise (NE, white bars), 1-day exercise (1DE), 5-day exercise (5DE), or 10-day exercise (10DE) (black bars), and 5DE followed by 5 days of rest (5DR, gray bars). Transcript analysis included *Hif1a* (hypoxia-inducible factor 1α), *Ldha* (lactate dehydrogenase A), *Slc2a1* (glucose transporter 1), *Slc16a1* (monocarboxylate transporter 1), *Slc16a7* (monocarboxylate transporter 2), and *Vegf* (vascular endothelial growth factor). Statistical analysis of significant changes was made versus the NE group. $^*P < 0.05$, significant. $N = 5$ mice per group.

increased arterial blood flow, and neuronal strengthening [24]. Smeyne *et al.* [25] reported differential roles of HIF-1α and HIF-2α in neuroprotection and neuronal survival, respectively, of dopaminergic neurons in a model of dopamine-depletion. HIF-1α plays an important link between exercise, angiogenesis, metabolism, and synaptogenesis [26]; however, it may be one of several mechanisms activated by exercise in both the normal and injured brain.

Conclusion

Together, both pharmacological and nonpharmacological approaches are emerging as critical components of the standard of care in treating these brain disorders with the goal of improved quality of life and potential disease modification [27,28]. Findings from these studies show that exercise leads to the activation of a subset of HIF-1α-dependent mRNA transcripts within the STR. Further analysis of changes in transcript expression supports the hypothesis that these changes occur, in part, in a circuit specific fashion and may be associated with exercise-enhanced neuroplasticity in those circuits engaged in exercise. These findings support the potentially important role of targeted exercise and physical activity to engage those circuits compromised or at risk in both aging and in neurodegenerative disorders.

Acknowledgements

A special thanks to friends of the USC Parkinson's Disease Research Group including George and Mary Lou Boone, Walter and Susan Doniger, Edna and John Ball, Team Parkinson, and the family of Don Gonzalez Barrera.

The authors also acknowledge the support of the NINDS RO1 NS44327, US Army NETRP (grant no. W81XWH-17-PRP-IIRA), the National Parkinson's Foundation, the Confidence Foundation, and the Plotkin Family Foundation.

Conflicts of interest

There are no conflicts of interest.

References

1 Stefanko DP, Shah VD, Yamasaki WK, Petzinger GM, Jakowec MW. Treadmill exercise delays the onset of non-motor behaviors and striatal pathology in the CAG140 knock-in mouse model of Huntington's disease. *Neurobiol Dis* 2017; **105**:15–32.

2 Fisher BE, Petzinger GM, Nixon K, Hogg E, Bremmer S, Meshul CK, *et al.* Exercise-induced behavioral recovery and neuroplasticity in the 1-methyl-4-phenyl-1,2,3,6-tetrahydropyridine-lesioned mouse basal ganglia. *J Neurosci Res* 2004; **77**:378–390.

3 Fisher BE, Li Q, Nacca A, Salem GJ, Song J, Yip J, *et al.* Treadmill exercise elevates striatal dopamine D2 receptor binding potential in patients with early Parkinson's disease. *Neuroreport* 2013; **24**:509–514.

4 Petzinger GM, Walsh JP, Akopian G, Hogg E, Abernathy A, Arevalo P, *et al.* Effects of treadmill exercise on dopaminergic transmission in the 1-methyl-4-phenyl-1,2,3,6-tetrahydropyridine-lesioned mouse model of basal ganglia injury. *J Neurosci* 2007; **27**:5291–5300.

5 Toy WA, Petzinger GM, Leyshon BJ, Akopian GK, Walsh JP, Hoffman MV, *et al.* Treadmill exercise reverses dendritic spine loss in direct and indirect striatal medium spiny neurons in the 1-methyl-4-phenyl-1,2,3,6-tetrahydropyridine (MPTP) mouse model of Parkinson's disease. *Neurobiol Dis* 2014; **63**:201–209.

6 Kintz N, Petzinger GM, Akopian G, Ptasnik S, Williams C, Jakowec MW, *et al.* Exercise modifies alpha-amino-3-hydroxy-5-methyl-4-isoxazolepropionic acid receptor expression in striatopallidal neurons in the 1-methyl-4-phenyl-1,2,3,6-tetrahydropyridine-lesioned mouse. *J Neurosci Res* 2013; **91**:1492–1507.

7 VanLeeuwen JE, Petzinger GM, Walsh JP, Akopian GK, Vuckovic M, Jakowec MW. Altered AMPA receptor expression with treadmill exercise in the 1-methyl-4-phenyl-1,2,3,6-tetrahydropyridine-lesioned mouse model of basal ganglia injury. *J Neurosci Res* 2010; **88**:650–668.

8 Dienel GA. Brain glucose metabolism: integration of energetics with function. *Physiol Rev* 2019; **99**:949–1045.

9 Sharp FR, Bernaudin M. HIF1 and oxygen sensing in the brain. *Nat Rev Neurosci* 2004; **5**:437–448.

10 Wang Z, Stefanko DP, Guo Y, Toy WA, Petzinger GM, Jakowec MW, *et al.* Evidence of functional brain reorganization on the basis of blood flow changes in the CAG140 knock-in mouse model of Huntington's disease. *Neuroreport* 2016; **27**:632–639.

11 Wang Z, Myers KG, Guo Y, Ocampo MA, Pang RD, Jakowec MW, *et al.* Functional reorganization of motor and limbic circuits after exercise training in a rat model of bilateral parkinsonism. *PLoS ONE* 2013; **8**:e80058.

12 Yang J, Sadler TR, Givrad TK, Maarek JM, Holschneider DP. Changes in brain functional activation during resting and locomotor states after unilateral nigrostriatal damage in rats. *Neuroimage* 2007; **36**:755–773.

13 Wang Z, Guo Y, Myers KG, Heintz R, Peng YH, Maarek JM, *et al.* Exercise alters resting-state functional connectivity of motor circuits in parkinsonian rats. *Neurobiol Aging* 2015; **36**:536–544.

14 Wang Z, Guo Y, Myers KG, Heintz R, Holschneider DP. Recruitment of the prefrontal cortex and cerebellum in parkinsonian rats following skilled aerobic exercise. *Neurobiol Dis* 2015; **77**:71–87.

15 Fisher BE, Wu AD, Salem GJ, Song J, Lin CH, Yip J, *et al.* The effect of exercise training in improving motor performance and corticomotor excitability in people with early Parkinson's disease. *Arch Phys Med Rehabil* 2008; **89**:1221–1229.

16 Vuckovic MG, Li Q, Fisher B, Nacca A, Leahy RM, Walsh JP, *et al.* Exercise elevates dopamine D2 receptor in a mouse model of Parkinson's disease: in vivo imaging with [(1)F]fallypride. *Mov Disord* 2010; **25**:2777–2784.

17 Olive PL, Aquino-Parsons C, MacPhail SH, Liao SY, Raleigh JA, Lerman MI, *et al.* Carbonic anhydrase 9 as an endogenous marker for hypoxic cells in cervical cancer. *Cancer Res* 2001; **61**:8924–8929.

18 Laughton JD, Bittar P, Charnay Y, Pellerin L, Kovari E, Magistretti PJ, *et al.* Metabolic compartmentalization in the human cortex and hippocampus: evidence for a cell- and region-specific localization of lactate dehydrogenase 5 and pyruvate dehydrogenase. *BMC Neurosci* 2007; **8**:35.

19 Torp R, Hoover F, Danbolt NC, Storm-Mathisen J, Ottersen OP. Differential distribution of the glutamate transporters GLT1 and rEAAC1 in rat cerebral cortex and thalamus: an in situ hybridization analysis. *Anat Embryol (Berl)* 1997; **195**:317–326.

20 Tang K, Xia FC, Wagner PD, Breen EC. Exercise-induced VEGF transcriptional activation in brain, lung and skeletal muscle. *Respir Physiol Neurobiol* 2010; **170**:16–22.

21 Fabel K, Tam B, Kaufer D, Baiker A, Simmons N, Kuo CJ, *et al.* VEGF is necessary for exercise-induced adult hippocampal neurogenesis. *Eur J Neurosci* 2003; **18**:2803–2812.

22 Chen H, Zhang SM, Schwarzschild MA, Hernan MA, Ascherio A. Physical activity and the risk of Parkinson disease. *Neurology* 2005; **64**:664–669.

23 Ohman H, Savikko N, Strandberg TE, Kautiainen H, Raivio MM, Laakkonen ML, *et al.* Effects of exercise on cognition: the Finnish Alzheimer Disease Exercise Trial: a randomized, controlled trial. *J Am Geriatr Soc* 2016; **64**:731–738.

24 Cotman CW, Berchtold NC, Christie LA. Exercise builds brain health: key roles of growth factor cascades and inflammation. *Trends Neurosci* 2007; **30**:464–472.

25 Smeyne M, Sladen P, Jiao Y, Dragatsis I, Smeyne RJ. HIF1alpha is necessary for exercise-induced neuroprotection while HIF2alpha is needed for dopaminergic neuron survival in the substantia nigra pars compacta. *Neuroscience* 2015; **295**:23–38.

26 Greer SN, Metcalf JL, Wang Y, Ohh M. The updated biology of hypoxia-inducible factor. *EMBO J* 2012; **31**:2448–2460.

27 Petzinger GM, Fisher BE, McEwen S, Beeler JA, Walsh JP, Jakowec MW. Exercise-enhanced neuroplasticity targeting motor and cognitive circuitry in Parkinson's disease. *Lancet Neurol* 2013; **12**:716–726.

28 Jakowec MW, Wang Z, Holschneider D, Beeler J, Petzinger GM. Engaging cognitive circuits to promote motor recovery in degenerative disorders. Exercise as a learning modality. *J Hum Kinet* 2016; **52**:35–51.

Received: 6 February 2019 | Revised: 29 March 2019 | Accepted: 3 April 2019

DOI: 10.1002/jnr.24430

RESEARCH ARTICLE

Exercise induces region-specific remodeling of astrocyte morphology and reactive astrocyte gene expression patterns in male mice

Adam J. Lundquist[1] | Jacqueline Parizher[1] | Giselle M. Petzinger[1,2] | Michael W. Jakowec[1,2]

[1]Department of Neurology, University of Southern California, Los Angeles, California

[2]Division of Biokinesiology and Physical Therapy, University of Southern California, Los Angeles, California

Correspondence
Adam J. Lundquist, Department of Neurology, University of Southern California, Los Angeles, CA 90033.
Email: alundqui@usc.edu

Funding information
Congressionally Directed Medical Research Programs, Grant/Award Number: W81XWH-04-1-0444

Abstract

Astrocytes are essential mediators of many aspects of synaptic transmission and neuroplasticity. Exercise has been demonstrated to induce neuroplasticity and synaptic remodeling, such as through mediating neurorehabilitation in animal models of neurodegeneration. However, the effects of exercise on astrocytic function, and how such changes may be relevant to neuroplasticity remain unclear. Here, we show that exercise remodels astrocytes in an exercise- and region-dependent manner as measured by GFAP and SOX9 immunohistochemistry and morphological analysis in male mice. Additionally, qRT-PCR analysis of reactive astrocyte gene expression showed an exercise-induced elevation in brain regions known to be activated by exercise. Taken together, these data demonstrate that exercise actively modifies astrocyte morphology and drives changes in astrocyte gene expression and suggest that astrocytes may be a central component to exercise-induced neuroplasticity and neurorehabilitation.

KEYWORDS

astrocyte, exercise, GFAP, morphology, plasticity, RRID:AB_10013382, RRID:AB_143157, RRID:AB_2239761, RRID:AB_2534017, RRID:AB_2535792

1 | INTRODUCTION

Once thought to be limited to a structural and developmental role, glia are now known to be involved in maintaining brain homeostasis and actively engaging in experience-dependent neuroplasticity (Khakh & Sofroniew, 2015). Astrocytes are a diverse class of glia found throughout the mammalian brain. They play a central role in several important processes including establishing and regulating the blood brain barrier, modulating blood flow, regulating synaptogenesis and physical remodeling of synapses, and participating in neuronal bioenergetics by providing key substrates for metabolism (Abbott, Rönnbäck, & Hansson, 2006; Chung et al., 2013; Eroglu & Barres, 2010; Suzuki et al., 2011). Such synergism between astrocytes and the neurons they contact reflects the close relationship that exists between these two cell types in regulating synaptic activity.

Neuroplasticity can simply be defined as changes in synaptic strength and structure in response to experience (Petzinger et al., 2015). One form of experience that can initiate neuroplasticity is physical activity or exercise. Studies from our laboratories have shown that exercise, in the form of intensive treadmill running, can lead to regional and circuit-specific changes in synaptic connectivity, blood flow, and behavior in normal rodents as well as neurotoxin-induced and genetic models of neurodegenerative disorders (Petzinger et al., 2013; Wang et al., 2013). Furthermore, others have shown that exercise leads to changes in astrocyte function, including glutamate-glutamine recycling (Bernardi et al., 2013),

Edited by Bradley Kerr.

All peer review communications can be found with the online version of the article.

Significance

Astrocytes are essential to neuroplasticity, or the brain's ability to dynamically change. Aerobic exercise is known to induce neuroplasticity in specific brain regions, but how astrocytes respond to exercise in these regions is relatively unknown. Here, we show that astrocytes can undergo structural changes and differentially regulate gene expression in response to exercise. This work demonstrates that aerobic exercise can modify astrocytes in a dynamic and region-specific fashion and provides additional insight into the effect of exercise on brain structure and function.

aquaporin-4 expression (Brockett, LaMarca, & Gould, 2015), and hippocampal proliferation (de Senna et al., 2017). Such findings clearly implicate a role for astrocytes in mediating exercise-dependent plasticity.

The purpose of this study was to build upon our findings on the mechanisms of neuroplasticity with exercise and to explore the potential role that astrocytes may play. Interestingly, studies have shown that exercise can cause astrocytic response, termed astrogliosis, based on the elevation of glial fibrillary acidic protein (GFAP) expression (Li et al., 2005), while others reporting its suppression (Bernardi et al., 2013). Such differences in the characterization of the astrocytic response to exercise may be partially explained by astrocyte heterogeneity (Khakh & Sofroniew, 2015), differences in the type of exercise intervention, including intensity and type (voluntary vs. forced) (Kinni et al., 2011), or by strain- or species-dependent difference in exercise ability (Billat, Mouisel, Roblot, & Melki, 2005). In this study, we utilized GFAP and SOX9 (*SRY*-related HMG-box gene 9, an astrocyte-specific nuclear marker) immunohistochemistry to determine changes in astrocyte morphology and proliferation in regions of the healthy mouse brain that display neuroplasticity in response to running on a motorized treadmill. Selection of brain regions of interest was based on our previous studies mapping exercise-induced changes in regional cerebral blood flow (rCBF), and synaptogenesis and synaptic plasticity (Kintz et al., 2013; Wang et al., 2013). Furthermore, we used quantitative RT-PCR to examine astrocyte-specific transcript expression of genes involved in metabolic responses to exercise. Together, these studies aimed to determine if exercise leads to changes in astrocyte morphology, proliferation, and gene expression; and to understand if such changes are associated with region specific responses in neuroplasticity, or simply reflect generalized and global changes in the brain.

2 | MATERIALS AND METHODS

2.1 | Mice

Male, 8–10 week old C57BL/6J mice (n = 28, The Jackson Laboratory, Bar Harbor, ME) were used for this study and were housed at University of Southern California vivarium. Female mice were not used, as estradiol (E2) has been shown to decrease GFAP expression and astrocytic morphology (Rozovsky et al., 2002). All procedures were approved by the Institutional Animal Care and Use Committee of the University of Southern California and conducted in accordance with the National Research Council's *Guide for the Care and Use of Laboratory Animals* (Committee for the Update of the Guide for the Care and Use of Laboratory Animals; National Research Council, 2010). Mice were housed in groups of four mice per cage and maintained on a reverse 12-hr light/dark cycle (lights off at 0,700) with ad libitum access to food and water.

2.2 | Animal groups and treadmill exercise

Mice were randomly divided into four groups: sedentary (n = 8), and exercise for 1 (n = 8), 2 (n = 8), or 4 (n = 4) weeks. Mice were exercised on motorized treadmills (EXER-6M, Columbus Instruments, Columbus, OH) for 1 hr/day, 5 days/week as previously described (Fisher et al., 2004) with slight modification. Briefly, mice begin in a warm-up phase, consisting of increasing speeds over the span of 15 min, before progressing to high speed running for 30 min and finishing with decreasing speed over the final 15 min. Sedentary animals were placed on a stationary treadmill adjacent to the exercising mice. The maximum speed for intensive running increased over time, reaching 12 m/min at the end of 1 week, and reaching 17.5 m/min at the end of 4 weeks.

2.3 | Brain tissue collection

Brain tissue was collected after the final exercise session at the end of 1 week of exercise (including sedentary mice), 2 weeks of exercise, and 4 weeks of exercise. One hour after the final exercise session, half of each group (n = 4 mice) was sedated with intraperitoneal injections of tribromoethanol (250 mg/kg body weight) and assessed for lack of toe-pinch response before being transcardially perfused with 50 ml of ice-cold 0.9% saline followed by 100 ml of ice-cold 4% paraformaldehyde in phosphate buffered saline, pH 7.2 (PFA-PBS). Whole brains were extracted and placed in 4% PFA-PBS at 4°C for 24 hr, followed by sinking in 20% sucrose. Whole brains were rapidly frozen by submersion in 2-methylbutane cooled on dry ice and stored at −80°C until use.

2.4 | Immunohistochemical analysis of astrocytic morphology

Astrocyte morphology was assessed using GFAP-stained sections. Whole brains were coronally sliced (30 μm thickness) on a sliding cryostat (Leica CM1900, Leica Microsystems, Wetzlar, Germany). Briefly, sections were washed in Tris-buffered saline, pH 7.2, with 0.2% Triton X-100 (TBST) for 1 hr at room temperature, blocked in 4% normal goat serum (NGS, S-1000, Vector Labs, Burlingame, CA) in TBST for 2 hr at room temperature, and incubated overnight at 4°C in primary antibody (2% NGS in TBST) with rabbit anti-GFAP

(1:2,000, Agilent Cat# Z0334, RRID:AB_10013382). Sections were washed with TBST (3 × 30 min) and incubated in secondary antibody (2% NGS in TBST) with Alexa 568-conjugated goat anti-rabbit (1:5,000, Thermo Fisher Scientific, Cat# A-11011, RRID:AB_143157) for 90 min. Sections were washed with TBST (3 × 30 min), mounted onto gelatin-coated slides, and coverslipped (Vectashield Hardset Antifade with DAPI; H-1500, Vector Labs, Burlingame, CA). Confocal images were taken on an IXB-DSU spinning disk Olympus BX-61 (Olympus America, Melville, NY) and captured with an ORCA-R2 digital CCD camera (Hamamatsu, Bridgewater, NJ) and MetaMorph Advanced software (Molecular Devices, San Jose, CA).

2.5 | Immunohistochemical analysis of astrocyte number

Astrocyte number in regions of interest was assessed using SOX9-stained sections (Sun et al., 2017). Whole brains were sliced as above, washed with TBST for 1 hr at room temperature, blocked in 4% NGS in TBST for 2 hr at room temperature, and incubated overnight at 4°C in primary antibody (2% NGS in TBST) with rabbit anti-SOX9 (1:2,000, Millipore Cat# AB5535, RRID:AB_2239761). Sections were washed with TBST (3 × 30 min) and incubated in secondary antibody (2% NGS in TBST) with Alexa 568-conjugated goat anti-rabbit (1:5,000, Thermo Fisher Scientific, Cat# A-11011, RRID:AB_143157) for 90 min. Sections were washed with TBST (3 × 30 min), mounted onto gelatin-coated slides, and coverslipped (Vectashield Hardset Antifade with DAPI, Vector Labs).

For SOX9-GFAP co-localization, sections were washed with TBST as before, blocked in 4% normal donkey serum (NDS, S30, EMD Millipore) in TBST for 2 hr at room temperature, and incubated overnight at 4°C in primary antibody (2% NDS in TBST) with rabbit anti-SOX9 (1:2,000, Millipore Cat# AB5535, RRID:AB_2239761). Sections were washed with TBST as before and incubated in secondary antibody (2% NDS in TBST) with Alexa 568-conjugated donkey anti-rabbit (1:5,000, Thermo Fisher Scientific Cat# A10042, RRID:AB_2534017). Sections were washed as before, and staining protocol was repeated with blocking (4% NDS in TBST) and overnight incubation at 4°C with primary antibody (2% NDS in TBST) with rabbit anti-GFAP (1:2,000, Agilent Cat# Z0334, RRID:AB_10013382). Sections were washed as before and incubated in secondary antibody (2% NDS in TBST) with Alexa 488-conjugated donkey anti-rabbit (1:5,000, Thermo Fisher Scientific Cat# A-21206, RRID:AB_2535792). Sections were washed as before, mounted onto gelatin-coated slides and coverslipped (Vectashield Hardset Antifade with DAPI, Vector Labs). A full list of antibodies used in this study are contained in Table 1.

2.6 | Morphological analysis of astrocytic structure

GFAP-positive astrocytes were morphologically analyzed for corrected total cellular fluorescence (CTCF, a measure of fluorescence intensity), distal to proximal length, and number of primary processes. Astrocytes were imaged at 10× magnification (UPlan FI, Olympus) and analyzed in three regions of the brain: (i) prefrontal cortex (PFC, Bregma +2.0 to +1.6 mm A.P., ±0.5 mm M.L., −1.5 to −3.0 mm D.V.); (ii) striatum (STR, +1.4 to −0.2 mm A.P., ±0.8–2.5 mm M.L., −2.5 to −4.5 mm D.V.); and (iii) ectorhinal cortex (ETC, −1.3 to −3.0 mm A.P., ±3.2–4.2 mm M.L., −3.0 to −3.5 mm D.V.). Selection of these anatomical regions was based upon previous findings of exercise-induced changes in regional blood flow in the PFC and STR but not in the ETC (Guo, Wang, Prathap, & Holschneider, 2017; Wang et al., 2013). Astrocytic area was determined by CTCF according to previously published guidelines (Burgess et al., 2010), with modifications. Intact astrocytes were manually traced and total area and integrated density determined and measured in Fiji (NIH, ver. 1.52b; Schindelin et al., 2012). Mean gray values for background adjacent to measured cells was recorded and CTCF calculated as: integrated density—(average background mean gray value × area of astrocyte). Distance between the most distal and proximal process was measured and reported in microns. The number of primary processes emanating from the soma was also counted. Morphological parameters measured by CTCF were captured in arbitrary units based upon the above calculation. At least three tissue sections through each anatomical region were analyzed per animal (n = 4 mice per group).

2.7 | Unbiased counting of astrocytes

SOX9-positive nuclei were analyzed using an unbiased counting approach. SOX9-positive nuclei were imaged at 10× magnification (UPlan FI, Olympus) with identical camera settings in the same three regions previously described (PFC, STR, ECT). A grid of 300 μm × 300 μm squares was overlaid on each image and SOX9-positive nuclei were manually counted in five nonadjacent squares, averaged across sections, and the percent change relative to sedentary was calculated. At least three sections through each anatomical region were analyzed per animal (n = 4 mice per group).

2.8 | Sholl analysis of astrocyte arborization

Astrocytic arborization (a measurement of process ramification and reactivity) was determined using Sholl analysis (Sholl, 1953). Individual, GFAP-positive astrocytes were randomly selected from areas of interest (including PFC, STR, and ETC as delineated above) and imaged using a 60× water-immersion objective (UplanSApo, Olympus) in z-stacks at 0.5 μm intervals. Images were manually traced using the Simple Neurite Tracer plug-in for Fiji before segments were max z-projected and measured using the Sholl Analysis plug-in (Ferreira et al., 2014). Forty concentric circles (with increasing radii in steps of 2 μm) centered around the soma were placed on top of segmented astrocytes and the number of intersections across each circle recorded. Data were plotted, as the distance from soma versus number of intersections, for comparisons including area under the curve (AUC). For representative astrocytes, segments were filled using the Simple Neurite Tracer plug-in with manually selected thresholds. At least three tissue sections through each anatomical region were analyzed per animal (n = 4 mice per group).

2.9 | Quantitative RT-PCR for astrocytic genes of interest

To explore astrocytic activation, we examined the pattern of expression of several genes including *Gfap* (Gene ID 14580), *Thbs2* (thrombospondin 2, Gene ID 21826), *Lif* (leukemia inhibitory factor, Gene ID 16878), and *Il6* (interleukin 6, Gene ID 16193). Immediately after the final exercise session, half of each exercise group (sedentary, 1 week and 2 weeks exercise; $n = 4$ mice per group) were sacrificed via cervical dislocation and whole brains were extracted. Fresh tissue was rapidly microdissected in blocks from (i) PFC (Bregma +2.0 to +1.4 mm A.P., rostral to corpus callosum; ± 1 mm M.L. from midline to the corpus callosum, and −1.5 to −3.0 mm D.V.) (Kintz, Petzinger, & Jakowec, 2017); (ii) STR (Bregma +1.2 to −0.2 mm A.P., including tissue bordered ventrally by the anterior commissure, dorsally by the corpus callosum, medially by the lateral ventricle, and ±2.5 mm laterally from the midline) (Kintz et al., 2013); and (iii) ETC (Bregma −2.0 to −3.0 mm A.P., laterally bounded by the edge of the cortex and extending 1 mm medially to the edge of the striatum, and −3.0 to −3.5 mm D.V.) Tissues were placed in RNA*later* Stabilization Solution (QIAGEN, Germantown, MD) and stored at 4°C overnight. RNA was extracted using RNEasy Mini Kit (QIAGEN, Germantown, MD) according to manufacturer's guidelines for animal tissue, with an additional chloroform extraction step. Total RNA concentration was measured by absorbance spectroscopy (BioPhotometer, Eppendorf, Hauppauge, NY). Complimentary DNA (cDNA) was generated by reverse transcription from 1 µg of sample RNA using QuantiTect Reverse Transcription Kit (QIAGEN, Germantown, MD) following manufacturer's guidelines. qRT-PCR was run with 1 µl cDNA and QuantiTect SYBR Green (QIAGEN, Germantown, MD) on an Eppendorf Mastercycler Ep Realplex (Eppendorf, Hauppauge, NY) using a program of 15 min at 95°C, followed by 40 cycles of 15 s at 94°C, 30 s at 55°C, and 30 s at 72°C. Following completion of cycling, a melting curve of products was generated. Data were collected and normalized on Eppendorf Realplex *ep* software (Eppendorf, Hauppauge, NY). Standard Δ ΔCT analysis (Livak & Schmittgen, 2001) was used to quantify fold changes in gene expression in exercise groups normalized to sedentary controls, with *Actb* serving as a housekeeping gene. The primers used are as follows (5′→3′): *Actb* forward GGCTGTATTCCCCTCCATCG; *Actb* reverse CCAGTTGGTAACAATGCCATG; *Gfap* forward CGGAGA CGCATCACCTCTG; *Gfap* reverse AGGGAGTGGAGGAGTCATTCG; *Il6* forward TAGTCCTTCCTACCCCAATTTCC; *Il6* reverse TTGG TCCTTAGCCACTCCTTC; *Lif* forward ATTGTGCCCTTACTGCT GCTG; *Lif* reverse GCCAGTTGATTCTTGATCTGGT; *Thbs2* forward CTGGGCATAGGGCCAAGAG; *Thbs2* reverse GCTTGACAATCCTGT TGAGATCA.

2.10 | Statistical analysis

All statistical tests were carried out and graphs made using Prism 8.0 (GraphPad, San Diego, CA), with statistical significance set at $p < 0.05$. For morphological and cell counting measurements, AUC, and qRT-PCR analysis, one-way ANOVA with Dunnett's multiple comparisons was used with the sedentary group serving as a control. For Sholl analysis, two-way ANOVA with Dunnett's multiple comparisons was used with the sedentary group serving as a control.

3 | RESULTS

The overall analysis approach used in these studies is shown in Figure 1. The upper row indicates the anatomical regions and Bregma range from which brain tissues were collected including the prefrontal cortex (PFC), striatum (STR), and ectorhinal cortex (ETC). The middle panel shows a representative *z*-stack of a GFAP-positive astrocyte. The bottom panel outlines the measurement criteria including CTCF (arbitrary units) of GFAP, maximal distal-proximal measurement of a single astrocyte (microns), the Sholl analysis of the astrocytic range of influence (number of intersections), and the number of primary processes that emerge from the cell body. A low and high magnification of representative GFAP-positive astrocytic immunohistochemical staining of sections through the selected regions of interest corresponding to the PFC, STR, and ETC are shown in Figure 2. A summary of morphological metrics (CTCF, distal-to-proximal distance, and number of primary processes; mean ± *SEM*) can be found in Table 2.

3.1 | Exercise increases the GFAP fluorescence of astrocytes

In the PFC, exercise resulted in a statistically significant increase in CTCF values (arbitrary units, au) with exercise ($n = 31–49$ cells, $F_{(3, 165)} = 11.27$, $p < 0.001$). CTCF values statistically significantly increased with 1 week of exercise (52% increase, $p < 0.001$) but not with 2 or 4 weeks of exercise ($p = 0.986$ and $p = 0.233$, respectively) compared to sedentary controls.

In the STR, CTCF statistically significantly changed with exercise ($n = 86–146$ cells, $F_{(3, 479)} = 38.98$, $p < 0.001$). Specifically, CTCF statistically significantly decreased at 1 week of exercise (34% decrease, $p < 0.001$) and significantly increased at 4 weeks of exercise (31% increase, $p < 0.001$) relative to sedentary animals, and did not significantly differ with 2 weeks of exercise ($p = 0.495$).

In the ETC, CTCF was significantly affected by exercise ($n = 25–55$ cells, $F_{(3, 181)} = 10.03$, $p < 0.001$). Specifically, CTCF increased significantly with 1 week of exercise (92% increase, $p < 0.001$) and 4 weeks of exercise (64% increase, $p = 0.0102$) and did not significantly differ from sedentary animals with 2 weeks of exercise ($p > 0.999$) (Figure 3a).

3.2 | Exercise modifies the distal-proximal distance of astrocyte processes

Distal-proximal (D-P) distances in GFAP-positive astrocytes reflected the findings in the CTCF measurements (Figure 3b).

In the PFC, exercise had a statistically significantly effect on D-P measurements ($n = 30–52$ cells, $F_{(3, 149)} = 5.97$, $p < 0.001$). Specifically,

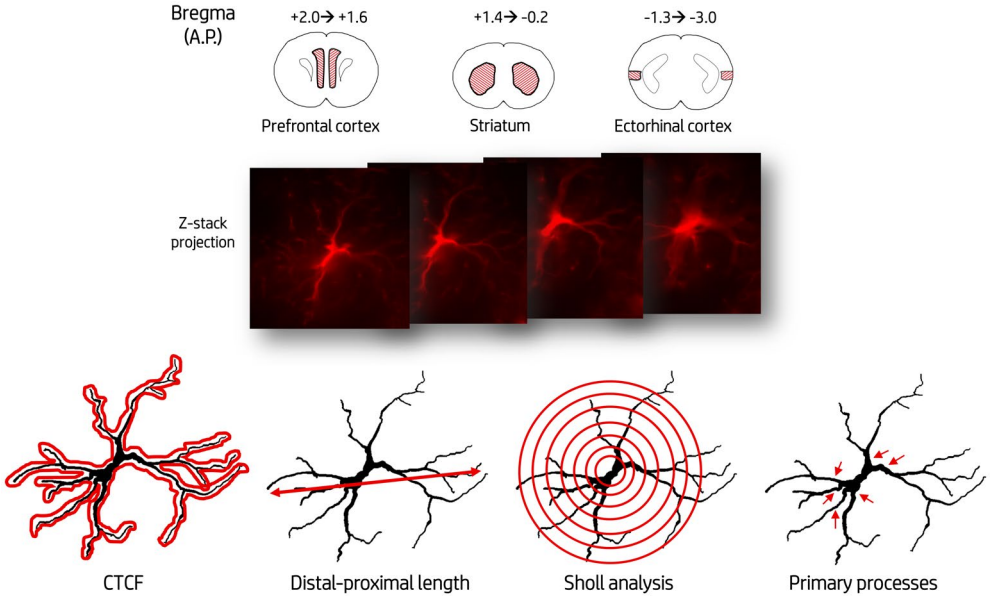

FIGURE 1 Morphological assessment of GFAP-positive astrocytes. Prefrontal cortex, striatum, and ectorhinal cortex (red-shaded regions, with anterior-posterior range given relative to Bregma) were included in morphological analysis. Examples of the morphological metrics are shown on a representative astrocyte, including corrected total cellular fluorescence (CTCF), distal-proximal distance, number of primary processes, and Sholl analysis [Color figure can be viewed at wileyonlinelibrary.com]

1 week of exercise significantly increased D-P distance (23% increase, $p < 0.001$) but 2 and 4 weeks of exercise had no significant effect on D-P distance ($p = 0.531$ and $p > 0.999$, respectively) compared to sedentary animals.

In the STR, exercise also statistically significantly changed D-P distance ($n = 35–86$ cells, $F_{(3, 334)} = 28.28$, $p < 0.001$). D-P distance decreased significantly with 1 week of exercise (24% decrease, $p < 0.001$) and significantly increased with 2 and 4 weeks of exercise (10% increase, $p = 0.0132$ and 19% increase, $p < 0.001$, respectively) relative to sedentary animals (Table 2).

In the ETC, D-P distance was also statistically significantly increased by exercise ($n = 38–55$ cells, $F_{(3, 181)} = 8.75$, $p < 0.001$). Interestingly, D-P distance significantly increased with 1 and 2 weeks of exercise (13 and 11% increase, respectively; $p = 0.023$ and $p < 0.001$, respectively), but was not significantly different from sedentary animals at 4 weeks of exercise ($p = 0.228$).

3.3 | Exercise changes the number of striatal astrocyte primary processes

The number of primary processes emanating from an identifiable astrocyte soma were counted in each brain region and exercise duration (Figure 3c). In the PFC ($n = 30–52$ cells, $F_{(3, 108)} = 0.68$, $p = 0.566$) and the ETC ($n = 38–55$ cells, $F_{(3, 139)} = 0.11$, $p = 0.956$), there was no exercise effect on the number of primary processes on GFAP-positive astrocytes.

In the STR, exercise did have a statistically significant effect on the number of primary processes ($n = 21–48$ cells, $F_{(3, 123)} = 13.11$, $p < 0.001$). The number of primary processes significantly decreased at 1 week (18% decrease, $p = 0.0060$) before showing a trend in increasing at 2 weeks (11% increase, $p = 0.0829$) and significantly increasing at 4 weeks of exercise (18% increase, $p = 0.0012$) relative to sedentary controls.

3.4 | Exercise does not influence astrocyte number

To assess the potential that aerobic exercise causes astrocyte proliferation in regions of interest (Li et al., 2005), we used immunohistochemistry to examine the astrocyte-specific nuclear protein SOX9 to sample the number of astrocytes (Sun et al., 2017). In the regions sampled (PFC, STR, and ETC), we did not see any statistically significant change in the number of SOX9-positive astrocytes in exercised animals relative to sedentary animals (PFC: $p = 0.430$, $n = 1,039$ nuclei; STR: $p = 0.811$, $n = 1,131$ nuclei; ETC: $p = 0.758$, $n = 799$ nuclei) (Figure 4).

3.5 | Exercise modulates astrocyte complexity

Figure 5 summarizes Sholl analysis of astrocyte arborization, process ramification, and morphological complexity in exercised animals relative to sedentary animals by counting astrocytic process intersections of overlaid concentric circles (Ferreira et al., 2014).

In the PFC, exercise showed a statistically significant effect on the number of intersections ($F_{(3, 1312)} = 73.82$, $p < 0.001$). One week of exercise did not significantly increase the number of intersections (Figure 5a) or AUC analysis ($n = 10$ cells, $p = 0.213$) (Figure 5b). In contrast, 2 weeks of exercise significantly decreased the number of intersections in distal parts of the cell (>40 μm from soma, $p = 0.0084$, $n = 9$ cells) but did not affect AUC analysis ($p = 0.840$), while 4 weeks of exercise significantly decreased both the number of intersections

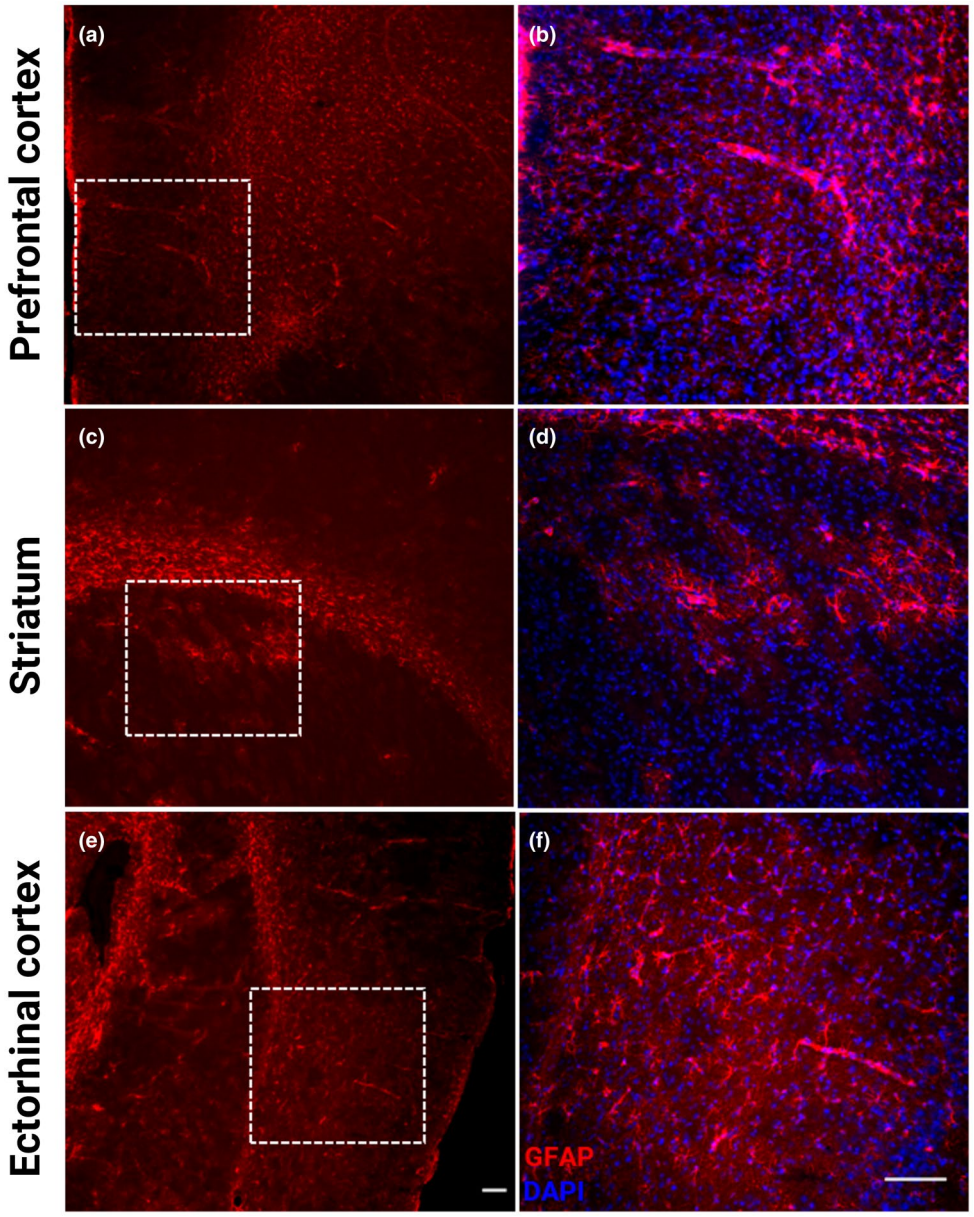

FIGURE 2 Representative GFAP immunohistochemistry of the three regions sampled. Left hand column shows low-magnification images of prefrontal cortex, striatum, and ectorhinal cortex (a, c, and e); right hand column shows corresponding high-magnification images of boxed area. Scale bars: 200 μm [Color figure can be viewed at wileyonlinelibrary.com]

TABLE 1 List of antibodies used in immunohistochemical analysis

Antibody	RRID	Host species	Immunogen	Manufacturer	Dilution
Rabbit anti-GFAP	AB_10013382	Rabbit	GFAP isolated from cow spinal cord	Agilent (Cat# Z0334)	1:2,000
Rabbit anti-SOX9	AB_2239761	Rabbit	KLH-conjugated linear peptide corresponding to the C-terminal sequence of human Sox9	Millipore (Cat# AB5535)	1:2,000
Goat anti-rabbit (568 nm)	AB_143157	Goat	Gamma Immunoglobins, Heavy and Light chains	Thermo Fisher Scientific (Cat# A11011)	1:5,000
Donkey anti-rabbit (488 nm)	AB_2535792	Donkey	Gamma Immunoglobins, Heavy and Light chains	Thermo Fisher Scientific (Cat# A21206)	1:5,000
Donkey anti-rabbit (568 nm)	AB_2534017	Donkey	Gamma Immunoglobin	Thermo Fisher Scientific (Cat# A10042)	1:5,000

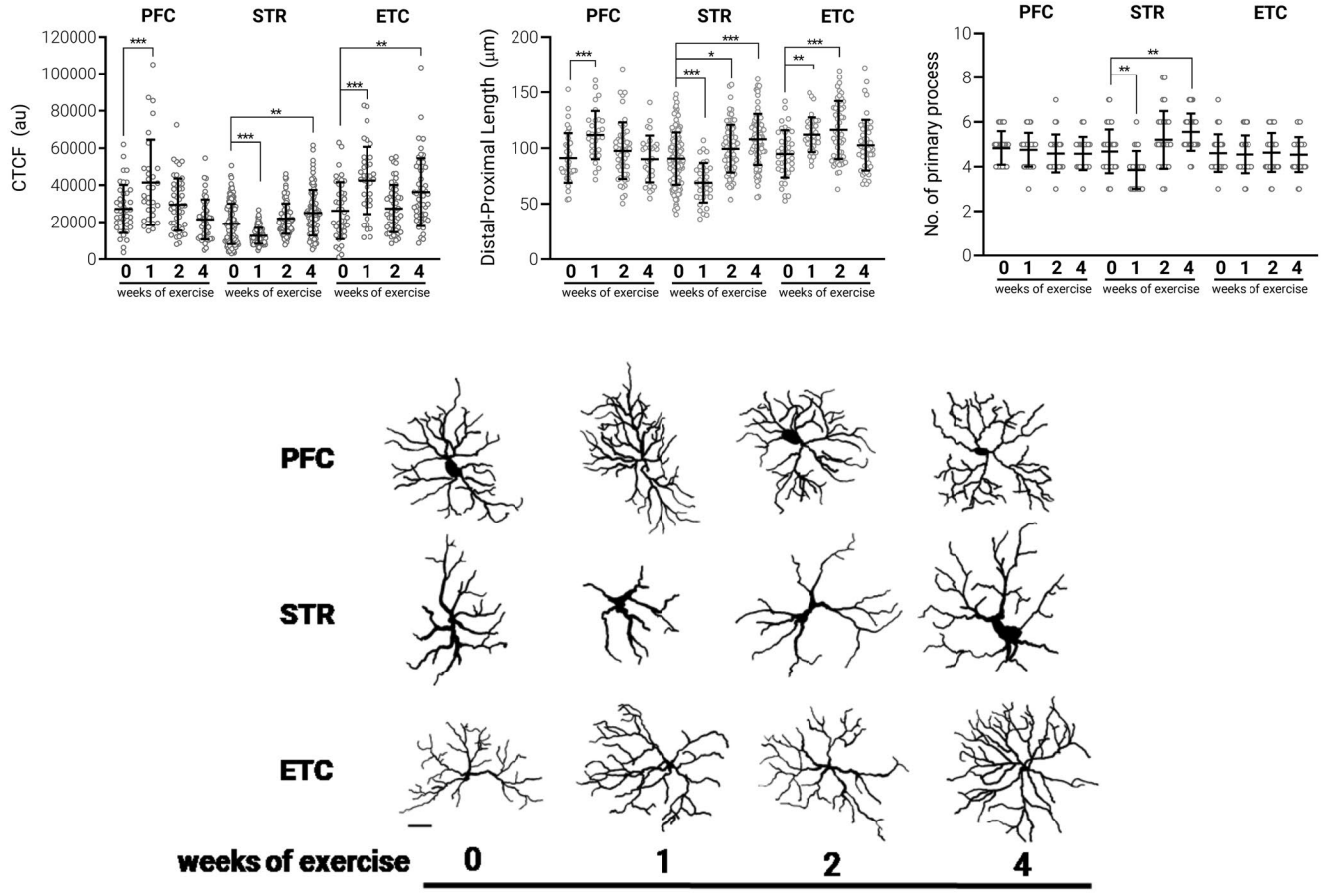

FIGURE 3 Aerobic exercise causes astrocyte morphological changes in a region- and time-specific manner. (a) Corrected total cellular fluorescence (CTCF) for intact, GFAP-positive astrocytes following 1, 2, or 4 weeks of exercise across regions of interest and measured in arbitrary fluorescent units. (b) Distal-proximal distance as measured from astrocytes quantified previously and measured in microns. (c) Number of primary processes projecting from astrocytes quantified previously. (d) Representative traces of prefrontal cortex, striatum, and ectorhinal cortex astrocytes (60× magnification) following 1, 2, or 4 weeks of exercise. Scale bar: 20 μm. $n = 4$ mice per time point; mean ± *SD* with all data points in gray. One-way ANOVA with Dunnett's multiple comparisons. $^{*}p < 0.05$; $^{**}p < 0.01$; $^{***}p < 0.001$ relative to sedentary control

TABLE 2 Mean ± *SD* for morphological analyses

Morphology metric	Duration of exercise	Prefrontal cortex	Striatum	Ectorhinal cortex
CTCF (au)	Sedentary	27,230 ± 12,639	19,163 ± 10,984	26,228 ± 15,387
	1 week	41,483 ± 22,992***	12,626 ± 4,280***	42,592 ± 18,117***
	2 weeks	29,540 ± 14,108	21,944 ± 8,179	27,401 ± 12,703
	4 weeks	21,533 ± 10,852	25,089 ± 12,325**	36,245 ± 18,297**
Distal-proximal (μm)	Sedentary	91.07 ± 22.12	90.52 ± 23.46	94.78 ± 21.13
	1 week	111.6 ± 21.57***	68.98 ± 17.78***	111.9 ± 15.41**
	2 weeks	97.62 ± 25.34	99.47 ± 21.34*	116.3 ± 25.94***
	4 weeks	90.16 ± 20.92	107.7 ± 22.81***	102.5 ± 22.67
Primary processes	Sedentary	4.84 ± 0.75	4.69 ± 0.97	4.61 ± 0.84
	1 week	4.56 ± 0.75	3.86 ± 0.85**	4.56 ± 0.84
	2 weeks	4.64 ± 0.84	5.21 ± 1.29	4.64 ± 0.87
	4 weeks	4.59 ± 0.73	5.55 ± 0.83**	4.54 ± 0.78

Note: One-way ANOVA with Dunnett's multiple comparisons.
$^{*}p < 0.05$; $^{**}p < 0.01$; $^{***}p < 0.001$ relative to sedentary control.

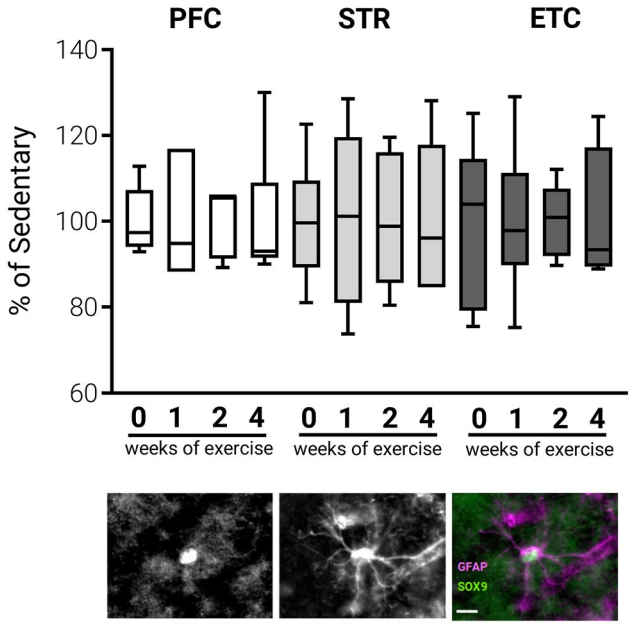

FIGURE 4 Aerobic exercise does not change astrocyte numbers. (a) Astrocyte counts were assessed using SOX9 immunostaining and unbiased counting of SOX9-positive nuclei in non-adjacent 300 μm × 300 μm squares. Average counts of SOX9-positive nuclei in sedentary animals (PFC: n = 45.2; STR: n = 45.7; ECT: n = 42.3) were set as 100% and percent relative changes in exercised animals were compared. (b) Representative image showing SOX9 colocalizes with GFAP in the STR (scale bar = 10 μm). n = 4 mice per time point. Data are shown as box-and-whisker plots, where the upper- and lower-bounds of the box represent the 75th and 25th percentile, respectively; the horizontal line represents the median; and the whiskers indicate the highest and lowest values. One-way ANOVA with Dunnett's multiple comparisons [Color figure can be viewed at wileyonlinelibrary.com]

(p < 0.05, n = 9 cells) as well as significantly decreasing AUC compared to sedentary (499.7 ± 111.9 vs. 680 ± 73.34 intersections • μm, p = 0.0298).

In the STR, exercise also showed a statistically significant effect on the number of intersections ($F_{(3, 1476)}$ = 67.09, p < 0.001). We found a significant exercise effect for AUC analysis (n = 10 cells per time point, $F_{(3, 36)}$ = 13.46, p < 0.001). One week of exercise significantly decreased the number of intersections (n = 10 cells, p < 0.05) as well as the AUC (411.7 ± 97.85 vs. 568.4 ± 78.64 intersections • μm, p = 0.0064), while 2 weeks of exercise had no effect on the number of intersections (n = 10 cells, p > 0.05) or AUC (p = 0.806). However, 4 weeks of exercise significantly increased the number of intersections (n = 10 cells, p < 0.05) but did not significantly increase the AUC (p = 0.676) (Figure 5c,d).

In the ETC, our analysis showed a statistically significant effect of exercise on the number of intersections ($F_{(3, 1189)}$ = 83.48, p < 0.001). We additionally showed a significant effect of exercise on AUC analysis (n = 8–9 cells per time point, $F_{(3, 29)}$ = 19.94, p < 0.001). One week of exercise showed a trend for increased intersections in proximal areas of astrocytes compared to sedentary (<40 μm from soma, p = 0.079, n = 8 cells) without any significant difference in AUC (p = 0.280). Two weeks of exercise also showed a trend for increased proximal intersections (p = 0.078, n = 9 cells) but had no effect on AUC (p = 0.435). Finally, 4 weeks of exercise increased intersections significantly both proximally (<40 μm from soma) and distally (>40 μm from soma) (p < 0.001, n = 8 cells) as well as increasing the AUC (909.4 ± 166.9 vs. 558.8 ± 86.01 intersections • μm, p < 0.001) (Figure 5e,f).

3.6 | Exercise induces differential gene expression in astrocytes

To examine the effect of exercise on astrocytic gene expression, we selected four genes of interest based upon previous analysis of reactive astrocytes (Zamanian et al., 2012) for qRT-PCR analysis (Figure 6), including *Gfap* (a marker of reactive astrocytes), *Lif* (a trophic and differentiation factor), *Thbs2* (an astrocyte-secreted synaptogenic factor), and *Il6* (a pro- and anti-inflammatory chemokine).

In the PFC, exercise resulted in a statistically significant increase in *Gfap* expression ($F_{(2, 9)}$ = 1,184, p < 0.001), at 2 weeks of exercise (7.39-fold increase relative to sedentary control, p < 0.001); an increase in *Thbs2* ($F_{(2, 9)}$ = 97.41, p < 0.001) at both 1 week (2.16-fold increase, p = 0.0066) and 2 weeks of exercise (4.1-fold increase, p < 0.001); and an increase in *Il6* ($F_{(2, 9)}$ = 29.32, p < 0.001) at 1 week (3.23-fold increase, p < 0.001) but not 2 weeks of exercise (p = 0.262), without any exercise effect on *Lif* expression ($F_{(2, 9)}$ = 0.57, p = 0.582).

In the STR, our analysis showed *Gfap* expression statistically significantly increased ($F_{(2, 9)}$ = 6.13, p = 0.0368) at 1 week (2.98-fold increase, p = 0.0146) and 2 weeks of exercise (2.80-fold increase, p = 0.0311); *Thbs2* expression increased ($F_{(2, 9)}$ = 6.48, p = 0.018) at 1 week (2.95-fold increase, p = 0.0211) and 2 weeks of exercise (2.89-fold increase, p = 0.0240); *Il6* expression showed an exercise effect ($F_{(2, 9)}$ = 86.97, p < 0.001) but in particular expression did not significantly increase at 1 week of exercise (1.52-fold increase, p = 0.145) but was significantly increased at 2 weeks of exercise (4.53-fold increase, p < 0.001); and *Lif* expression increased significantly ($F_{(2, 9)}$ = 6.02, p = 0.0219) at 1 week (2.06-fold increase, p = 0.0203) and 2 weeks of exercise (1.93-fold increase, p = 0.0377).

In the ETC, exercise did not result in any statistically significant change in expression of the four sampled genes, excluding a statistically significant increase of Il6 expression at 2 weeks of exercise (9.25-fold increase, p < 0.001).

4 | DISCUSSION

Astrocytes comprise 15–20% of all cells in the rodent brain and support neurotransmission through recycling of neurotransmitters and energetic and trophic substrate delivery (Bélanger, Allaman, & Magistretti, 2011; Khakh & Sofroniew, 2015; Sun et al., 2017). Astrocytes orchestrate rCBF and synaptic plasticity by regulating synaptogenesis and modulating the blood–brain barrier to promote experience-dependent neuroplasticity (Abbott et al., 2006;

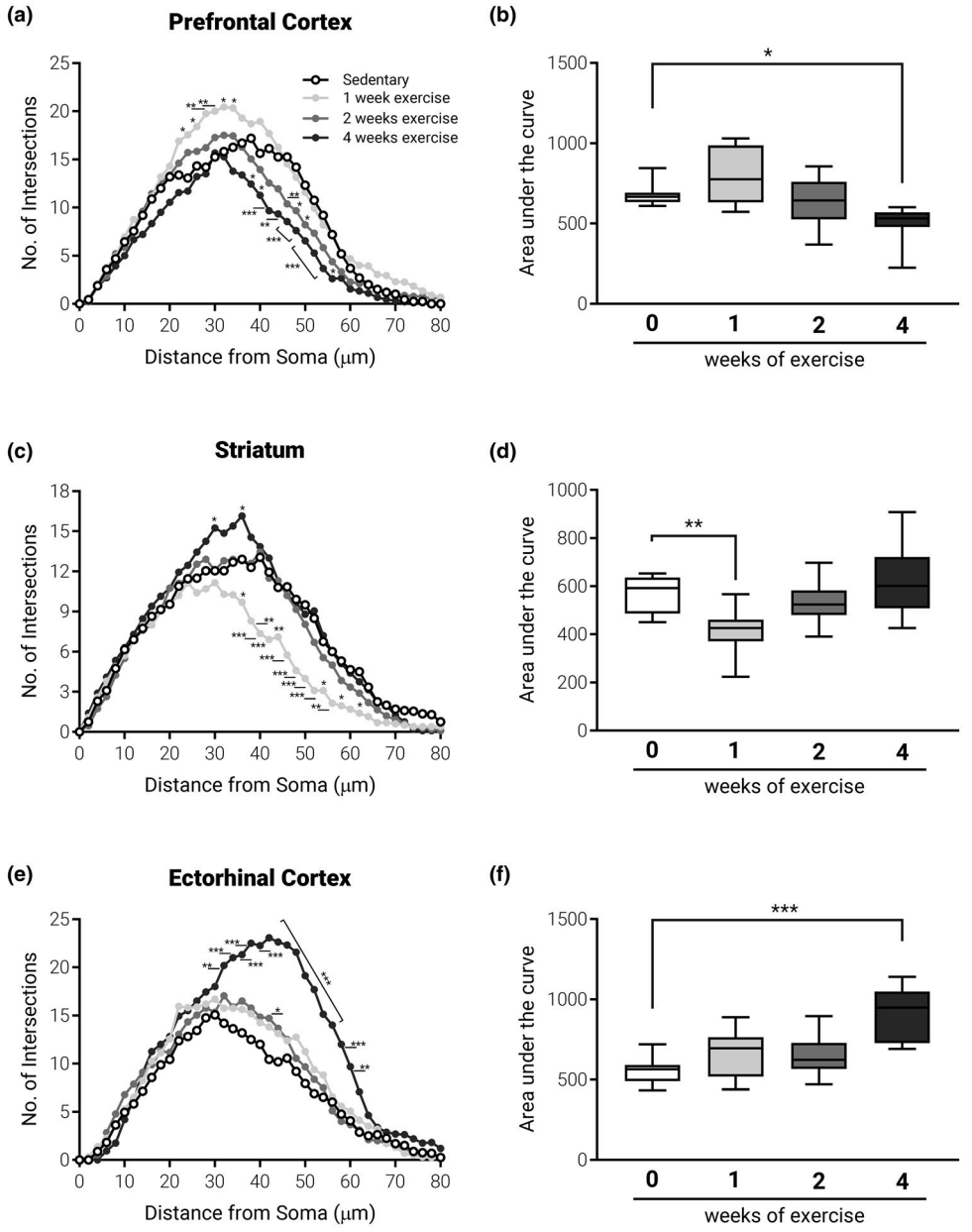

FIGURE 5 Sholl analysis of astrocytes reveals distinct arborization patterns across regions and exercise duration. (a, c, and e) Number of intersections for prefrontal cortex, striatum, and ectorhinal cortex astrocytes per 2 μm step. (b, d, and f) Area-under-the-curve analysis of Sholl plots for a, c, and e, respectively. $n = 4$ mice per time point. Data are shown as mean intersections every 2 μm (Sholl plot) or box-and-whisker plots, where the upper- and lower-bounds of the box represent the 75th and 25th percentile, respectively; the horizontal line represents the median; and the whiskers indicate the highest and lowest values (AUC, intersections × μm). Two-way ANOVA with Dunnett's multiple comparisons (Sholl) and one-way ANOVA with Dunnett's multiple comparisons (AUC). $^{*}p < 0.05$; $^{**}p < 0.01$; $^{***}p < 0.001$ relative to sedentary control

Christopherson et al., 2005; Eroglu & Barres, 2010). Astrocytes respond to changes in brain activity and homeostasis by entering a reactive state (Sofroniew & Vinters, 2010). One aspect of reactive astrocytes is a change in cellular morphology, as demonstrated by increased expression of GFAP (an intermediate filament), and cellular hypertrophy (Wilhelmsson et al., 2006); while the activation of GFAP has been predominantly characterized in the context of brain injury and disease, increased expression of GFAP has also been implicated as a surrogate marker of astrocyte reactivity in response to aerobic exercise (Li et al., 2005; Saur et al., 2014; Sofroniew & Vinters, 2010). Aerobic exercise is a form of experience-dependent neuroplasticity that changes rCBF in a circuit-specific manner and rescues cognitive and motor behaviors in animal models of dopamine dysfunction. (Fisher et al., 2004; Kintz et al., 2013; Petzinger et al., 2007; Toy et al., 2014; Wang et al., 2013). Astrocytes monitor synaptic activity by close contact between distal processes and neurons, and changes in GFAP expression and astrocyte morphology are regulated in response to synaptic activity (Bernardinelli et al., 2014).

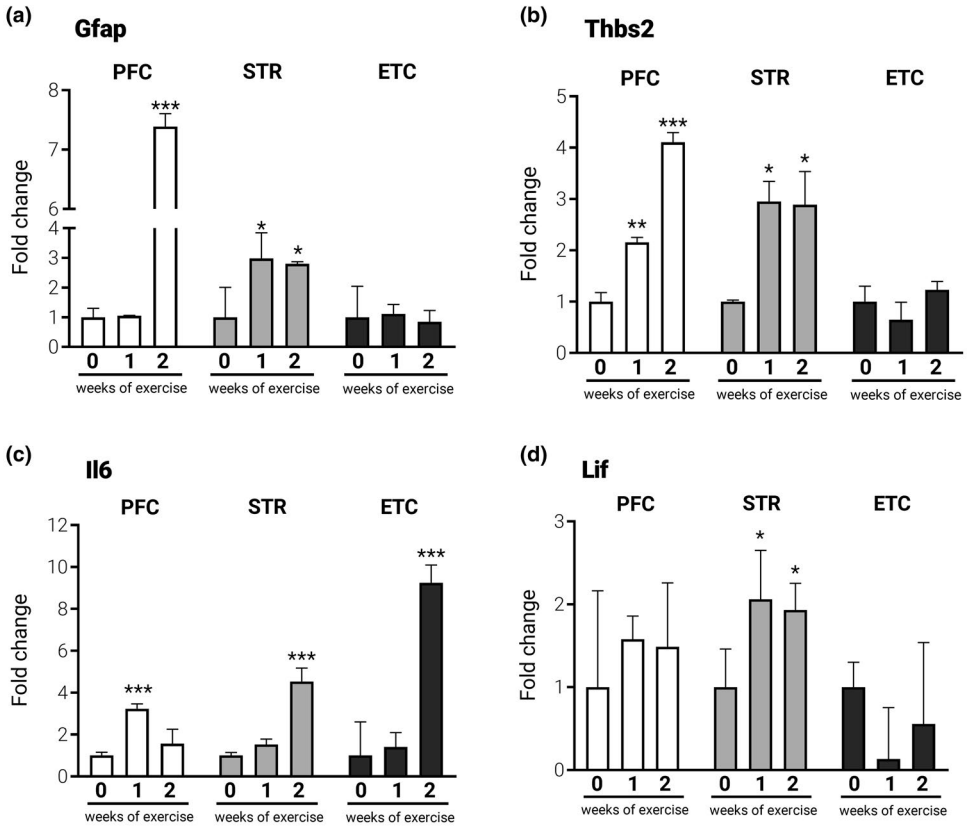

FIGURE 6 Aerobic exercise induces reactive astrocyte gene expression. (a) Fold induction of *Gfap* with 1 and 2 weeks of exercise. (b) Fold induction of *Thbs2* with 1 and 2 weeks of exercise. (c) Fold induction of *Il6* with 1 and 2 weeks of exercise. (d) Fold induction of *Lif* with 1 and 2 weeks of exercise. $n = 4$ mice per time point; mean + *SD*. One-way ANOVA with Dunnett's multiple comparisons. $^{*}p < 0.05$; $^{**}p < 0.01$; $^{***}p < 0.001$ relative to sedentary control

Our results demonstrate that exercise increases the expression of GFAP and mediates changes in astrocyte morphology. In this study, we focused on specific neuroanatomical regions of interest (PFC, STR, and ETC) based upon published changes in rCBF following exercise (Wang et al., 2013). We found that astrocytes within the PFC increased GFAP expression, increased their distal-to-proximal span, and increased overall arborization following 1 week of exercise before returning to baseline morphology even with the continuation of exercise. This contrasts with findings in the STR that showed astrocytes initially decreased GFAP expression (and less morphological complexity) following 1 week of exercise but increased GFAP expression and morphological complexity with the continuation of exercise. We found distinct changes in astrocyte morphology and GFAP expression in the ETC. For example, distal-to-proximal length increased at 1 and 2 weeks of exercise but did not change with 4 weeks of exercise as it did in the STR. Alternately, the number of astrocyte primary processes did not change with exercise in the ETC, similarly to the PFC but in contrast to the STR. While the PFC and STR showed similar temporal and structural differences in morphology in response to exercise, the ETC showed both similarities and differences in astrocytic phenotype that may be reflective of regional astrocyte heterogeneity (Chai et al., 2017). While some morphological features of astrocytes appear to be region-specific based on circuit activation, other morphological features may be more global. In a mouse model of Alzheimer's disease, increased GFAP expression was found throughout the brain (Kamphuis et al., 2012) but no morphological analysis was done on these astrocytes to delineate in greater detail astrocyte reactivity and its functional correlate. Future studies using GFAP as a surrogate marker of morphology should incorporate more detailed morphological metrics to link GFAP activation and astrocyte function. These differences in region-specific morphological changes of astrocytes may reflect differences in the role they play in supporting synaptic integrity and mediating synaptogenesis, as well as modulating metabolic functions at the blood brain barrier.

Astrocytes can respond to changes in synaptic activity by altering messenger RNA transcript expression. These astrocyte-specific transcripts are involved in a wide array of mechanisms, including synaptogenesis, metabolism, and angiogenesis. (Abbott et al., 2006; Christopherson et al., 2005; Stogsdill et al., 2017). To explore the effects of exercise on astrocyte function and their contribution to synaptogenesis, we analyzed by qRT-PCR the expression of four genes associated with astrocyte reactivity (*Gfap*, *Thbs2*, *Lif*, and *Il6*) (Zamanian et al., 2012). Exercise resulted in the increased expression in *Gfap* in the PFC and STR, but not in ETC, suggesting an exercise-mediated association between activated astrocytes and circuits

involved in motor behavior, especially cortico-striatal circuits. In support of the role of astrocytes in mediating synaptogenesis, we found that expression of the synaptogenic molecule *Thbs2* also increased in the PFC and STR, but not in ETC, reflecting region-specific activation. Thrombospondins promote the formation of synapses and previous work from our group has shown an increase in synaptogenesis following exercise within these same regions (Christopherson et al., 2005; Morel et al., 2017; Toy et al., 2014). The cytokine LIF (leukemia inhibitor factor) plays a role in neural development and plasticity. We found increased expression of *Lif* in the STR following exercise, further supporting exercise-dependent neuroplasticity (Bauer, Kerr, & Patterson, 2007; Petzinger et al., 2007). Unlike *Gfap*, *Thbs2*, and *Lif*, the expression of the cytokine IL6 increased across all regions of interest following exercise. IL6 works in both a pro- and anti-inflammatory capacity and its elevated expression may suggest a global response to exercise (Gruol & Nelson, 1997). The expression of *Il6* can be mediated in multiple ways, including by peripheral lactate derived from muscles during exercise (Andersson, Rönnbäck, & Hansson, 2005; Erta, Quintana, & Hidalgo, 2012); however, the precise role of IL6 in the brain following exercise remains unknown. Previous work has shown an exercise-induced increase in *Il6* expression in the hippocampus but not in the cortex or cerebellum of mice; however, such changes were observed following acute exercise which is in contrast to our chronic exercise paradigm (Rasmussen et al., 2011). Taken together, changes in gene expression associated with reactive and synaptogenic astrocyte function occur in a region-specific manner, while those genes associated with neuropoietic function occur in both a region-specific and global pattern. Such patterns suggest that exercise differentially activates astrocytic gene expression and may ultimately reflect differences in astrocytic structure and function.

Exercise-induced GFAP, morphological, and transcriptional changes of astrocytes suggest that aerobic exercise can modulate astrocyte function to enhance exercise-induced neuroplasticity. Our immunohistochemical analysis of the astrocyte-specific transcription factor SOX9 did not reveal any changes in astrocyte number in our regions of interest, contrary to previous reports (Li et al., 2005). Our studies support that exercise increases GFAP expression and morphological changes, but do not show that astrocyte proliferation is occurring. Adult hippocampal neurogenesis has been shown to be elevated with exercise but evidence for neurogenesis or gliogenesis in the striatum following exercise is lacking (van Praag, 2005; van Praag, Kempermann, & Gage, 1999). Thus, future studies should explore the impact of different exercise paradigms on cellular proliferation in regions activated by motor behavior, such as the striatum. These results suggest that exercise is not changing the relative astrocyte composition in these regions, but instead is modifying astrocytic function. Aerobic exercise enhances experience-dependent neuroplasticity and synaptogenesis, leading to cognitive and motor circuit connectivity (Fisher et al., 2004; Petzinger et al., 2013). In the context of normal brain function, exercise can act as a mechanism for brain maintenance, allowing motor and cognitive learning to occur (Davies et al., 2017). In the context of neurodegenerative diseases, such as Parkinson's or Huntington's disease, where motor and cognitive dysfunction is evident, skilled exercise can be harnessed to restore dysfunctional circuits, including cortico-striatal circuitry (Petzinger et al., 2015; Wang et al., 2016). While much of motor learning and exercise-induced neuroplasticity has focused on the protection and restoration of neurons, studies from our group are beginning to identify and support an important role for astrocytes. We hypothesize that astrocytes physically remodel to locally support neurons as new, exercise-specific circuits are activated. As plasticity begins to refine such circuits in an activity-dependent manner (i.e., with more exercise), astrocytes respond to facilitate synaptogenesis and provide neurotrophic support to contribute to exercise-induced neuroplasticity. In the rat hippocampus, gene expression patterns for important neuroplasticity markers, such as BDNF, synaptotagmin, and NMDA receptors, undergo exercise-dependent changes over various lengths of exercise duration, supporting the notion that chronic exercise is capable of remodeling neuronal function (Molteni, Ying, & Gómez-Pinilla, 2002). Increased synaptic activity, which occurs during exercise, is energetically demanding (Attwell & Laughlin, 2001), and astrocytes can provide energetic support by supplying neurons with lactate via the astrocyte-neuron lactate shuttle (ANLS) (Pellerin & Magistretti, 1994). The maintenance of the ANLS has been shown to be important for learning, exhaustive exercise capacity, and memory (Boury-Jamot et al., 2016; Matsui et al., 2017; Suzuki et al., 2011). Exercise effects on the ANLS and metabolic cooperation between neurons and astrocytes may be important for exercise-induced neuroplasticity. Additionally, future studies should seek to understand the connection between peripheral and central factors, including muscle-derived sources of lactate and cytokines (E, Lu, Selfridge, Burns, & Swerdlow, 2013; Fischer, 2006). Lactate is capable of inducing angiogenesis through the $G_{i/o}$-protein coupled receptor HCA1 and may likely play a role in facilitating region-specific, exercise-induced blood flow changes that map with circuit-specific neuroplasticity (Morland et al., 2017).

In conclusion, findings from this study, based on changes in astrocytic morphology and gene expression, support astrocytic roles in neuroplasticity and synaptogenesis as mediated through exercise. While astrocytes are important in neuroplasticity and synaptogenesis, the underlying mechanisms that drive such a response remain incompletely known. Future studies should seek to explain the precise molecular components that may play a role in driving astrocytic response to exercise, and whether they are derived from local neurons and other glial cells or peripheral sources. Additionally, how exercise modifies the blood–brain barrier and astrocytic regulation of blood flow may also be an important avenue for more completely understanding exercise-induced neuroplasticity and synaptogenesis.

ACKNOWLEDGMENTS

The authors would like to acknowledge the support of the U.S. Army NETRP (Grant No. W81XWH-04-1-0444), the National Parkinson's Foundation, the Confidence Foundation, and the Plotkin Family Foundation. A special thanks to Friends of the USC Parkinson's

Disease Research Group including George and Mary Lou Boone, Walter and Susan Doniger, Edna and John Ball, Team Parkinson, and the family of Don Gonzalez Barrera. The authors declare no competing financial interests.

CONFLICT OF INTEREST

The authors declare no conflict of interest.

AUTHOR CONTRIBUTIONS

All authors take full responsibility for the integrity and analysis of all data presented. *Conceptualization*, A.J.L., G.M.P., and M.W.J.; *Methodology*, A.J.L., G.M.P., and M.W.J.; *Investigation*, A.J.L., J.P., G.M.P., and M.W.J.; *Formal Analysis*, A.J.L., G.M.P., and M.W.J.; *Writing—Original Draft*, A.J.L., J.P., G.M.P., and M.W.J.; *Writing—Review & Editing*, A.J.L., J.P., G.M.P., and M.W.J.; *Visualization*, A.J.L. and M.W.J.; *Supervision*, G.M.P. and M.W.J.; *Funding Acquisition*, G.M.P. and M.W.J.

DATA ACCESSIBILITY

Further information regarding resources, reagents, and data availability should be directed to the corresponding author (alundqui@usc.edu) and will be fulfilled upon reasonable request.

ORCID

Adam J. Lundquist https://orcid.org/0000-0002-0704-2567

REFERENCES

Abbott, N. J., Rönnbäck, L., & Hansson, E. (2006). Astrocyte–endothelial interactions at the blood–brain barrier. *Nature Reviews Neuroscience*, *7*(1), 41–53. https://doi.org/10.1038/nrn1824

Andersson, A. K., Rönnbäck, L., & Hansson, E. (2005). Lactate induces tumour necrosis factor-α, interleukin-6 and interleukin-1β release in microglial- and astroglial-enriched primary cultures. *Journal of Neurochemistry*, *93*(5), 1327–1333. https://doi.org/10.1111/j.1471-4159.2005.03132.x

Attwell, D., & Laughlin, S. B. (2001). An energy budget for signaling in the grey matter of the brain. *Journal of Cerebral Blood Flow & Metabolism*, *21*(10), 1133–1145. https://doi.org/10.1097/00004647-200110000-00001

Bauer, S., Kerr, B. J., & Patterson, P. H. (2007). The neuropoietic cytokine family in development, plasticity, disease and injury. *Nature Reviews Neuroscience*, *8*(3), 221–232. https://doi.org/10.1038/nrn2054

Bélanger, M., Allaman, I., & Magistretti, P. J. (2011). Brain energy metabolism: Focus on Astrocyte-neuron metabolic cooperation. *Cell Metabolism*, *14*(6), 724–738. https://doi.org/10.1016/j.cmet.2011.08.016

Bernardi, C., Tramontina, A. C., Nardin, P., Biasibetti, R., Costa, A. P., Vizueti, A. F., … Gonçalves, C. A. (2013). Treadmill exercise induces hippocampal astroglial alterations in rats. *Neural Plasticity*, *2013*, 1–10. https://doi.org/10.1155/2013/709732

Bernardinelli, Y., Randall, J., Janett, E., Nikonenko, I., König, S., Jones, E. V., … Muller, D. (2014). Activity-dependent structural plasticity of perisynaptic astrocytic domains promotes excitatory synapse stability. *Current Biology*, *24*(15), 1679–1688. https://doi.org/10.1016/j.cub.2014.06.025

Billat, V. L., Mouisel, E., Roblot, N., & Melki, J. (2005). Inter- and intra-strain variation in mouse critical running speed. *Journal of Applied Physiology*, *98*(4), 1258–1263. https://doi.org/10.1152/japplphysiol.00991.2004

Boury-Jamot, B., Carrard, A., Martin, J. L., Halfon, O., Magistretti, P. J., & Boutrel, B. (2016). Disrupting astrocyte–neuron lactate transfer persistently reduces conditioned responses to cocaine. *Molecular Psychiatry*, *21*(8), 1070–1076. https://doi.org/10.1038/mp.2015.157

Brockett, A. T., LaMarca, E. A., & Gould, E. (2015). Physical exercise enhances cognitive flexibility as well as astrocytic and synaptic markers in the medial prefrontal cortex. *PLoS ONE*, *10*(5), e0124859. https://doi.org/10.1371/journal.pone.0124859

Burgess, A., Vigneron, S., Brioudes, E., Labbé, J.-C., Lorca, T., & Castro, A. (2010). Loss of human Greatwall results in G2 arrest and multiple mitotic defects due to deregulation of the cyclin B-Cdc2/PP2A balance. *Proceedings of the National Academy of Sciences*, *107*(28), 12564–12569. https://doi.org/10.1073/pnas.0914191107

Chai, H., Diaz-Castro, B., Shigetomi, E., Monte, E., Octeau, J. C., Yu, X., … Khakh, B. S. (2017). Neural circuit-specialized astrocytes: Transcriptomic, proteomic, morphological, and functional evidence. *Neuron*, *95*(3), 531–549.e9. https://doi.org/10.1016/j.neuron.2017.06.029

Christopherson, K. S., Ullian, E. M., Stokes, C. C. A., Mullowney, C. E., Hell, J. W., Agah, A., … Barres, B. A. (2005). Thrombospondins are astrocyte-secreted proteins that promote CNS synaptogenesis. *Cell*, *120*(3), 421–433. https://doi.org/10.1016/j.cell.2004.12.020

Chung, W.-S., Clarke, L. E., Wang, G. X., Stafford, B. K., Sher, A., Chakraborty, C., … Barres, B. A. (2013). Astrocytes mediate synapse elimination through MEGF10 and MERTK pathways. *Nature*, *504*(7480), 394–400. https://doi.org/10.1038/nature12776

Committee for the Update of the Guide for the Care and Use of Laboratory Animals; National Research Council. (2010). *Guide for the care and use of laboratory animals* (8th Ed.). Washington, DC: The National Academies Press. https://doi.org/10.2307/1525495

Davies, J. M. S., Cillard, J., Friguet, B., Cadenas, E., Cadet, J., Cayce, R., … Davies, K. J. A. (2017). The oxygen paradox, the French paradox, and age-related diseases. *GeroScience*, *39*(5–6), 499–550. https://doi.org/10.1007/s11357-017-0002-y

de Senna, P. N., Bagatini, P. B., Galland, F., Bobermin, L., do Nascimento, P. S., Nardin, P., … Xavier, L. L. (2017). Physical exercise reverses spatial memory deficit and induces hippocampal astrocyte plasticity in diabetic rats. *Brain Research*, *1655*, 242–251. https://doi.org/10.1016/j.brainres.2016.10.024

E, L., Lu, J., Selfridge, J. E., Burns, J. M., & Swerdlow, R. H. (2013). Lactate administration reproduces specific brain and liver exercise-related changes. *Journal of Neurochemistry*, *127*(1), 91–100. https://doi.org/10.1111/jnc.12394

Eroglu, C., & Barres, B. A. (2010). Regulation of synaptic connectivity by glia. *Nature*, *468*(7321), 223–231. https://doi.org/10.1038/nature09612

Erta, M., Quintana, A., & Hidalgo, J. (2012). Interleukin-6, a major cytokine in the central nervous system. *International Journal of Biological Sciences*, *8*(9), 1254–1266. https://doi.org/10.7150/ijbs.4679

Ferreira, T. A., Blackman, A. V., Oyrer, J., Jayabal, S., Chung, A. J., Watt, A. J., … van Meyel, D. J. (2014). Neuronal morphometry directly from bitmap images. *Nature Methods*, *11*(10), 982–984. https://doi.org/10.1038/nmeth.3125

Fischer, C. P. (2006). Interleukin-6 in acute exercise and training: What is the biological relevance? *Exercise Immunology Review*, *12*(6–33), 41. https://doi.org/10.1016/j.metabol.2015.10.028

Fisher, B. E., Petzinger, G. M., Nixon, K., Hogg, E., Bremmer, S., Meshul, C. K., & Jakowec, M. W. (2004). Exercise-induced behavioral recovery

and neuroplasticity in the 1-methyl-4-phenyl-1,2,3,6-tetrahydropyridine-lesioned mouse basal ganglia. *Journal of Neuroscience Research*, *77*(3), 378–390. https://doi.org/10.1002/jnr.20162

Gruol, D. L., & Nelson, T. E. (1997). Physiological and pathological roles of interleukin-6 in the central nervous system. *Molecular Neurobiology*, *15*(3), 307–339. https://doi.org/10.1007/BF02740665

Guo, Y., Wang, Z., Prathap, S., & Holschneider, D. P. (2017). Recruitment of prefrontal-striatal circuit in response to skilled motor challenge. *NeuroReport*, *28*(18), 1187–1194. https://doi.org/10.1097/WNR.0000000000000881

Kamphuis, W., Mamber, C., Moeton, M., Kooijman, L., Sluijs, J. A., Jansen, A. H. P., … Hol, E. M. (2012). GFAP isoforms in adult mouse brain with a focus on neurogenic astrocytes and reactive astrogliosis in mouse models of Alzheimer disease. *PLoS ONE*, *7*(8), e42823. https://doi.org/10.1371/journal.pone.0042823

Khakh, B. S., & Sofroniew, M. V. (2015). Diversity of astrocyte functions and phenotypes in neural circuits. *Nature Neuroscience*, *18*(7), 942–952. https://doi.org/10.1038/nn.4043

Kinni, H., Guo, M., Ding, J. Y., Konakondla, S., Dornbos, D., Tran, R., … Ding, Y. (2011). Cerebral metabolism after forced or voluntary physical exercise. *Brain Research*, *1388*, 48–55. https://doi.org/10.1016/j.brainres.2011.02.076

Kintz, N., Petzinger, G. M., Akopian, G., Ptasnik, S., Williams, C., Jakowec, M. W., & Walsh, J. P. (2013). Exercise modifies α-amino-3-hydroxy-5-methyl-4-isoxazolepropionic acid receptor expression in striatopallidal neurons in the 1-methyl-4-phenyl-1,2,3,6-tetrahydropyridine-lesioned mouse. *Journal of Neuroscience Research*, *91*(11), 1492–1507. https://doi.org/10.1002/jnr.23260

Kintz, N., Petzinger, G. M., & Jakowec, M. W. (2017). Treadmill exercise modifies dopamine receptor expression in the prefrontal cortex of the 1-methyl-4-phenyl-1,2,3,6-tetrahydropyridine-lesioned mouse model of Parkinson's disease. *NeuroReport*, *28*(15), 987–995. https://doi.org/10.1097/WNR.0000000000000865

Li, J., Ding, Y. H., Rafols, J. A., Lai, Q., McAllister, J. P., & Ding, Y. (2005). Increased astrocyte proliferation in rats after running exercise. *Neuroscience Letters*, *386*(3), 160–164. https://doi.org/10.1016/j.neulet.2005.06.009

Livak, K. J., & Schmittgen, T. D. (2001). Analysis of relative gene expression data using real-time quantitative PCR and the 2 ⌥ ⌬⌬ C T method. *Gene Expression*, *408*, 402–408. https://doi.org/10.1006/meth.2001.1262

Matsui, T., Omuro, H., Liu, Y.-F., Soya, M., Shima, T., McEwen, B. S., & Soya, H. (2017). Astrocytic glycogen-derived lactate fuels the brain during exhaustive exercise to maintain endurance capacity. *Proceedings of the National Academy of Sciences*, *114*(24), 6358–6363. https://doi.org/10.1073/pnas.1702739114

Molteni, R., Ying, Z., & Gómez-Pinilla, F. (2002). Differential effects of acute and chronic exercise on plasticity-related genes in the rat hippocampus revealed by microarray. *European Journal of Neuroscience*, *16*(6), 1107–1116. https://doi.org/10.1046/j.1460-9568.2002.02158.x

Morel, L., Chiang, M. S. R., Higashimori, H., Shoneye, T., Iyer, L. K., Yelick, J., … Yang, Y. (2017). Molecular and functional properties of regional astrocytes in the adult brain. *The Journal of Neuroscience*, *37*(36), 8706–8717. https://doi.org/10.1523/JNEUROSCI.3956-16.2017

Morland, C., Andersson, K. A., Haugen, Ø. P., Hadzic, A., Kleppa, L., Gille, A., … Bergersen, L. H. (2017). Exercise induces cerebral VEGF and angiogenesis via the lactate receptor HCAR1. *Nature Communications*, *8*, 15557. https://doi.org/10.1038/ncomms15557

Pellerin, L., & Magistretti, P. J. (1994). Glutamate uptake into astrocytes stimulates aerobic glycolysis: A mechanism coupling neuronal activity to glucose utilization. *Proceedings of the National Academy of Sciences of the United States of America*, *91*(22), 10625–10629. https://doi.org/10.1073/pnas.91.22.10625

Petzinger, G. M., Fisher, B. E., McEwen, S., Beeler, J. A., Walsh, J. P., & Jakowec, M. W. (2013). Exercise-enhanced neuroplasticity targeting motor and cognitive circuitry in Parkinson's disease. *The Lancet Neurology*, *12*(7), 716–726. https://doi.org/10.1016/S1474-4422(13)70123-6

Petzinger, G. M., Holschneider, D. P., Fisher, B. E., McEwen, S., Kintz, N., Halliday, M., … Jakowec, M. W. (2015). The effects of exercise on dopamine neurotransmission in Parkinson's disease: Targeting neuroplasticity to modulate basal ganglia circuitry. *Brain Plasticity*, *1*(1), 29–39. https://doi.org/10.3233/BPL-150021

Petzinger, G. M., Walsh, J. P., Akopian, G., Hogg, E., Abernathy, A., Arevalo, P., … Jakowec, M. W. (2007). Effects of treadmill exercise on dopaminergic transmission in the 1-Methyl-4-Phenyl-1,2,3,6-tetrahydropyridine-lesioned mouse model of basal ganglia injury. *Journal of Neuroscience*, *27*(20), 5291–5300. https://doi.org/10.1523/JNEUROSCI.1069-07.2007

Rasmussen, P., Vedel, J.-C., Olesen, J., Adser, H., Pedersen, M. V., Hart, E., … Pilegaard, H. (2011). In humans IL-6 is released from the brain during and after exercise and paralleled by enhanced IL-6 mRNA expression in the hippocampus of mice. *Acta Physiologica*, *201*(4), 475–482. https://doi.org/10.1111/j.1748-1716.2010.02223.x

Rozovsky, I., Wei, M., Stone, D. J., Zanjani, H., Anderson, C. P., Morgan, T. E., & Finch, C. E. (2002). Estradiol (E2) enhances neurite outgrowth by repressing glial fibrillary acidic protein expression and reorganizing laminin. *Endocrinology*, *143*(2), 636–646. https://doi.org/10.1210/endo.143.2.8615

Saur, L., Baptista, P. P. A., de Senna, P. N., Paim, M. F., Nascimento, P. D., Ilha, J., … Xavier, L. L. (2014). Physical exercise increases GFAP expression and induces morphological changes in hippocampal astrocytes. *Brain Structure and Function*, *219*(1), 293–302. https://doi.org/10.1007/s00429-012-0500-8

Schindelin, J., Arganda-Carreras, I., Frise, E., Kaynig, V., Longair, M., Pietzsch, T., … Cardona, A. (2012). Fiji: An open-source platform for biological-image analysis. *Nature Methods*, *9*(7), 676–682. https://doi.org/10.1038/nmeth.2019

Sholl, D. A. (1953). Dendritic organization in the neurons of the visual and motor cortices of the cat. *Journal of Anatomy*, *87*, 387–406.

Sofroniew, M. V., & Vinters, H. V. (2010). Astrocytes: Biology and pathology. *Acta Neuropathologica*, *119*(1), 7–35. https://doi.org/10.1007/s00401-009-0619-8

Stogsdill, J. A., Ramirez, J., Liu, D. I., Kim, Y. H., Baldwin, K. T., Enustun, E., … Eroglu, C. (2017). Astrocytic neuroligins control astrocyte morphogenesis and synaptogenesis. *Nature*, *551*(7679), 192–197. https://doi.org/10.1038/nature24638

Sun, W., Cornwell, A., Li, J., Peng, S., Osorio, M. J., Aalling, N., … Nedergaard, M. (2017). SOX9 is an astrocyte-specific nuclear marker in the adult brain outside the neurogenic regions. *The Journal of Neuroscience*, *37*(17), 4493–4507. https://doi.org/10.1523/JNEUROSCI.3199-16.2017

Suzuki, A., Stern, S. A., Bozdagi, O., Huntley, G. W., Walker, R. H., Magistretti, P. J., & Alberini, C. M. (2011). Astrocyte-neuron lactate transport is required for long-term memory formation. *Cell*, *144*(5), 810–823. https://doi.org/10.1016/j.cell.2011.02.018

Toy, W. A., Petzinger, G. M., Leyshon, B. J., Akopian, G. K., Walsh, J. P., Hoffman, M. V., … Jakowec, M. W. (2014). Treadmill exercise reverses dendritic spine loss in direct and indirect striatal medium spiny neurons in the 1-methyl-4-phenyl-1,2,3,6-tetrahydropyridine (MPTP) mouse model of Parkinson's disease. *Neurobiology of Disease*, *63*, 201–209. https://doi.org/10.1016/j.nbd.2013.11.017

van Praag, H. (2005). Exercise enhances learning and hippocampal neurogenesis in aged mice. *Journal of Neuroscience*, *25*(38), 8680–8685. https://doi.org/10.1523/JNEUROSCI.1731-05.2005

van Praag, H., Kempermann, G., & Gage, F. H. (1999). Running increases cell proliferation and neurogenesis in the adult mouse dentate gyrus. *Nature Neuroscience*, *2*(3), 266–270. https://doi.org/10.1038/6368

Wang, Z., Myers, K. G., Guo, Y., Ocampo, M. A., Pang, R. D., Jakowec, M. W., & Holschneider, D. P. (2013). Functional reorganization of motor

and limbic circuits after exercise training in a rat model of bilateral parkinsonism. *PLoS ONE*, *8*(11), e80058. https://doi.org/10.1371/journal.pone.0080058

Wang, Z., Stefanko, D. P., Guo, Y., Toy, W. A., Petzinger, G. M., Jakowec, M. W., & Holschneider, D. P. (2016). Evidence of functional brain reorganization on the basis of blood flow changes in the CAG140 knock-in mouse model of Huntington's disease. *NeuroReport*, *27*(9), 632–639. https://doi.org/10.1097/WNR.0000000000000587

Wilhelmsson, U., Bushong, E. A., Price, D. L., Smarr, B. L., Phung, V., Terada, M., … Pekny, M. (2006). Redefining the concept of reactive astrocytes as cells that remain within their unique domains upon reaction to injury. *Proceedings of the National Academy of Sciences*, *103*(46), 17513–17518. https://doi.org/10.1073/pnas.0602841103

Zamanian, J. L., Xu, L., Foo, L. C., Nouri, N., Zhou, L., Giffard, R. G., & Barres, B. A. (2012). Genomic analysis of reactive astrogliosis. *Journal of Neuroscience*, *32*(18), 6391–6410. https://doi.org/10.1523/JNEUROSCI.6221-11.2012

How to cite this article: Lundquist AJ, Parizher J, Petzinger GM, Jakowec MW. Exercise induces region-specific remodeling of astrocyte morphology and reactive astrocyte gene expression patterns in male mice. *J Neuro Res*. 2019;97:1081–1094. https://doi.org/10.1002/jnr.24430